NASA TECHNICAL REPORT

NASA TR R-393

NASA TR R-393

A STUDY OF THE MICROSTRUCTURE AND OPTICAL PROPERTIES OF THIN LEAD-DIELECTRIC CERMET FILMS

by Robert B. Owen

George C. Marshall Space Flight Center
Marshall Space Flight Center, Ala. 35812

NATIONAL AERONAUTICS AND SPACE ADMINISTRATION • WASHINGTON, D. C. • DECEMBER 1972

TECHNICAL REPORT STANDARD TITLE PAGE

1. REPORT NO.	2. GOVERNMENT ACCESSION NO.	3. RECIPIENT'S CATALOG NO.
TR R-393		

4. TITLE AND SUBTITLE	5. REPORT DATE
A Study of the Microstructure and Optical Properties of Thin Lead-Dielectric Cermet Films	December 1972
	6. PERFORMING ORGANIZATION CODE
7. AUTHOR(S)	8. PERFORMING ORGANIZATION REPORT #
Robert B. Owen	
9. PERFORMING ORGANIZATION NAME AND ADDRESS	10. WORK UNIT NO.
	11. CONTRACT OR GRANT NO.
George C. Marshall Space Flight Center Marshall Space Flight Center, Alabama 35812	13. TYPE OF REPORT & PERIOD COVERED
12. SPONSORING AGENCY NAME AND ADDRESS	Technical Report
National Aeronautics and Space Administration Washington, D.C. 20546	14. SPONSORING AGENCY CODE

15. SUPPLEMENTARY NOTES Prepared by Astrionics Laboratory, Science and Engineering. This work was submitted to the Graduate Faculty of Virginia Polytechnic Institute and State University in partial fulfillment of the requirements for the degree of Doctor of Philosophy in Physics and was done under the guidance of Dr. H. Y. Loy.

16. ABSTRACT

A transmission electron microscopy study involving direct and replicating techniques is directed to a definition of the microstructure of radio frequency-sputtered, thin lead-dielectric cermet films. Once defined, this microstructure is used to obtain theoretical film refractive indices. The Maxwell Garnett theory provides a basis for the theoretical results. Measurements of film transmission and reflectivity are used to obtain rough experimental values for film refractive indices by the Tekucheva method. More exact values are obtained via ellipsometry. The rough Tekucheva values are used to determine the range over which computer calculations interpreting the ellipsometric results must be made. This technique yields accurate values for the film refractive indices. The films are radio frequency-sputtered from lead glass targets with varying amounts of lead attached to their faces. Three different targets are used, resulting in three sets of films, each containing a different percentage of lead. The lead content of the films is measured by microprobe analysis as well as visual inspection of micrographs. The lower content lead films are seen to consist of tiny balls of lead embedded in the dielectric, as are the intermediate lead content films; but the higher lead content films form metallic networks throughout the dielectric. The lower and intermediate lead content films have indices which agree with the predictions of the Maxwell Garnett theory; but the higher lead content films, whose structure fails to conform to the Maxwell Garnett configuration, have indices whose values diverge from the Maxwell Garnett predictions. It is thus shown that the theory of Maxwell Garnett is valid for thin cermet films whose structure consists of tiny metal balls embedded in a dielectric medium.

17. KEY WORDS	18. DISTRIBUTION STATEMENT
Thin Films Film Structure Optical Properties Refractive Index Cermet Films	

19. SECURITY CLASSIF. (of this report)	20. SECURITY CLASSIF. (of this page)	21. NO. OF PAGES	22. PRICE
Unclassified	Unclassified	110	$3.00

* For sale by the National Technical Information Service, Springfield, Virginia 22151

TABLE OF CONTENTS

LIST OF ILLUSTRATIONS

LIST OF ILLUSTRATIONS (Continued)

LIST OF ILLUSTRATIONS (Concluded)

LIST OF TABLES

ACKNOWLEDGMENTS

All equipment and materials used in this study belong to the Technology Division, Astrionics Laboratory, George C. Marshall Space Flight Center, National Aeronautics and Space Administration, Huntsville, Alabama. Of special aid to this work were James C. Taylor, Technology Division Chief, who sponsored this study; S.V. Caruso, Hybrid Circuit Research Section Chief, who suggested cermet films sputtered from a single target as a material for study; James L. Zurasky, without whom the ellipsometric measurements in this study would have been impossible; R.F. DeHaye, who aided greatly in the laboratory work; and all members of the MSFC Hybrid Circuit Research Section, who were always helpful and patient.

The author would like to thank his advisor, Dr. H.Y. Loh of the Virginia Polytechnic Institute and State University, for his guidance throughout this project.

The author offers an expression of gratitude to his wife, Lyn, for her cooperation and understanding during the preparation of this manuscript.

LIST OF SYMBOLS

A	Analyzer reading, amplitude coefficient
$\bar{A}$	Magnetic vector potential
a	Semiaxis of ellipse, radius of metal spheres
a_i	Component amplitude, analyzer angle
$\bar{B}$	Magnetic induction
b	Semiaxis of ellipse
c	Velocity of light in free space
$\bar{D}$	Electric displacement
d_i	Thickness
$\bar{E}^i$	Electric vector
f	Frequency
$\bar{H}$	Magnetic vector
I_i	Light intensity
$\bar{j}$	Current density
k_i	Imaginary part of refractive index
$\bar{M}$	Magnetic polarization
N	Number of molecules per unit volume
N'	Number of metal spheres per unit volume
$n_j{}^i$	Refractive index
$\bar{n}$	Refractive index, unit normal
P	Polarizer reading
$\bar{P}^i$	Electric polarization
p	Polarizer angle
$\bar{p}$	Electric dipole moment

LIST OF SYMBOLS (Continued)

q	Volume factor
R	Distance
R_i	Reflection coefficient
r_i^j	Reflection amplitude coefficient, Fresnel amplitude coefficient
S_i	Strokes parameter
t	Time
V	Volume
v	Velocity of light in medium
a_i	Absorption coefficient, mean polarizability
Δ	Phase difference
δ	Phase difference
ϵ_0 , ϵ_v	Permittivity of free space
ϵ_i	Permittivity of medium
ϵ^i	Dielectric constant
η^i	Dielectric susceptibility
θ	Relative phase retardation
2θ	Microprobe detector location
κ	Absorption index
λ_i	Wavelength
μ	Refractive index, percent metal per unit volume
μ_0 , μ_v	Permeability of free space
σ_i	Conductivity

LIST OF SYMBOLS (Concluded)

υ	Refractive index of glass
ϕ	Electric scaler potential, azimuth of light
χ	Ellipticity of light
ω	Angular frequency

A STUDY OF THE MICROSTRUCTURE AND OPTICAL PROPERTIES OF THIN LEAD-DIELECTRIC CERMET FILMS

I. INTRODUCTION

Thin cermet films, similar to other vacuum-deposited thin films, are formed through a process of nucleation that starts with the appearance of isolated three-dimensional nuclei [1-5]. If deposition continues, the nuclei grow, intergrow, and finally form a continuous deposit film at an average thickness of 5 to 100 nm [6].

Previous studies [7-9] have shown that composite dielectric-metal (cermet) films consist of metallic grains embedded in a dielectric network. Miller and Shirn [7] studied the conductive properties of co-sputtered Au-SiO_2, thin film cermets. The electric resistance was found to vary exponentially with gold concentration. The microstructure was examined briefly by transmission electron microscopy and was found to consist of discontinuous networks of Au and SiO_2. A similar study of flash-evaporated Cr-SiO films involving film structure, resistivity, and temperature coefficient of resistance was carried out by Gland, et al. [8]. Electron microscopy revealed a discontinuous microstructure that varied with metallic content. Another study of the structure and resistivity of co-sputtered metal-dielectric films was made by Beckerman and Thun [9]. Various metal-dielectric combinations of percentages and materials revealed a discontinuous, grainy microstructure.

Because of their microstructure, cermet films are intimately related to the extensively studied but poorly understood ultrathin metallic films which consist entirely of the initial, isolated nuclei or grains. Therefore, we shall briefly review the studies made of ultrathin metal films, most of which are concerned with the electrical conductivity of the films.

The problem of conduction by tunneling between isolated, conducting grains was analyzed in 1930 by Frenkel [10]. Further studies on conduction through thin dielectric barriers were made by Emtage and Tantraporn [11], who considered Schottky emission through thin insulating films; Stratton [12], who extended previous tunneling theory by including temperature dependence and image force corrections; Hartman, et al. [13], who made extensive experimental measurements of electrical conduction through SiO films; Hill [14], who did an excellent survey of the various proposed mechanisms and relevant experimental results; and Gundlach and Simmons [15], who analyzed the range of validity of the WKB approximations used in some of the proposed mechanisms.

The first detailed investigation of conduction in ultrathin metal films was done by Neugebauer and Webb [16], who concluded that the conduction process consisted of, first, thermally activated charge carrier creation involving charge transfer between initially neutral particles and, second, the drift velocity of those charges in an applied field. Charge

transfer between charges occurred by tunneling. Neugebauer's and Webb's mechanism was supported by experimental results. An alternate mechanism was then proposed by Hartman [17], who assumed tunneling between neutral grains. Hartman's mechanism, which was also in agreement with experiment, involved an activation energy corresponding to differences in energy levels of the band structure of the individual particles, which was assumed to be discrete because of the small size of the particles. The Neugebauer and Webb mechanism suggested that a certain number of the microparticles must be charged, thus requiring a thermal activation energy to move the appropriate electrons, with tunneling then occurring between charged and uncharged microparticles. Workers agreed that some kind of activation energy was required to reconcile theory and experiment, but it was questionable as to which theoretical form it would take. Experimental results slightly favoring the Hartman theory were obtained by measurements of electrical resistance-strain characteristics of thin metal films made by Parker and Krinsky [18], but then a further modification of the Neugebauer and Webb thermal activation mechanism by Weitzenkamp and Bashara [19] brought that theory more in line with experiment.

At this time a different mechanism was proposed by Herman and Rhodin [20], who suggested that conduction should include contributions caused by electron tunneling between regions in the substrate surface immediately under the metallic particles. Charge carriers would be contributed to the insulator surface regions by the metallic microparticles. Their activation energy, which also produced results agreeable with experiment, was electrostatic in nature and depended upon the average size and separation of the metal grains.

A modification of the tunneling process common to all the previously described mechanisms was made by Milgram and Lu [21], who assumed that trapping centers existed in the substrate. They considered charge carriers created both by thermal excitation and by field injection coupled with a charge transportation mechanism consisting of tunneling via the trapping centers.

Further modification of the Neugebauer and Webb model was done by Swanson, et al. [22], who considered electron transfer between charged particles other than charged-to-neutral particle transfers.

The confusion was finally resolved by Hill [23], who, in an extensive theoretical and experimental work, established a mechanism similar to that of Neugebauer and Webb, but with an activation energy that considered substrate electrical properties and microparticle dimension and a tunneling mechanism that incorporated temperature dependence and the effects of an active substrate.

It should be noted that an interesting proposal by Morris [24] suggested correlated conductivity and Hall-effect measurements on cermet films as a method of finally determining which of the above mechanisms was correct. Unfortunately cermet films never showed a measureable Hall effect.[1]

1. J.E. Morris, Private Communication, April 28, 1970.

The only examinations of cermet films have been in the form of conduction and structural studies. In addition to those studies mentioned, a detailed conduction study was made by Christen and Hewitt [25], who measured resistivities and temperature coefficients of resistance for radiofrequency, co-sputtered gold-silicon dioxide and vacuum-evaporated gold-silicon monoxide films. Their results are compatible with the mechanism of Neugebauer and Webb.

No optical studies have been made on thin cermet films until the present study, although such films would be roughly included in the general study of the optical properties of thin absorbing films made by Abelés [26]. Related optical studies have been made by workers examining ultrathin metal films.

The theory of Maxwell Garnett [27] applies to island structure films, such as ultrathin metal films. Studies of the optical properties of such films have been made and are reviewed by Heavens [28]. Maxwell Garnett assumed spherical metal particles that were small with respect to a wavelength of light. His results agree with the more general theory of Mie [29] for light absorption and scattering by an arbitrarily-sized sphere in the limit of small, widely-separated spheres. Some investigators [30, 31] reported disagreement with the Maxwell Garnett theory and assumed nonspherical microparticles without any direct evidence for the necessity of this assumption. The resultant treatments are extremely complex. However, it was shown in the later work of Doremus [32, 33] that previous results could be understood in terms of the Maxwell Garnett theory and that it was not necessary to assume that the particles were nonspherical or to make any other modifications of the theory. It might be noted that while in the original formulation of the theory it was stated that for thin films the Maxwell Garnett expression for the dielectric constant might have to be modified for light falling on the film at an oblique angle, the results of Doremus indicate that no such modification is necessary. It is shown in the present study that the Maxwell Garnett model applies with equal validity to thin cermet films.

In this study, variations in surface structure are correlated with variations in the internal metallic distribution. This is done by electron microscopy, using both replicating techniques and direct observation of films, and by microprobe analysis. The structural model found is approximated by the Maxwell Garnett model, which is then used to generate theoretical refractive indices. Rough indices of refraction experimentally using the Tekucheva method [34] for interpretation of transmission and reflectivity measurements and more exact experimental values found using ellipsometry [35, 36] are compared to the theoretical Maxwell Garnett refractive index values.

II. MICROSTRUCTURE EXAMINATION

This section presents the experimental procedure used in this study for the examination of the microstructure of thin cermet films.

A. Film Formation

The films were made in a Consolidated Vacuum Corporation (CVC) Plasmavac AST-200 sputtering unit, which may be seen in Figure 1. The unit utilizes an RF-sputtering technique which enables one to sputter dielectrics as well as conductors. This technique is well discussed in Holland [37]. Plasmavac chamber pressures were less than 10^{-5} torr before argon was introduced and sputtering began.

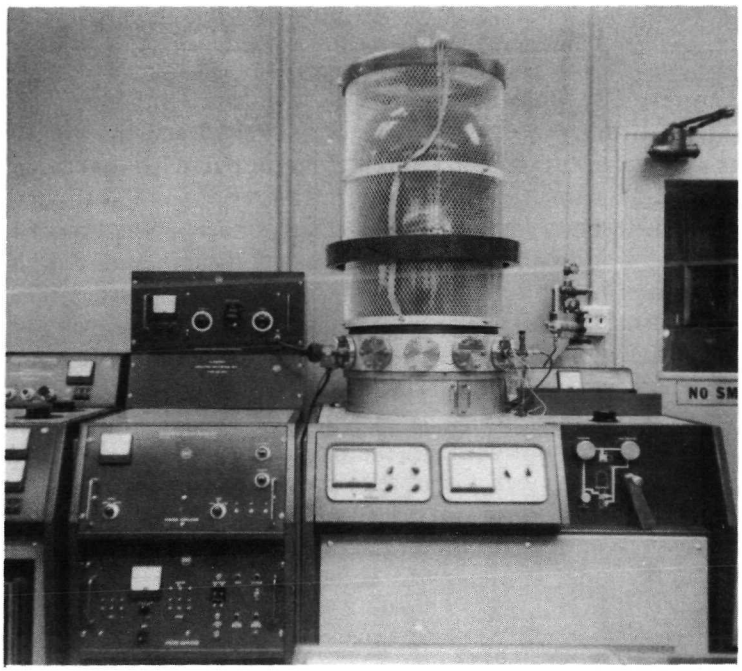

Figure 1. Photograph of CVC Plasmavac AST-200 sputtering unit.

Single sputtering targets were used. This technique should ultimately yield films more uniform and reproducible than those resulting from the dual-target techniques used by others [7, 8]. The targets consisted of a nickel backing, lead glass, and varying amounts of pure lead. A typical target was formed by firing a coating of Corning 7572 or 7575 lead glass onto a 0.157-cm-thick square of nickel and fusing strips or dots of pure lead to the glass. The glass fired at about 500°C. This technique was suggested by R.F. DeHaye, Marshall Space Flight Center (MSFC). Three targets were made, having 10-, 25-, and 50-percent pure lead by surface area, respectively, soldered to their fronts. The targets were mechanically polished before each deposition to remove any lead oxide.

Film thickness and sputtering rates were monitored by a Sloan 103-850 quartz crystal monitor. This unit uses a newly developed round quartz crystal which mounts inside a shielded stainless steel cap. Both the crystal mounting surface and its signal contact are shielded from the evaporant stream. Thus, unlike previous monitors, the unit gives stable readings while in a plasma. Monitor calibration was done by Tolansky interferometry [38] in a Sloan M-100 Angstrometer. Measurement by quartz crystal monitor is described by Holland [37]. Sputtering rates of about 10 nm/min were typical.

Films with thicknesses of 20, 40, 60, and 80 nm were made from each of the targets, and additional films of 100 nm and 100 and 140 nm were made from 25- and 10-percent lead targets, respectively.

B. Examination by Microprobe

An Advanced Metals Research (AMR) Corporation X-ray spectrometer attachment for the Philips EM-300 transmission electron microscope was used to measure the actual lead content of the films. All films measured were deposited onto electron microscope grids that were precovered with a Formvar film. Thus, the films could be inserted directly into the electron microscope for analysis. A 40 nm-thick, evaporated-lead film was used as a standard, and a simple ratio measurement of peak heights was used to determine the percentage of lead in the cermet films. Peak heights are taken to be proportional to lead content. This procedure is described in References 39 and 40.

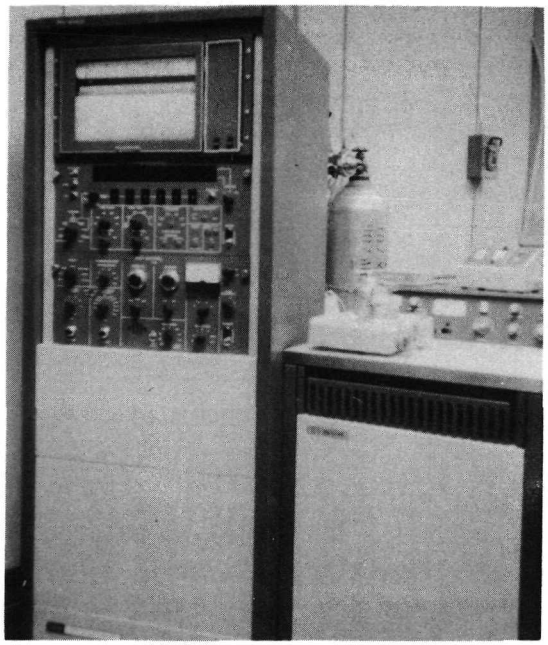

Figure 2. Photograph of AMR X-ray Spectrometer attachment and Norelco Mark III Data Control and Processor.

The AMR X-ray spectrometer attachment and the associated Norelco Mark III Data Control and Processor may be seen in Figure 2. With this equipment attached to the electron microscope, one bombards the sample with the microscope's electron beam and examines the intensity of the emitted X-rays as a function of the X-ray energy. Because of the discrete emissions characteristic of any given element, one is able to determine which elements are present in the sample by comparing the resultant peaks or lines with known, tabulated values. By comparing the intensities of the lines with line intensities from the appropriate known standards, it is also possible to determine quantitative values for sample composition.

C. Examination by Electron Microscopy

Replicas suitable for electron microscopy were made from each film. This was done by the following well-established procedure [41]. Presoftened replicating tape was pressed onto each film and left to set for at least 3 hours. These surface impressions were then removed, coated with a thin vacuum-sputtered carbon film which followed the contours of the impressions, and shadowed with chromium from a source angled at 30 deg with respect to the replica plane. The replicating tape was then desolved away in an acetone bath, leaving the shadowed carbon replicas which were scooped out of the bath onto a microscope grid. The resulting specimens show the surface structure of the films under study.

It was also possible to examine the films directly by electron microscopy. Some films were deposited directly onto 3.05-mm, 200-mesh Fullum electron microscope grids that were precovered with a Formvar film. These specimens could be inserted directly into the electron microscope and examined. All electron microscope examinations were made on a Philips EM-300 transmission scope, which may be seen in Figure 3.

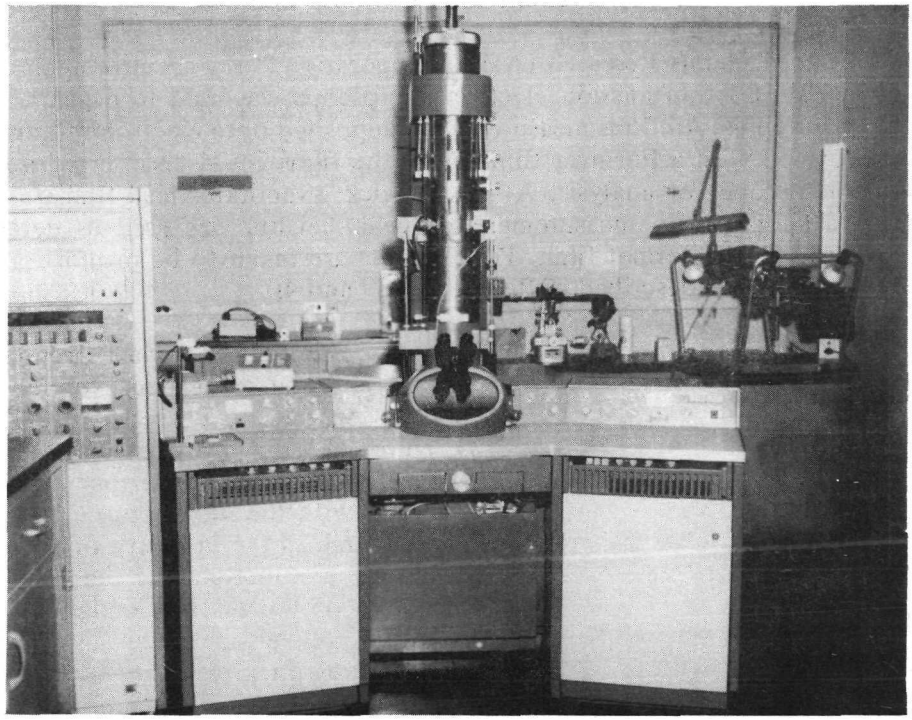

Figure 3. Photograph of Phillips EM-300 transmission electron microscope.

III. MEASUREMENT OF OPTICAL PROPERTIES

This section presents the experimental techniques used in this study for measurement of optical properties of thin cermet films. The films were formed in the same manner as before except that they were deposited onto Kodak B351 cover glass substrates.

A. Through Absorption and Reflection

It is possible to determine thin film indices of refraction by measuring the intensity of monochromatic light reflected by and transmitted through both the bare substrate and the film-substrate system. The approach used in this study is the method of Tekucheva [34], whose method requires knowledge of the light source wavelength, the film thickness, the substrate index of refraction, and the appropriate transmission and reflection measurements. For this study, Kodak B351 slide cover glass was used as substrates. The index of refraction of Kodak B351 glass has been determined to be 1.538 ± 0.001 at 546.1 nm,[2] and this value as well as the film thicknesses measured by the Sloan 103-850 quartz crystal monitor were the values utilized in the calculations in this study. These were also the values used in evaluating ellipsometric measurements.

2. J.L. Zurasky, Private Communication, Marshall Space Flight Center, Alabama, 1970.

A Cary Model 14 recording spectrophotometer was used to make transmission and reflection measurements. The instrument automatically records transmission and reflection spectra over the 186 to 2600 nm wavelength region with accuracies of ±3 percent, using assorted light sources, energy receivers, slits, collimators, prisms, and gratings. In this report, measurements were confined to the 325- to 800-nm region, where a tungsten lamp acted as source and a 1P28 multiplier phototube acted as energy receiver.

Measurements were taken on all the cermet films under study, but meaningful results were obtained only for the more absorbent films from the 50-percent pure lead sputtering target, since the accuracy of the Cary Model 14 was insufficient to detect the transmission variances required to use the Tekucheva method. A presentation of this method follows. However, the values obtained acted as a rough guide in the determination of the iteration range utilized in the McCrackin program for solution of the Drude equations.

Refractive Indices by the Tekucheva Method. Tekucheva's [34] method allows one to obtain refractive indices of thin films from measurements of film transmission and reflection. A derivation of this method follows.

Consider an absorbing medium of thickness d, reacting with monochromatic light of wavelength λ_0 and initial intensity I_0. We know that the transmitted light has intensity I, where

$$I = I_0 e^{-\alpha d} , \tag{1}$$

and α is the absorption coefficient of the medium. We may relate α to the medium's optical constants by

$$\alpha = 4\pi n\kappa/\lambda_0 , \tag{2}$$

where

n = refractive index of medium

κ = absorption index of medium.

Note that the complex refractive index $\bar{n}'$ would be defined here as

$$\bar{n}' = n(1 - i\kappa) . \tag{3}$$

Equation (1) is valid only if there is little reflection at the boundaries. For a medium without a substrate but with reflection at both boundaries, equation (1) becomes

$$I = I_0 (1 - r)^2 e^{-\alpha d} \quad , \tag{4}$$

where r is the reflection coefficient for the air-medium boundary, and the incident light is normal.

Now consider an absorbing film on a substrate, as shown in Figure 4. Here, we have reflection at three boundaries – the air-film, the film-substrate, and the substrate-air boundaries. Also, in addition to film absorption we have absorption by the substrate. Assuming film and substrate thicknesses of d_1 and d_2 and film and substrate absorption coefficients of α_1 and α_2, respectively, we may write

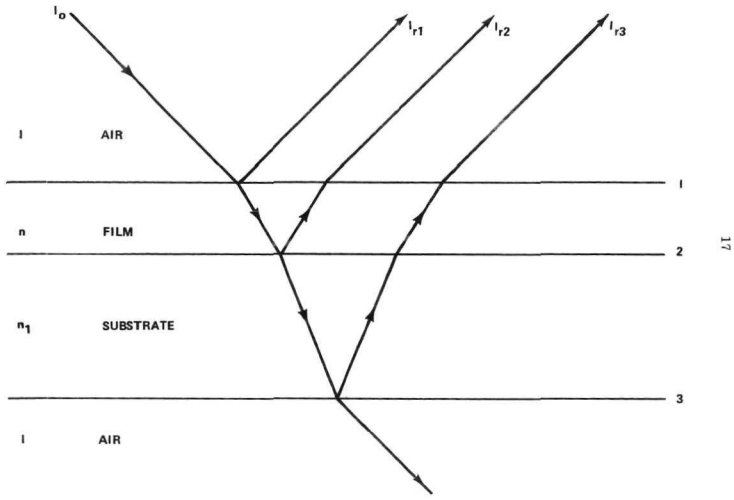

Figure 4. Film substrate system in unprimed mode.

$$I_1 = I_0 (1 - R_1)(1 - R_2)(1 - R_3) e^{-\alpha_1 d_1} e^{-\alpha_2 d_2} \quad , \tag{5}$$

where R_1, R_2, and R_3 are the reflection coefficients at boundaries 1, 2, and 3, respectively, as shown in Figure 4, and I_1 is the intensity of the light transmitted by the film and substrate. We are considering the incident light to be normal, and we are neglecting multiple-reflection terms, which are relatively small at normal incidence for the films under study.

We note that if we consider the intensity of the light transmitted by the bare substrate only, I_2, we may write

$$I_2 = I_0 (1 - R_3)^2 e^{-\alpha_2 d_2} \quad . \tag{6}$$

Solving for $e^{-\alpha_2 d_2}$ in equation (6) and substituting into equation (5) yield

$$I_1 = I_2(1 - R_1)(1 - R_2)e^{-\alpha_1 d_1}/(1 - R_3) \quad ,$$

or

$$e^{-\alpha_1 d_1} = \frac{I_1(1 - R_3)}{I_2(1 - R_1)(1 - R_2)} \quad . \tag{7}$$

We define the overall reflection coefficient for reflection from all three boundaries as

$$R = I_r/I_0 \quad ,$$

where I_r is the intensity of light reflected from all three boundaries, and the system is arranged as in Figure 4.

Approximating as before, we may write the reflected intensity of normally incident light as

$$I_r = I_0R_1 + I_0(1 - R_1)^2 R_2 e^{-2\alpha_1 d_1} + I_0(1 - R_1)^2 (1 - R_2)^2 R_3 e^{-2\alpha_2 d_2} e^{-2\alpha_1 d_1} \quad , \tag{8}$$

and by neglecting terms that contain R_iR_j we have

$$R \approx R_1 + R_2 e^{-2\alpha_1 d_1} + R_3 e^{-2\alpha_1 d_1} e^{-2\alpha_2 d_2} \quad . \tag{9}$$

Now, if the system is arranged as in Figure 5, which will be called the primed system, a similar expression may be derived for R', in which

$$R' = I_r'/I_0 \quad ;$$

that is,

$$R' = R_3 + R_2 e^{-2\alpha_2 d_2} + R_1 e^{-2\alpha_1 d_1} e^{-2\alpha_2 d_2} \quad . \tag{10}$$

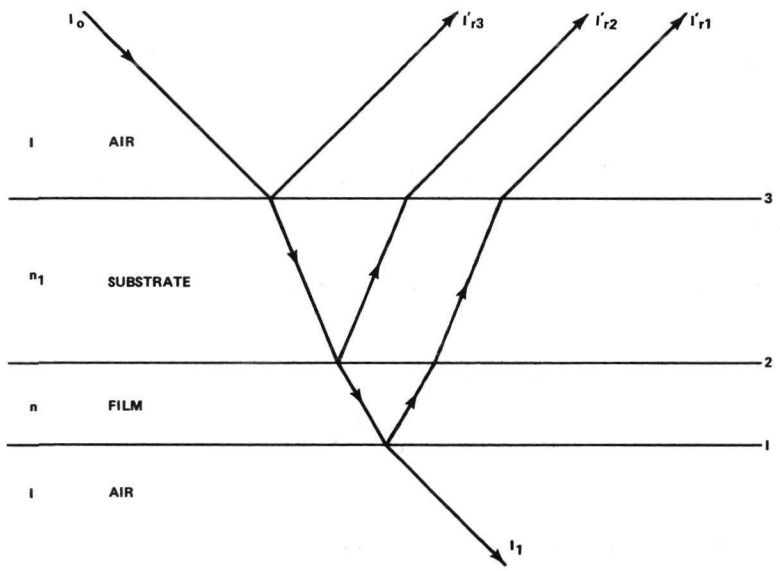

Figure 5. Film-substrate system in primed mode.

Noting that for normal incidence the Fresnel formulas for reflection at a boundary, as derived in Appendix B, reduce to

$$R_1 = (n - 1)^2/(n + 1)^2 \quad ,$$

$$R_2 = (n - n_1)^2/(n + n_1)^2 \quad , \tag{11}$$

$$R_3 = (n_1 - 1)^2/(n_1 + 1)^2 \quad ,$$

where 1, n, and n_1 are the refractive indices of air, film, and substrate, respectively, and solving equations (9), (10), and (11) simultaneously for n yields

$$n^2 - 2n \frac{p^2(1 - z^4) + p^2(R - R_3z^2p^2) - z^2(R' - R_3)}{p^2(1 - z^4) - p^2(R - R_3z^2p^2) + z^2(R' - R_3)} + 1 = 0 \ , \qquad (12)$$

where

$$z = e^{-\alpha_1 d_1} \text{ and } p = e^{-\alpha_2 d_2} \ .$$

For a thick substrate, R_3 terms may be neglected and equation (12) becomes

$$n^2 - 2n \frac{1 - z^4 + R - R'z^2/p^2}{1 - z^4 - R + R'z^2/p^2} + 1 = 0 \ . \qquad (13)$$

Making some further approximations, we note that for small $\alpha_i d_i$, equation (9) may be written as

$$R = R_1 + R_2 + R_3 - (2\alpha_1 d_1 R_2 + 2\alpha_1 d_1 R_3 + 2\alpha_2 d_2 R_3) \ , \qquad (14)$$

which may be further written, for thin ($d \leq 100$ nm) and not too strongly absorbing films on a thick substrate, as

$$R = R_1 + R_2 + R_3 \ . \qquad (15)$$

Thus, putting $(1 - R_1)(1 - R_2) \cong 1 - R_1 - R_2$ and using equation (15), we have

$$(1 - R_1)(1 - R_2) \approx 1 - R + R_3 \ . \qquad (16)$$

Substituting equation (16) into equation (7) yields

$$z = e^{-\alpha_1 d_1} \cong \frac{I_1(1 - R_3)}{I_2(1 - R + R_3)} \ . \qquad (17)$$

Now, we may calculate n and κ for the film from transmission and reflectivity data for monochromatic light of a known wavelength λ_0 if the film thickness d_1 and the substrate refractive index n_1 are known. We proceed as follows:

a. Measure the transmission of the bare substrate; this yields I_2.

b. Calculate R_3 using n_1 in equation (11).

c. Calculate p using equation (6).

d. Measure the total reflectivity of the film-substrate system in the primed and unprimed modes as shown in Figures 4 and 5; this yields R and R'.

e. Measure the transmission of the film-substrate system; this yields I_1.

f. Use the now-known values of I_1, I_2, R_3, and R in equation (17) to obtain z.

g. Use z, p, R, and R' values in equation (12) to obtain a value for n.

h. Use the known d_1 and the calculated z values in the definition of z to obtain a value for α_1.

i. Use $\alpha_1 = 4\pi n\kappa/\lambda_0$ to obtain κ.

In this manner, the Tekucheva method yields quick, rough values for n and κ which may be used as first approximations in more sophisticated techniques.

B. Through Ellipsometry

The indices of refraction for the cermet films under study were measured on a Gaertner Model L119 ellipsometer. This instrument and its peripheral equipment include the following: an external-filtered mercury light source emitting 546.1 nm monochromatic light; the appropriate collimators and shutters; two Nicol prisms, one rotatable about the source beam axis and one rotatable about the source beam axis and a vertical axis; a quarter-wave plate, rotatable about the source beam axis and situated between the two prisms; and a photomultiplier tube with associated power amplifier and digital voltmeter. The photomultiplier tube measures the intensity of the light after it leaves the source; passes through the collimator, first Nicol prism and the quarter-wave plate; bounces off the specimen; and passes through the second Nicol prism. The specimen is rotatable about the same vertical axis as is the second prism. All rotational orientations can be read directly to within 0.01 deg. With this equipment, changes in the polarization of the reference beam upon reflection from the specimen can be measured.

The classical treatment concerning the change in the state of polarization of light upon reflection from a bare surface or a surface with a film on it is the old and very elegant

approach of Drude [42], whose theory and equations are essentially exact. By using Fosterling's theory of reflection and refraction by a plane-parallel homogeneous thin film, a derivation of Drude's equations is given in Appendix B. Drude's equations cannot be solved in closed form, necessitating trial-and-error and iteration methods. Thus, before the availability of electronic computers, the routine application of the exact equations was practically impossible. However, computer programs to solve the Drude equations now exist, and, in this study, the National Bureau of Standards program of McCrackin [36] is used.

The McCrackin program was rewritten in Fortran 4H as modified for the Xerox Data Systems (XDS) Sigma Five computer used in this study, and, after extensive debugging efforts, the program worked well in evaluating ellipsometric measurements of the cermet films under study. The exact procedure used in this stage of the study is outlined in Appendix A.

IV. RESULTS OF OPTICAL EXAMINATION

In this section, the results of the examination of cermet films of various thicknesses sputtered from targets with different lead contents are presented.

A. Microprobe Results

The AMR microprobe attachment gave values of 58 ± 6, 45 ± 5, and 30 ± 3 percent lead by volume for films from the 50-, 25-, and 10-percent lead targets, respectively. The data for these films are shown in Figures 6 through 9. The peak height of the PbM (1, 2) doublet [43] was taken to be directly proportional to the percent lead by volume contained in each film. The peak height of the pure lead film in Figure 6 was used as a standard. The errors arise mostly from the simple ratio technique used to obtain quantitative values, which is not strictly accurate for the complex metal-dielectric matrix at hand. The PbLB (1, 2) and MB lines are distorted by the proximity of the barium LB1, LB2 (with satellites), LB3, LB4, and LB6 lines, and the platinum M3-01 line (arising from the sample holder), and may be disregarded. It might be noted here that the dielectric part of the films consisted of the oxides of zinc, aluminum, silicon, boron, and traces of barium. These compounds are contained in the Corning 7575 and 7572 lead glasses.[3]

B. Electron Microscope Results

1. Direct Transmission Studies. Examination of the films deposited onto Formvar-covered grids revealed that the films from each sputtering target had their own characteristic structure, which may be seen in the following sections.

3. Brent W. Springford, Private Communication, Corning Glass Works, Corning, New York, 1970.

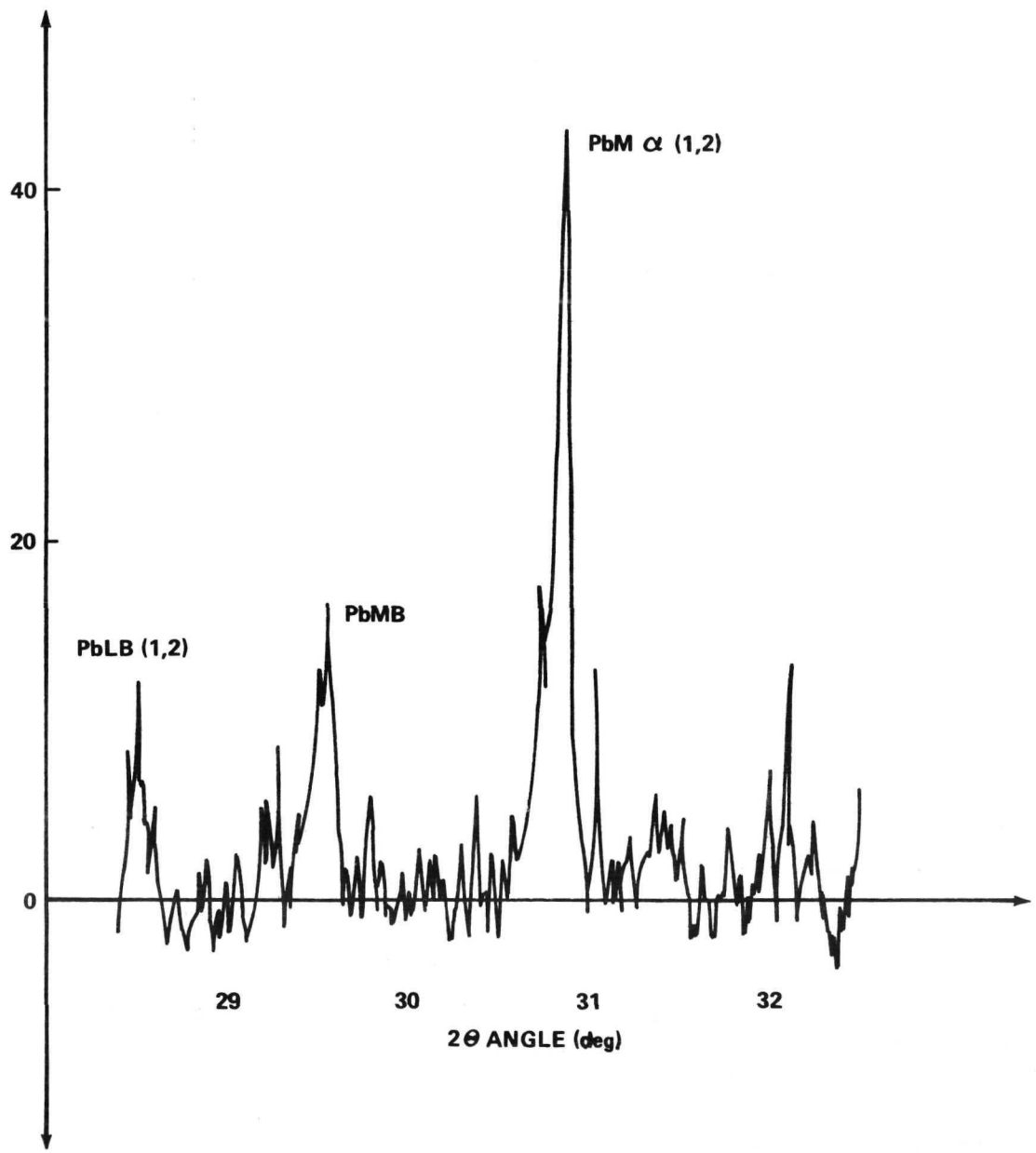

Figure 6. Spectral pattern from pure lead film.

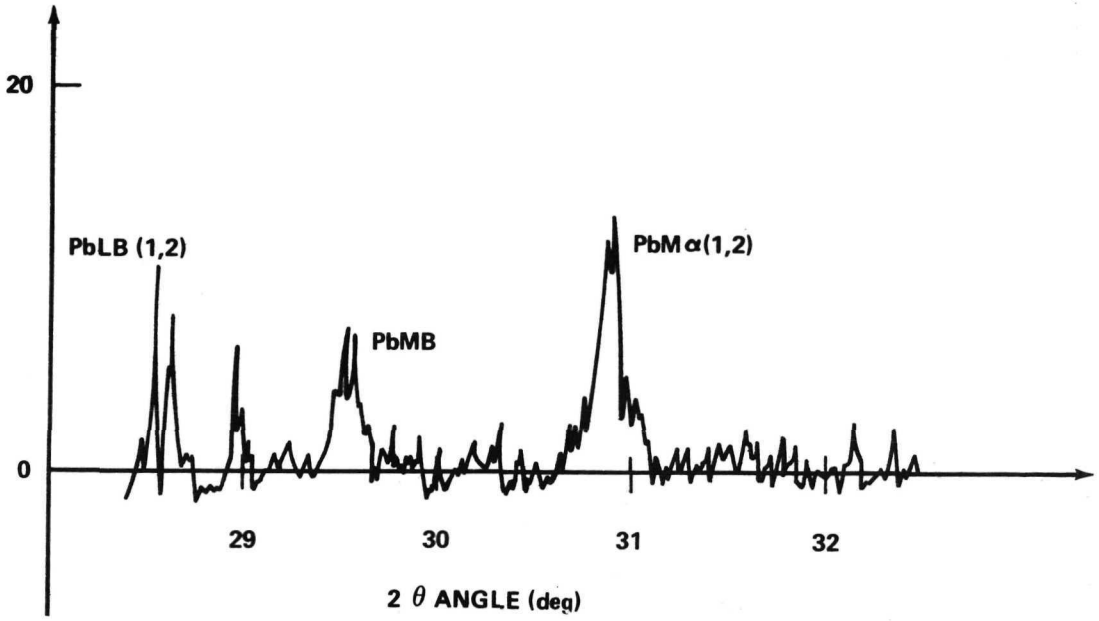

Figure 7. Spectral pattern of film sputtered from 10-percent pure lead target.

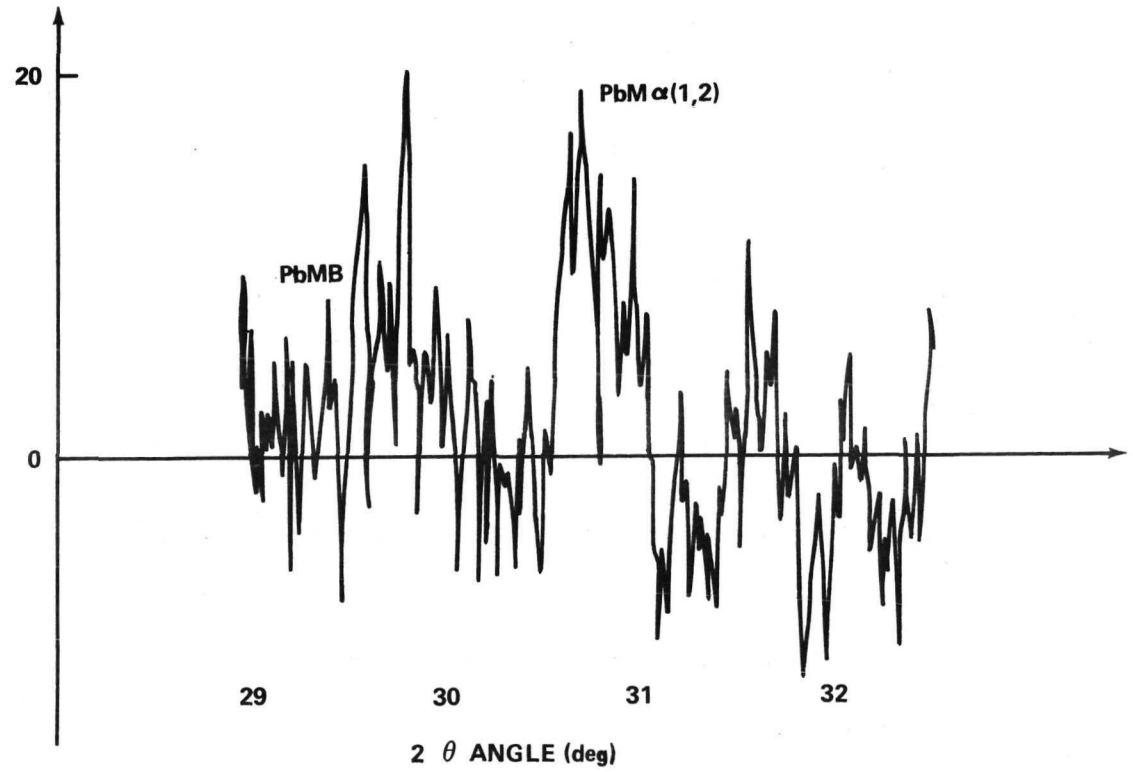

Figure 8. Spectral pattern of film sputtered from 25-percent pure lead target.

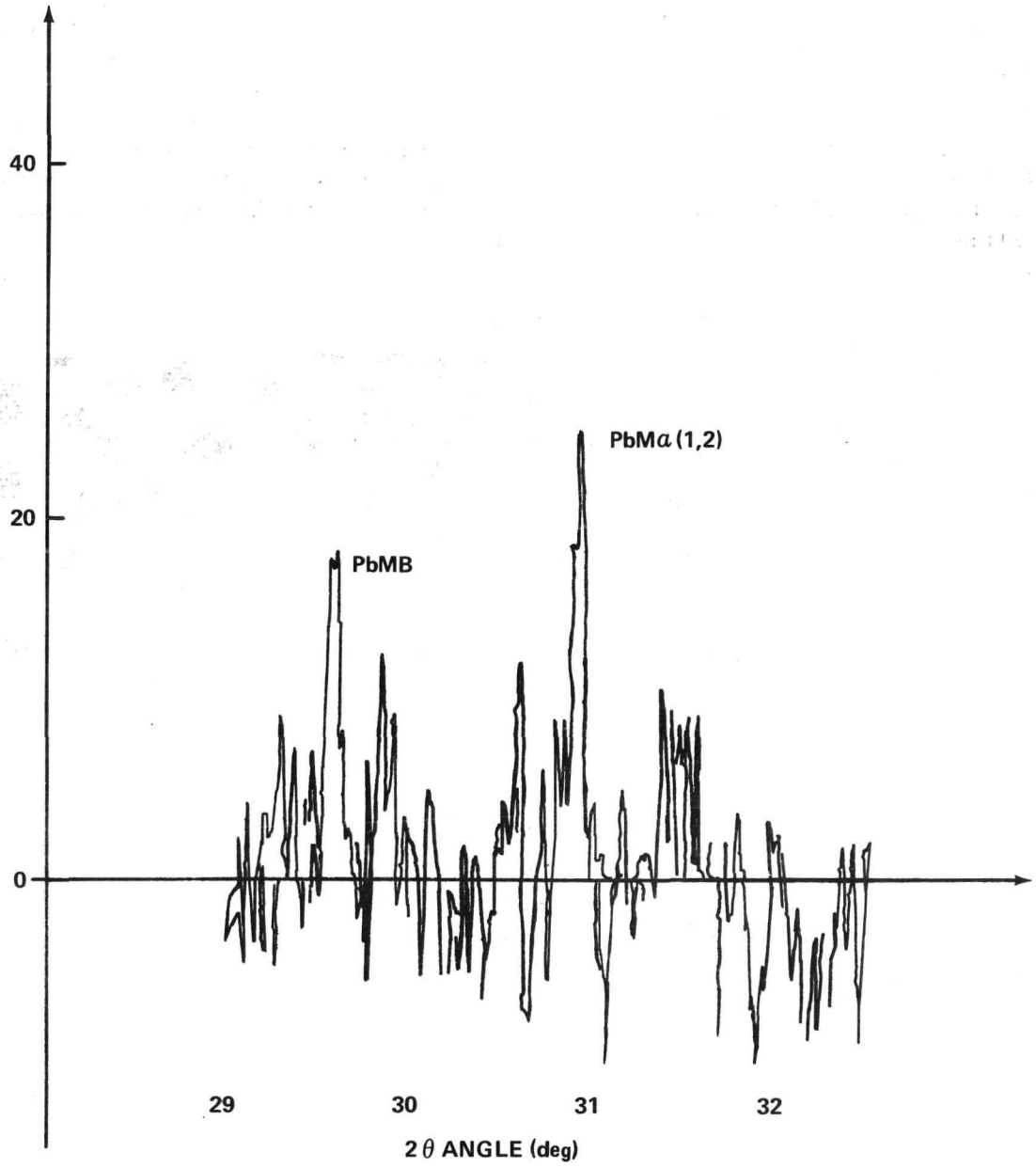

Figure 9. Spectral pattern of film sputtered from 50-percent pure lead target.

a. Low-Lead Content Films (30 Percent by Volume). Films deposited from the 10-percent pure lead target had a structure consisting of small spheres of lead embedded in dielectric. The spheres were typically 10 to 30 nm in diameter and had their centers separated by about 40 nm. The lead spheres occupied about 15 percent of the film volume. This structure may be seen in Figure 10. The film was stable under the microscope electron beam.

b. Intermediate-Lead Content Films (45 Percent by Volume). As the metallic content increased, the lead balls seemed to grow in size, typically to about 400 to 800 nm in diameter, although a number of balls less than 100 nm in diameter may be seen (Fig. 11). In other photographs, some of the smaller balls are in the process of combining with some of the larger balls, and some of the larger balls are intergrowing (Figs. 11 and 12). A higher magnification of one of the larger balls (Fig. 13) shows an outer edge consisting of a number of smaller balls the size of those observed in the low-lead content films. The larger balls are usually separated by a center-to-center distance on the order of 1300 nm.

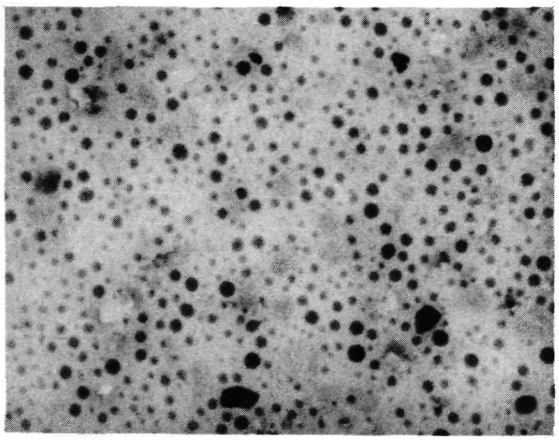

Figure 10. A 30-percent lead film on Formvar-covered grid (260 000 x).

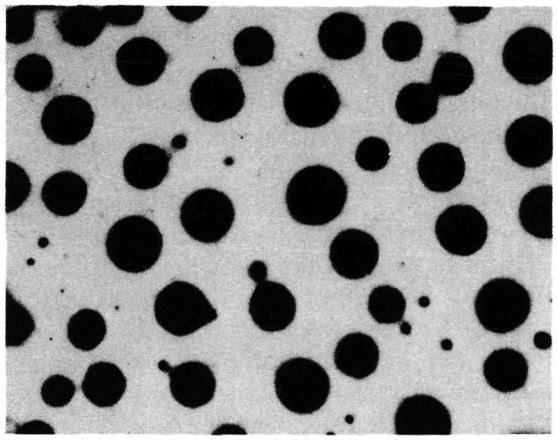

Figure 11. A 45-percent lead film on Formvar-covered grid (31 500 x).

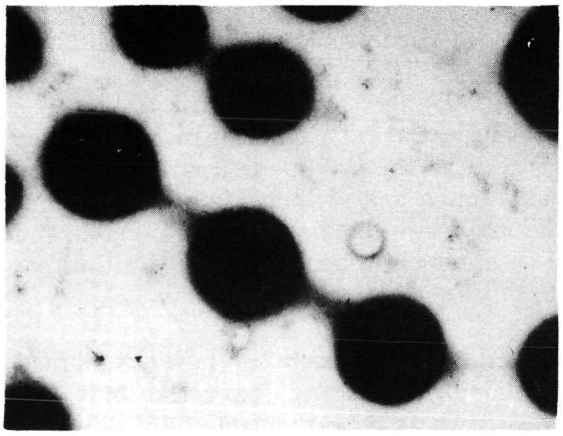

Figure 12. A 45-percent lead film on Formvar-covered grid (76 000 x).

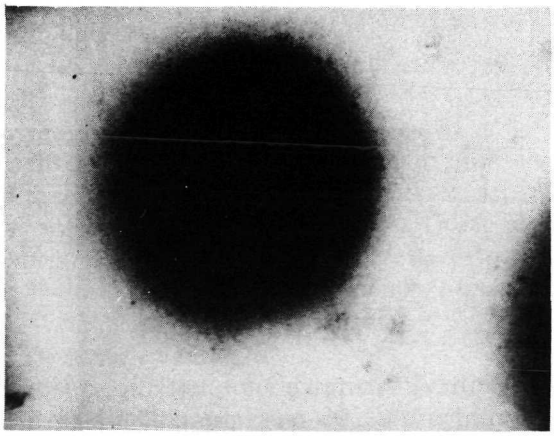

Figure 13. A 45-percent lead film on Formvar-covered grid (260 000 x).

Since the films are only 40 to 50 nm thick and are only 45-percent lead, insufficient metal exists in the films to form spheres of the sizes and distributions observed. A more likely shape for the metal particles is some type of disk.

Let us assume that the particles are oblate spheroids and that they contain all the lead in the film (45 percent by volume). This shape is not unreasonable and does not conflict with the micrographs.

Furthermore, the high contrast between the spheroids and the remaining film in Figure 11 leads one to believe that almost all the lead is contained in the particles. Let us further assume that the rotated ellipses forming the oblate spheroids have the same eccentricity. A rough volume calculation based on the above assumptions implies that such spheroids have eccentricities of about 0.96.

The above model infers that the larger spheroids have a maximum thickness of 200 nm. They should therefore be jutting out of the surface as manifestations of the underlying metal structure.

It should be noted here that it is possible that Figures 11 through 13 do not represent the totally undisturbed metallic structure. Some lead migration, as a result of film heating in the electron beam, was observed; thus, the original film structure may be different from that recorded. Such migratory effects have been noted in pure lead films [38, 39]. The effect is not surprising since under certain matrix conditions the electron beam can heat the sample to temperatures as high as 1000°C [40]. It is difficult to estimate the degree of the migration since the effect occurred very rapidly, usually while the microscope was being focused.

It might be further noted that no migration occurred in the high- or low-lead content films except immediately before film breakdown. Apparently, in the highly metallic films, conduction to prevent extreme heating existed, and in the slightly metallic films the relatively small amount of lead was held in place by the heat-resistive dielectric.

An indication of the accuracy of Figures 11 through 13 is obtained in the replica study presented later in this report.

c. High-Lead Content Films (58 Percent by Volume). In the extreme case, the metal particles remain about the same size as in the intermediate case, but more numerous and closely packed; they touch or nearly touch and form an almost continuous network (Fig. 14). However, there is not nearly as much contrast between the metallic and dielectric areas as there was in the intermediate case, which indicates that lead atoms are diffused throughout the dielectric.

In some areas (Fig. 15) the metal particles have combined completely, forming a metallic medium containing dielectric particles that are approximately 200 nm across. The lack of contrast in these areas indicates a diffused lead content.

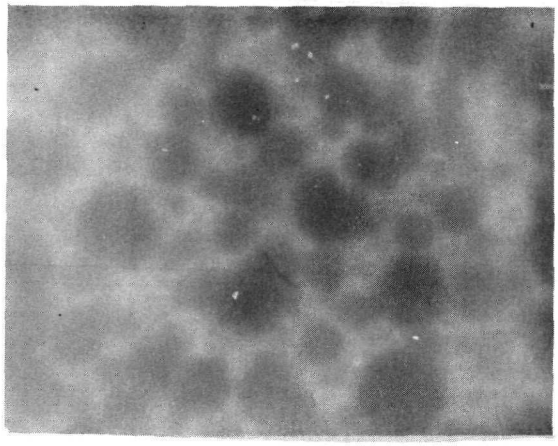

Figure 14. A 58-percent lead film on Formvar-covered grid (76 000 x).

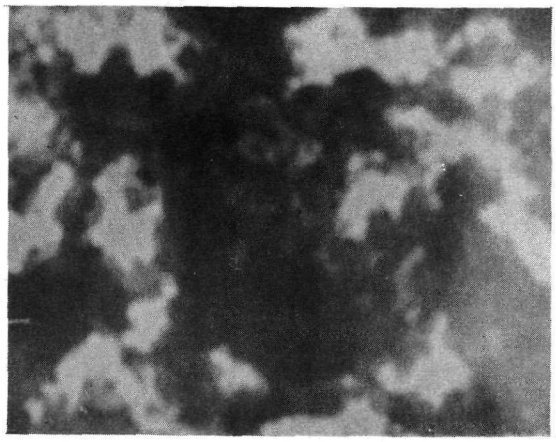

Figure 15. A 58-percent lead film on Formvar-covered grid (260 000 x).

2. Replica Studies. Replicas were made as follows. Impressions were made with replica tape of the various films. The impressions were coated with a sputtered-carbon film. This carbon film was shadowed with chromium, and the replicating tape was dissolved away in acetone. This is a standard technique [41].

a. Low-Lead Content Films (30 Percent by Volume). Films that were 20, 40, 60, 80, 100, and 140 nm thick were examined by the replicating technique. No surface trend with the thickness was seen. All films seemed to be continuous and exhibited pits and mounds. It is possible that some of the features of the thinner films are caused by substrate effects.

Since the limit of replica resolution is about 5 nm, one might expect difficulty in spotting surface features caused by the underlying 20-nm-diameter lead spheres. However, some surface details that could be so caused can be seen in Figure 16.

Figure 16. Replica of 20-nm, 30-percent lead film (79 300 x).

b. Intermediate-Lead Content Films (45 Percent by Volume). For this case, films with thicknesses of 20, 40, 60, 80, and 100 nm were examined by the replicating technique. Again no trend with thickness was established; all films seemed to be continuous. However, several features can be seen that could be surface manifestations of the lead spheroids observed in Figures 11 through 13. The surface features in Figures 17 and 18 correspond especially well in size and distribution to the spheroids. This is evidenced because the spheroids are not totally a product of heating in the electron beam. The shape of the features implies that the oblate spheroid model is correct in some instances, at least. In

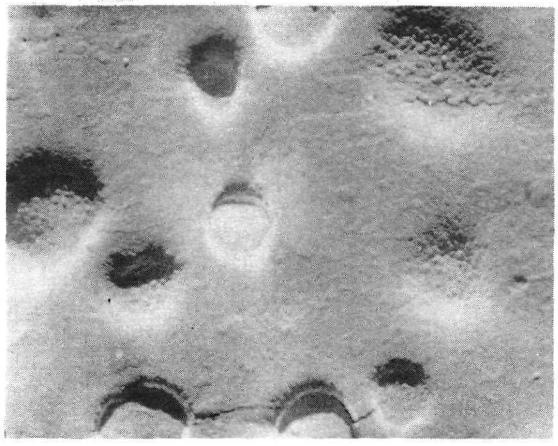

Figure 17. Replica of 60-nm, 45-percent lead film (31 000 x).

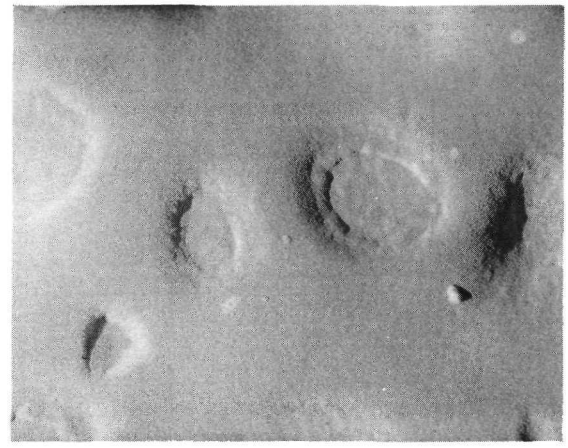

Figure 18. Replica of 60-nm, 45-percent lead film (63 000 x).

these instances, most of the lead in the film is contained in the spheroids. It is possible that in areas which do not exhibit such sharp surface features the lead is simply more dispersed through the dielectric.

c. High-Lead Content Films (58 Percent by Volume). Films that were 20, 40, 60, and 80 nm thick were examined by the replicating technique. A trend with thickness appeared and can be seen in Figures 19 through 22. By assuming that most of the surface features are a manifestation of the underlying metal network, the plates imply that the network becomes more defined and connected as film thickness increases. Metal particles seem to form and join together as the film thickens. Definite pits and protrusions were seen (Fig. 23) which matched well with the sizes and distributions of the metal particles observed in Figure 14.

Figure 19. Replica of 20-nm, 58-percent lead film (31 300 x).

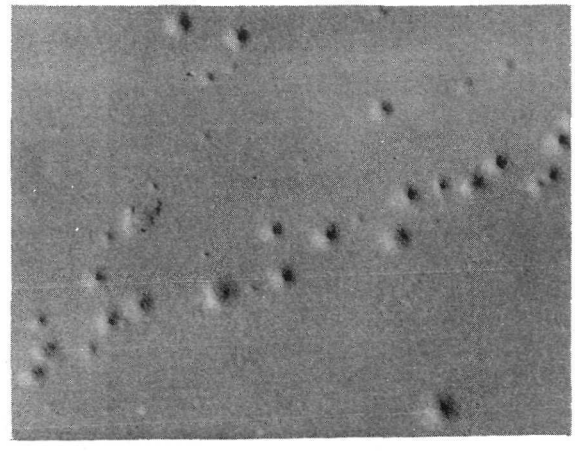

Figure 20. Replica of 40-nm, 58-percent lead film (33 600 x).

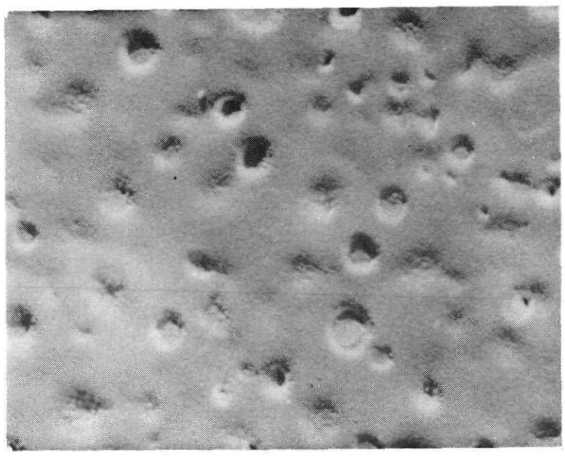

Figure 21. Replica of 60-nm, 58-percent lead film (30 500 x).

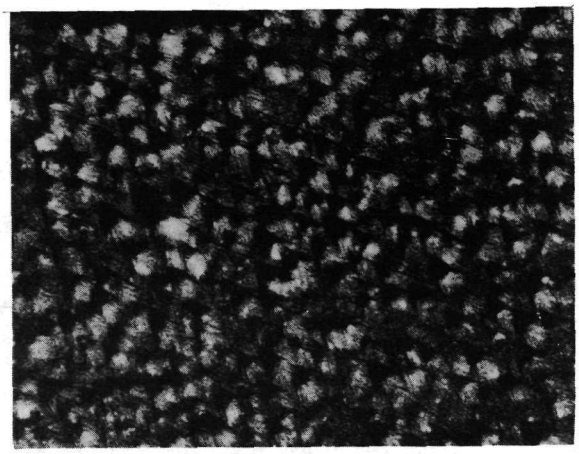

Figure 22. Replica of 80-nm, 58-percent lead film (176 000 x).

Figure 23. Replica of 60-nm, 58-percent lead film (100 000 x).

C. Interpretation of Electron Microscopy Observations

1. Internal Film Structure. Direct transmission electron microscopic examination of lead-dielectric cermet films indicates that increases in the lead content of the films from 30 to 45 to 58 percent vary the film structure drastically. In the 30-percent lead films the structure consists of 10- to 30-nm-diameter lead spheres embedded in a slightly homogeneous dielectric medium. As the lead content is increased to 45 percent, the spheres grow to well-defined oblate spheroids which are 400 to 800 nm in diameter. Further addition of lead (to 58 percent) results in many additional spheroids in the 400- to 800-nm-size range that join to form a connecting network as the film thickens.

2. Film Surface Structure. Replicas of film surfaces reveal mounds and pits that are roughly the size of the underlying metal particles. These features can be interpreted as manifestations of the film's metal structure, which juts out of the film plane in some areas and depresses the film surface in other areas. Thus, there appears to be a gratifying correspondence between the replica and direct electron microscopy studies.

3. Effects of Film Thickness Variations. No outstanding thickness trend appeared in the range observed except for the case of the 58-percent lead films, which seemed to show an increase in the definition of their metallic structures as film thickness increased. All films were continuous at 20 nm.

V. RESULTS OF MEASUREMENT OF OPTICAL PROPERTIES

This section presents the results of measurement of optical properties of thin cermet films.

A. Refractive Indices from Reflection and Transmission Measurements

Since the noise level in the Cary Model 14 recording spectrophotometer was higher than the differences in reflection and transmission that were measured in the less absorbent films, physically meaningful refractive indices were obtained only for the 58-percent lead films. These values are presented in Table 1 and in Figures 24 and 25. It is difficult to estimate the error in these indices; it is merely known that it is large. It should be noted that the usefulness of these rough values was in their specification of the initial iteration range to be used in the McCrackin computer program; in this sense, they were extremely valuable. It is interesting that the rough values for n indicate the same thickness dependence that is obtained from the final ellipsometric values.

TABLE 1. REFRACTIVE INDICES FROM REFLECTION AND TRANSMISSION MEASUREMENTS

Lead Content of Film (Percent by Volume)	Film Thickness (nm)	n′(Real Part of Index)	Kappa (κ')
58 ± 6	80 ± 4	3.9 ± ?	0.60 ± ?
58 ± 6	60 ± 3	4.3 ± ?	0.30 ± ?
58 ± 6	40 ± 2	5.0 ± ?	0.50 ± ?
58 ± 6	20 ± 1	2.5 ± ?	0.60 ± ?

B. Refractive Indices from Ellipsometry

Successive iterations of decreasing range and increment values on the XDS Sigma Five and 3 hours of computer time yielded the refractive indices shown in Table 2 and Figures 26 through 31. The data used are shown in Table 3. Figures 26 through 28 indicate a thickness dependence for the real part of the refractive index. No analysis of this dependence will be attempted in this study.

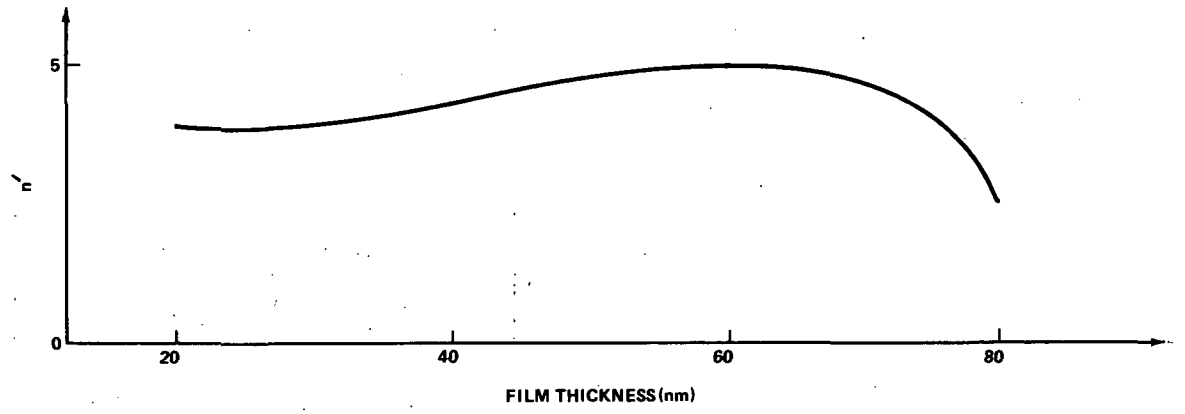

Figure 24. Approximate values of n′ from reflectivity and transmission measurements for 58-percent lead films.

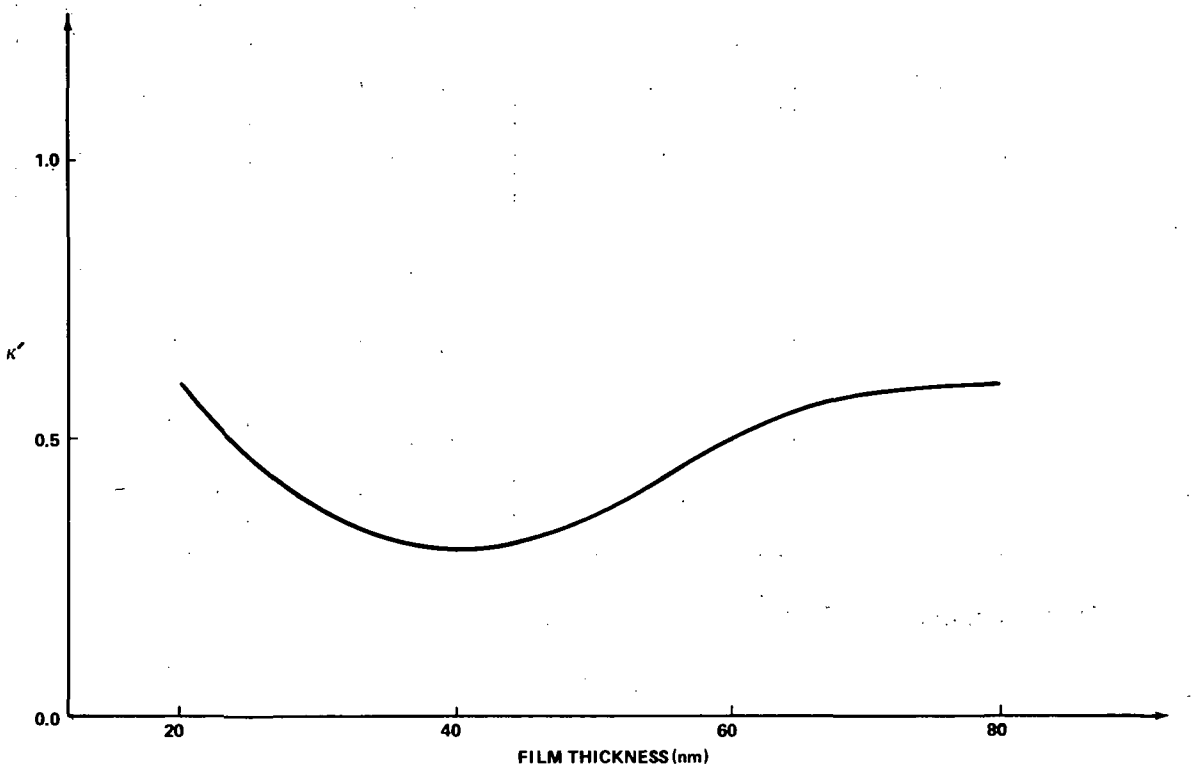

Figure 25. Approximate values of κ_i' from reflectivity and transmission measurements for 58-percent lead films.

TABLE 2. REFRACTIVE INDICES FROM ELLIPSOMETRY

Lead Content of Film (Percent by Volume)	Film Thickness (nm)	n′(Real Part of Index)	Kappa (κ′)
58 ± 6	80 ± 4	1.94 ± 0.06	0.35 ± 0.02
58 ± 6	60 ± 3	2.75 ± 0.08	0.51 ± 0.06
58 ± 6	40 ± 2	2.69 ± 0.20	0.79 ± 0.08
58 ± 6	20 ± 1	1.81 ± 0.08	0.99 ± 0.05
45 ± 5	80 ± 4	2.15 ± 0.02	0.10 ± 0.03
45 ± 5	60 ± 3	2.31 ± 0.01	0.08 ± 0.02
45 ± 5	40 ± 2	2.30 ± 0.02	0.06 ± 0.02
45 ± 5	20 ± 1	2.13 ± 0.03	0.05 ± 0.02
30 ± 3	80 ± 4	2.05 ± 0.02	0.17 ± 0.02
30 ± 3	60 ± 3	2.16 ± 0.02	0.05 ± 0.02
30 ± 3	40 ± 2	2.13 ± 0.02	0.04 ± 0.01
30 ± 3	20 ± 1	1.98 ± 0.03	0.020 ± 0.004

Note: $n_{complex} \equiv n' - n'\kappa'i$

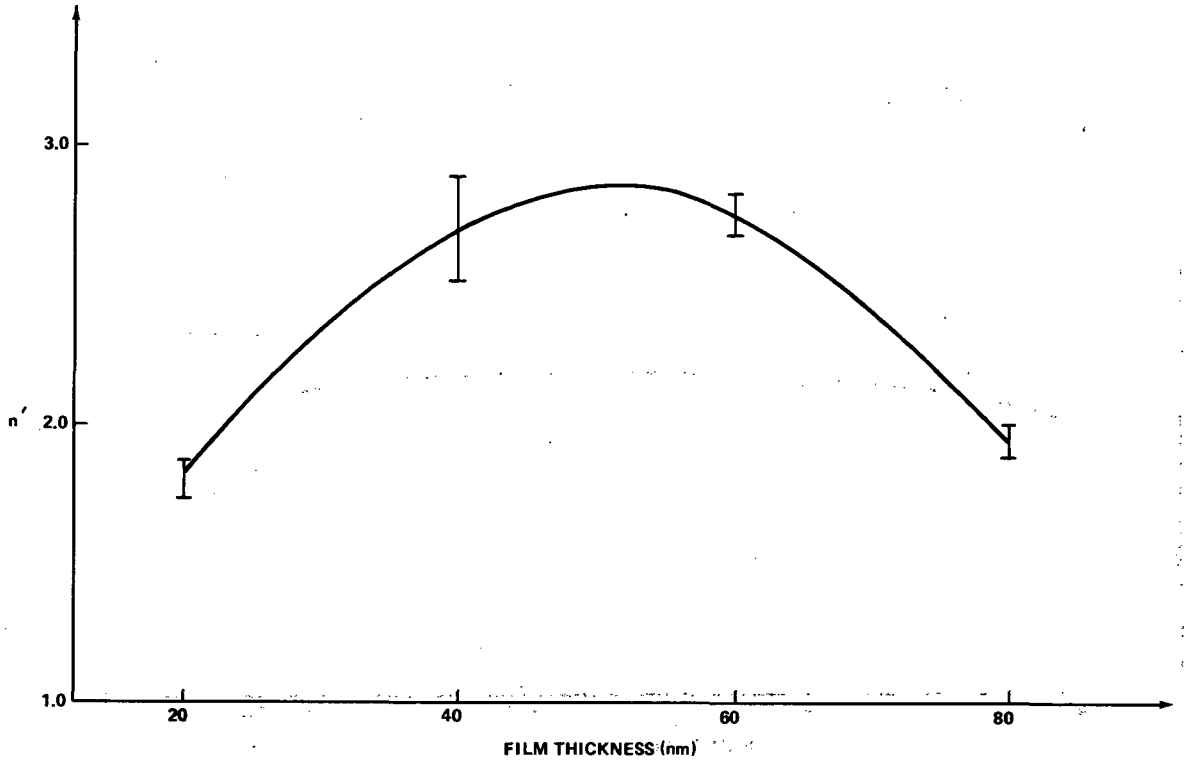

Figure 26. n′ versus film thickness for 58-percent lead films.

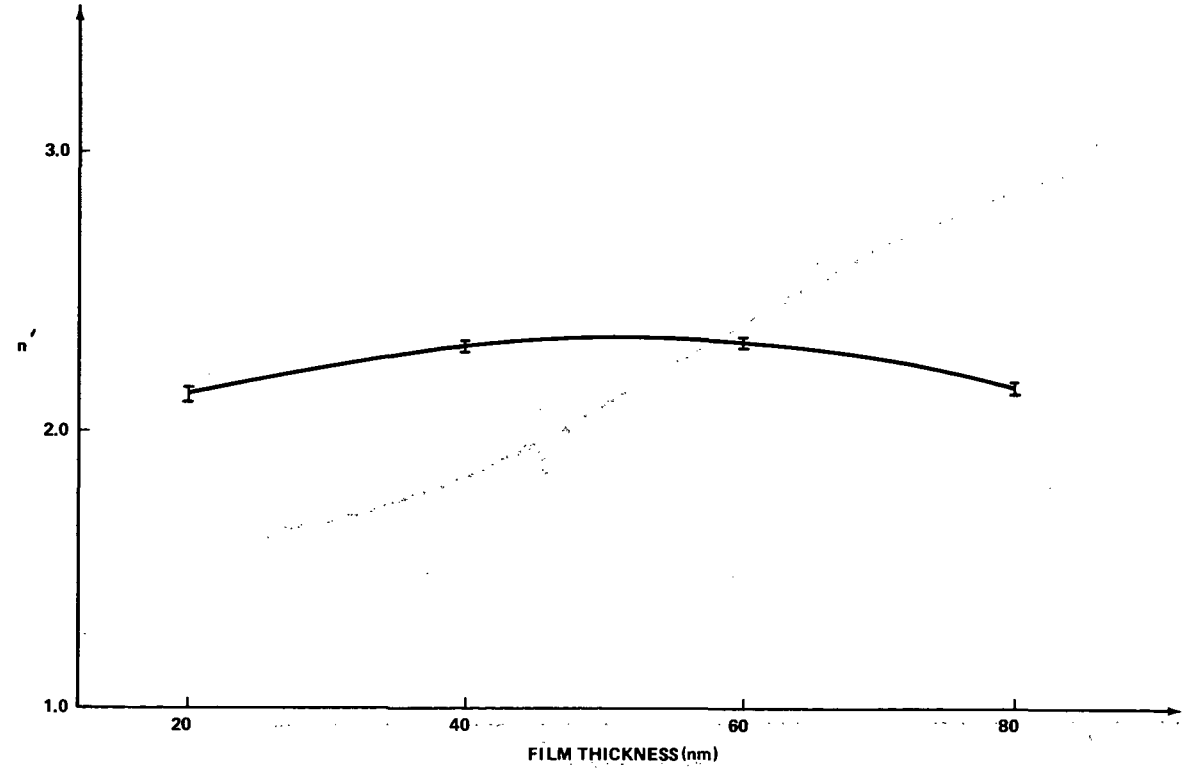

Figure 27. n′ versus film thickness for 45-percent lead films.

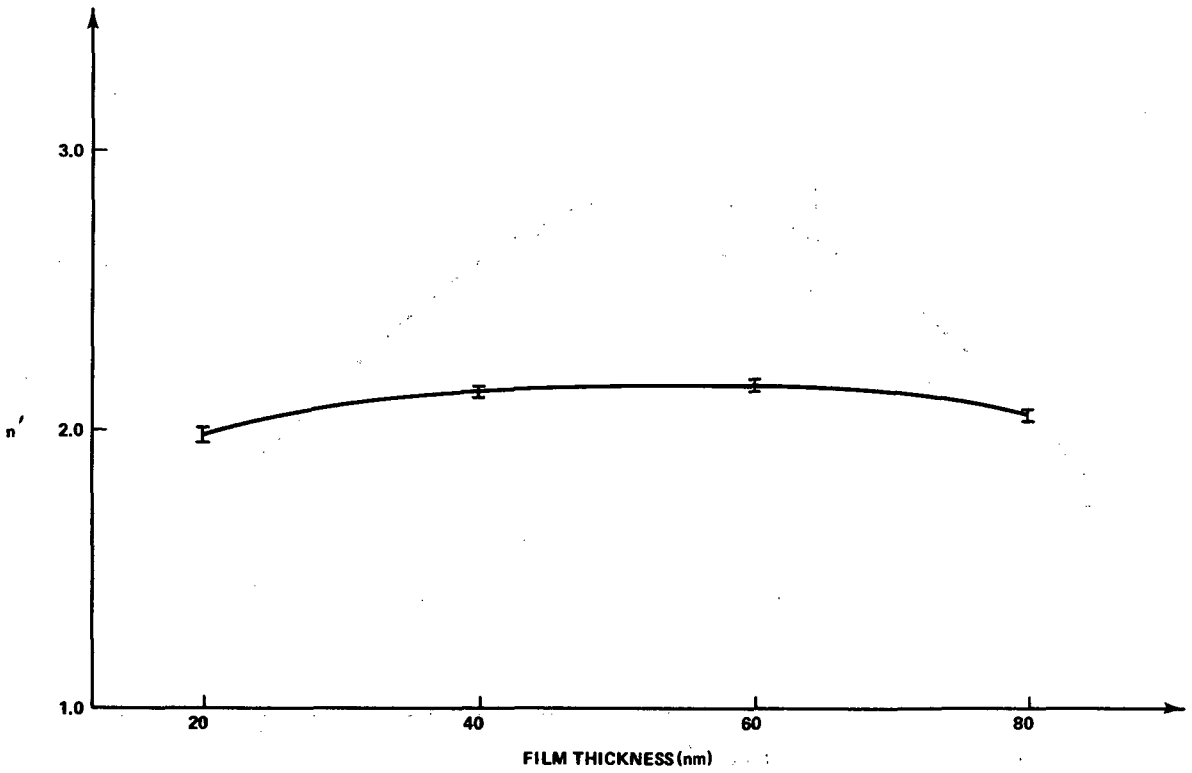

Figure 28. n′ versus film thickness for 30-percent lead films.

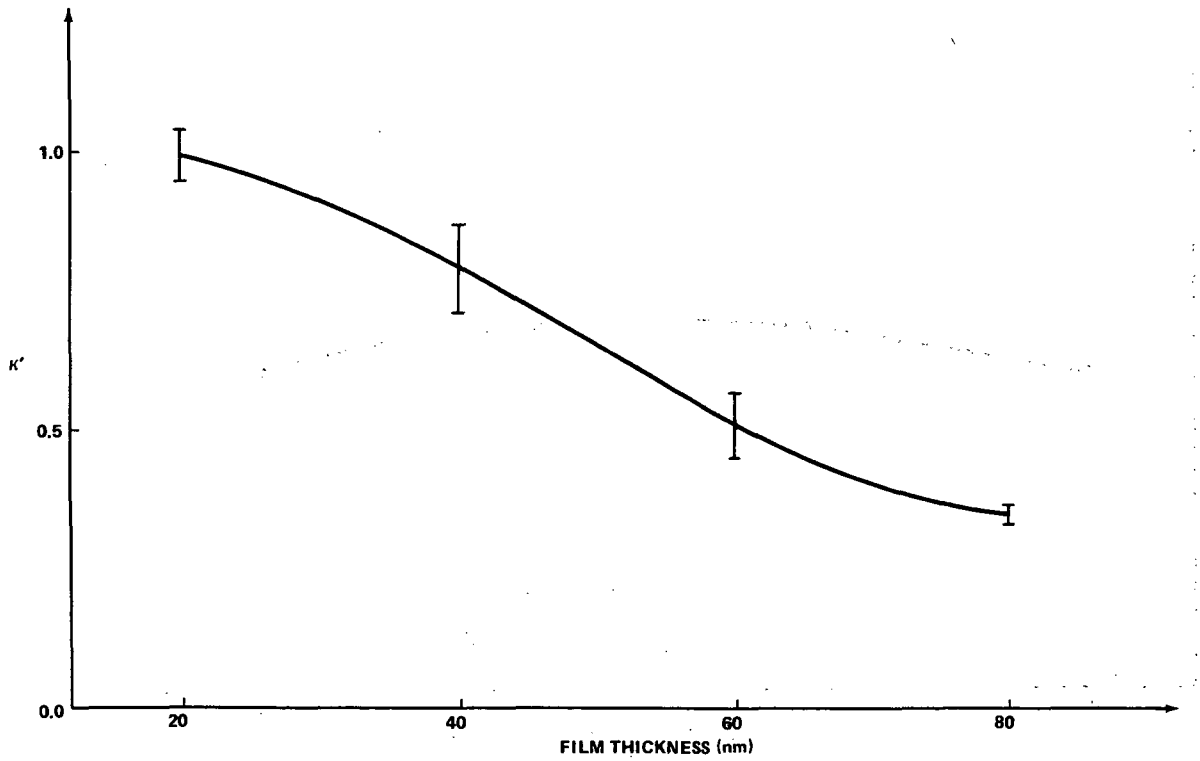

Figure 29. κ' versus film thickness for 58-percent lead films.

TABLE 3. ELLIPSOMETER READINGS

1. Typical Bare Substrate (Kodak B351 Cover Glass)

Angle of Incidence: 55 deg

a. Quarter Wave Plate: +45 deg

Polarizer (deg)	Analyzer (deg)
48.85	178.49
139.38	2.09

b. Quarter Wave Plate: -45 deg

Polarizer (deg)	Analyzer (deg)
47.72	178.09
137.33	2.18

2. 80-nm, 58-Percent Lead Film on Kodak B351 Cover Glass

Angle of Incidence: 55 deg

a. Quarter Wave Plate: +45 deg

Polarizer (deg)	Analyzer (deg)
155.09	21.44
65.02	161.60

b. Quarter Wave Plate: -45 deg

Polarizer (deg)	Analyzer (deg)
30.45	160.28
120.39	20.53

TABLE 3. (Continued)

3. 60-nm, 58-Percent Lead Film on Kodak B351 Cover Glass	
Angle of Incidence: 55 deg	
a. Quarter Wave Plate: +45 deg	
Polarizer (deg)	Analyzer (deg)
148.44	32.45
58.20	152.67
b. Quarter Wave Plate: -45 deg	
Polarizer (deg)	Analyzer (deg)
36.65	151.89
126.78	31.59
4. 40-nm, 48-Percent Lead Film on Kodak B351 Cover Glass	
Angle of Incidence: 55 deg	
a. Quarter Wave Plate: +45 deg	
Polarizer (deg)	Analyzer (deg)
59.36	150.40
149.48	34.81
b. Quarter Wave Plate: -45 deg	
Polarizer (deg)	Analyzer (deg)
125.72	33.82
35.61	149.46

TABLE 3. (Continued)

5. 20-nm, 58-Percent Lead Film on Kodak B351 Cover Glass

Angle of Incidence: 55 deg

a. Quarter Wave Plate: +45 deg

Polarizer (deg)	Analyzer (deg)
151.70	27.39
61.54	156.93

b. Quarter Wave Plate: -45 deg

Polarizer (deg)	Analyzer (deg)
33.22	156.09
123.20	26.51

6. 80-nm, 45-Percent Lead Film on Kodak B351 Cover Glass

Angle of Incidence: 55 deg

a. Quarter Wave Plate: +45 deg

Polarizer (deg)	Analyzer (deg)
51.37	155.28
141.53	17.10

b. Quarter Wave Plate: -45 deg

Polarizer (deg)	Analyzer (deg)
123.65	21.98
33.08	160.25

TABLE 3. (Continued)

7. 60-nm, 45-Percent Lead Film on Kodak B351 Cover Glass

Angle of Incidence: 55 deg

a. Quarter Wave Plate: +45 deg

Polarizer (deg)	Analyzer (deg)
139.32	24.48
49.20	159.23

b. Quarter Wave Plate: -45 deg

Polarizer (deg)	Analyzer (deg)
45.85	158.48
135.60	25.00

8. 40-nm, 45-Percent Lead Film on Kodak B351 Cover Glass

Angle of Incidence: 55 deg

a. Quarter Wave Plate: +45 deg

Polarizer (deg)	Analyzer (deg)
130.70	22.28
39.88	160.66

b. Quarter Wave Plate: -45 deg

Polarizer (deg)	Analyzer (deg)
54.30	160.77
144.64	23.26

TABLE 3. (Continued)

9. 20-nm, 45-Percent Lead Film on Kodak B351 Cover Glass

Angle of Incidence: 55 deg

a. Quarter Wave Plate: +45 deg

Polarizer (deg)	Analyzer (deg)
31.83	167.09
120.20	13.22

b. Quarter Wave Plate: -45 deg

Polarizer (deg)	Analyzer (deg)
152.47	14.57
64.31	167.71

10. 80-nm, 30-Percent Lead Film on Kodak B351 Cover Glass

Angle of Incidence: 55 deg

a. Quarter Wave Plate: +45 deg

Polarizer (deg)	Analyzer (deg)
57.98	163.21
148.14	20.26

b. Quarter Wave Plate: -45 deg

Polarizer (deg)	Analyzer (deg)
126.86	19.73
37.93	162.76

TABLE 3. (Concluded)

11. 60-nm, 30-Percent Lead Film on Kodak B351 Cover Glass	
Angle of Incidence: 55 deg	
Quarter Wave Plate: -45 deg	
Polarizer (deg)	Analyzer (deg)
46.85	161.05
136.64	22.14
12. 40-nm, 30-Percent Lead Film on Kodak B351 Cover Glass	
Angle of Incidence: 55 deg	
Quarter Wave Plate: -45 deg	
Polarizer (deg)	Analyzer (deg)
144.04	20.20
54.55	163.46
13. 20-nm, 30-Percent Lead Film on Kodak B351 Cover Glass	
Angle of Incidence: 55 deg	
Quarter Wave Plate: -45 deg	
Polarizer (deg)	Analyzer (deg)
65.57	169.45
154.94	11.79

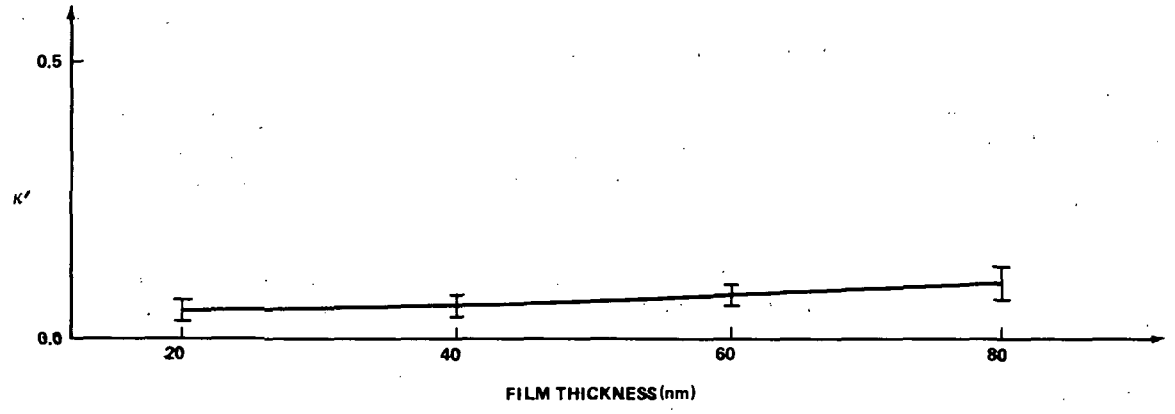

Figure 30. κ' versus film thickness for 45-percent lead films.

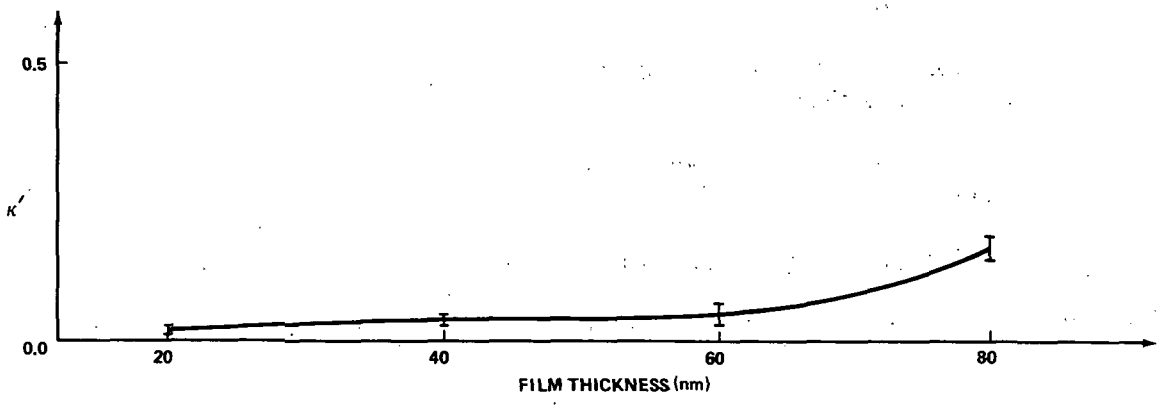

Figure 31. κ' versus film thickness for 30-percent lead films.

VI. REFRACTIVE INDICES FROM THE MAXWELL GARNETT THEORY

The theory of Maxwell Garnett [27] describes the optical properties of a medium containing minute metal particles. Maxwell Garnett assumed that the metallic particles were spherical and small with respect to the wavelength of light. His results agree with the more general theory of Mie [29] for light absorption and scattering by a sphere of arbitrary size in the limit of small spheres far apart.

The Maxwell Garnett theory has received considerable elaboration in the hands of Schopper [30], who assumed nonspherical particles, but it was later shown by Doremus [32, 33] that it was not necessary to assume that the particles were nonspherical or to make other modifications of the theory. Doremus [32, 33] obtained good agreement with experimental data for thin island gold films by use of the Maxwell Garnett theory.

The theory of Maxwell Garnett will be used in this study to derive theoretical values which will then be compared to the experimental values already obtained. The method of Malé [44] will be used to obtain optical constants from the Maxwell Garnett theory.

In the Maxwell Garnett theory [27], the effective complex refractive index for the film is related to the complex refractive index of the metallic particles contained in the film by:

$$\frac{\bar{n}'^2 - \upsilon^2}{\bar{n}'^2 + 2\upsilon^2} = \mu \frac{n^2 - \upsilon^2}{n^2 + 2\upsilon^2} \quad , \tag{18}$$

where

$n' = n'(1 - i\kappa')$ = effective complex refractive index for this film

μ = volume factor = fraction of volume taken up by the metal particles

$n = \hat{n}(1 - i\kappa)$ = complex refractive index for the metal particles

υ = refractive index of the dielectric medium.

Equation (18) is the basic equation of the Maxwell Garnett theory and is derived in the following subsection.

A. The Maxwell Garnett Theory

Maxwell Garnett [27] dealt with the problem of light passing through a dielectric medium that contained many small metallic spheres in a volume with linear dimensions on

the order of wavelength. In this classical treatment, Maxwell Garnett showed that such an assembly is equivalent to a medium with a certain complex refractive index $\bar{n}' = n'(1 - i\kappa')$, and he obtained expressions for $\bar{n}'$ in terms of the optical characteristics of the metallic spheres and the dielectric medium. His expressions will be derived in this section.

We shall first need to derive the Lorentz-Lorenz formula. Its derivation follows the treatment of Born and Wolf [45].

Let us consider the electromagnetic field in a nonconducting medium in a region where the current and charge densities ($\vec{j}$ and ρ, respectively) are zero. Using the rationalized mks system of units, Maxwell's general equations are:

$$\begin{aligned} \nabla \times \bar{H} &= \bar{j} + \partial\bar{D}/\partial t \quad , \\ \nabla \times \bar{E} &= -\partial\bar{B}/\partial t \quad , \\ \nabla \cdot \bar{D} &= \rho \quad , \\ \nabla \cdot \bar{B} &= 0 \quad , \end{aligned} \tag{19}$$

where

$\bar{E}$ = electric vector

$\bar{B}$ = magnetic induction

$\vec{j}$ = current density

$\bar{D}$ = electric displacement

$\bar{H}$ = magnetic vector.

The last three vectors are needed to describe the effect of the field on material objects.

We describe the interaction of field and matter through the following relations:

$$\begin{aligned} \bar{j} &= \sigma\bar{E} \quad , \\ \bar{D} &= \epsilon_0\bar{E} + \bar{P} \quad , \\ \bar{B} &= (\bar{H} + \bar{M})\mu_0 \quad , \end{aligned} \tag{20}$$

where

σ = specific conductivity of medium

$\bar{P}$ = electric polarization of medium

$\bar{M}$ = magnetic polarization of medium

ϵ_0 = permittivity of free space

μ_0 = permeability of free space.

The terms $\bar{P}$ and $\bar{M}$ vanish in a vacuum.

For the medium under consideration, we have

$$\sigma = 0$$

and

$$\bar{j} = \rho = 0 \quad . \tag{21}$$

Substituting equations (20) into equations (19) and imposing the conditions of equation (21) yield

$$\begin{aligned} \nabla \times \bar{B} - \mu_0 \epsilon_0 \frac{\partial \bar{E}}{\partial t} &= \mu_0 (\nabla \times \bar{M} + \partial \bar{P}/\partial t) \quad , \\ &= \tilde{j} \mu_0 \quad , \end{aligned} \tag{22}$$

where

$$\tilde{j} = \partial \bar{P}/\partial t + \nabla \times \bar{M} \quad , \tag{23}$$

$$\nabla \times \bar{E} + \partial \bar{B}/\partial t = 0 \quad , \tag{24}$$

$$\nabla \cdot \bar{E} = - \frac{\nabla \cdot \bar{P}}{\epsilon_0} = \frac{\tilde{\rho}}{\epsilon_0} \quad , \tag{25}$$

where

$$\tilde{\rho} = - \nabla \cdot \bar{P} \quad ,$$

= free charge density,

and

$$\nabla \cdot \bar{B} = 0 \quad . \tag{26}$$

Since the divergence of the curl of any vector is zero, equation (26) is satisfied by

$$\bar{B} = \text{curl } \bar{A} , \tag{27}$$

where $\bar{A}$ is an arbitrary vector function of position and time. Substituting equation (27) into equation (24) and interchanging the curl and time derivation operators yield

$$\nabla \times (\bar{E} + \partial \bar{A}/\partial t) = 0 \quad ; \tag{28}$$

and since $\nabla \times \nabla \phi = 0$, where ϕ is an arbitrary scalar function, equation (28) is satisfied if

$$\bar{E} = - \partial \bar{A}/\partial t - \text{grad } \phi \quad . \tag{29}$$

Now $\bar{A}$ and ϕ, which are called the magnetic vector potential and the electric scalar potential, respectively, must be defined to satisfy the remaining Maxwell equations [equations (22) and (25)].

Substituting equations (27) and (29) into equations (22) and (25) and noting that

$$\nabla \times (\nabla \times \bar{Z}) = \nabla (\nabla \cdot \bar{Z}) - \nabla^2 \bar{Z} \text{ and } (\nabla \cdot \nabla)\bar{Z} = \nabla^2 \bar{Z} ,$$

where $\bar{Z}$ is any vector, we obtain

$$\begin{aligned} &\nabla^2 \bar{A} - \mu_0 \epsilon_0 \partial^2 \bar{A}/\partial t^2 - \nabla(\nabla \cdot \bar{A} + \mu_0 \epsilon_0 \partial \phi/\partial t) = - \mu_0 \tilde{j} \quad ; \\ &\nabla^2 \phi - \mu_0 \epsilon_0 \partial^2 \phi/\partial t^2 + \partial/\partial t(\nabla \cdot \bar{A} + \mu_0 \epsilon_0 \partial \phi/\partial t) = - \tilde{\rho}/\epsilon_0 \quad . \end{aligned} \tag{30}$$

If we now impose the Lorentz condition

$$\nabla \cdot \bar{A} + \mu_0 \epsilon_0 \partial \phi / \partial t = 0 \quad , \tag{31}$$

equations (30) reduce to the inhomogeneous wave equations

$$\begin{aligned} \nabla^2 \bar{A} - \mu_0 \epsilon_0 \partial^2 \bar{A} / \partial t^2 &= - \mu_0 \tilde{j} \quad ; \\ \nabla^2 \phi - \mu_0 \epsilon_0 \partial^2 \phi / \partial t^2 &= - \tilde{\rho} / \epsilon_0 \quad . \end{aligned} \tag{32}$$

We should note that since $\nabla \cdot \nabla \times \bar{Z} = 0$, equation (22) requires that

$$- \nabla \cdot \partial \bar{E} / \partial t = \nabla \cdot \tilde{j} / \epsilon_0 \quad , \tag{33}$$

and by using equation (25), equation (33) becomes

$$\partial \tilde{\rho} / \partial t + \nabla \cdot \tilde{j} = 0 \quad . \tag{34}$$

Equation (34), the equation of continuity, is satisfied by $\tilde{\rho}$ and $\tilde{j}$ and may be seen from the definitions of $\tilde{\rho}$ and $\tilde{j}$ [equations (23) and (25)] by applying the vector identity $\nabla \cdot \nabla \times \bar{Z} = 0$.

The solution of equations (32) may be expressed in terms of the polarization and magnetization in the form

$$\phi(\bar{r}, t) = - \frac{1}{4\pi\epsilon_0} \int (1/R) [\mathrm{div}' \bar{P}] dV' \quad , \tag{35}$$

and

$$\bar{A}(\bar{r}, t) = \frac{\mu_0}{4\pi} \int (1/R) [\mathrm{curl}' \bar{M} + \partial \bar{P} / \partial t] dV' \quad , \tag{36}$$

where the differential operators div′ and curl′ are taken with respect to the coordinates (x′, y′, z′) of the variable point of integration $\bar{r}'$ at which the volume element dV' is situated. The square brackets denote retarded time values; i.e., t is replaced by $t \sqrt{\mu_0 \epsilon_0}$ R inside each bracket. Further,

$$R = | \bar{r} - \bar{r}' | = \{(x - x')^2 + (y - y')^2 + (z - z')^2\}^{1/2} \qquad (37)$$

is the distance from the point $\bar{r}(x, y, z)$ to the volume element dV' at $\bar{r}'(x', y', z')$. The integration is performed over all space.

Let us verify that equation (35) is a solution for the scalar potential in equation (32). Imagine that the point $\bar{r}$ is surrounded by a sphere of radius a, centered on $\bar{r}$. Divide equation (35) into two parts:

$$\phi = \phi_1 + \phi_2 \quad , \qquad (38)$$

where

ϕ = contribution to the integral from the interior of the sphere

ϕ_2 = contribution from the rest of space.

Since $R \neq 0$ for every point $r'(x', y', z')$, there are no singularities in the ϕ_2 contribution, and ϕ_2 may be differentiated under the integral sign.

It should be noted that equation (35) may be written

$$\phi(\bar{r}, t) = \frac{1}{4\pi\epsilon_0} \int \tilde{\rho}(\bar{r}, t - \sqrt{\mu_0\epsilon_0}R)/R \, dV' \quad . \qquad (39)$$

In spherical coordinates when considering solutions representing spherical waves, i.e., solutions of the form $V = V(r, t)$, we have

$$\nabla^2 V = (1/r^2)\partial/\partial r(r^2 \partial V/\partial r) \quad , \qquad (40)$$

and we may write

$$\nabla^2(\tilde{\rho}/r) = (1/r)\partial^2\tilde{\rho}/\partial r^2 \quad , \qquad (41)$$

thus showing that ϕ_2 satisfies the homogeneous wave equation

$$\nabla^2\phi_2 - \mu_0\epsilon_0\partial^2\phi_2/\partial t^2 = 0 \qquad (42)$$

since

$$\nabla^2\phi_2 - \mu_0\epsilon_0\partial^2\phi_2/\partial t^2 = \frac{1}{r}\,\frac{\partial^2\tilde{\rho}(\bar{r}, t - \sqrt{\mu_0\epsilon_0}\,r)}{\partial r^2}$$

$$- \frac{\mu_0\epsilon_0}{r}\,\frac{\partial^2\tilde{\rho}(\bar{r}, t - \sqrt{\mu_0\epsilon_0}\,r)}{\partial t^2} = 0 \quad . \tag{43}$$

Now the case of ϕ_1 will be considered, noting that the integrand has a singularity at $R = 0$. It will be assumed that $\tilde{\rho}$ is a continuous function of $\bar{r}$ and t.

By making the radius of the sphere sufficiently small, we can assure that for all r' inside the sphere

$$\tilde{\rho}(\bar{r}', t - \sqrt{\mu_0\epsilon_0}\,R) - \tilde{\rho}(\bar{r}, t) < \delta \tag{44}$$

for any prescribed δ, where $\delta > 0$. Thus, as the radius $\Rightarrow 0, \nabla^2\phi_1$ approaches more closely the electrostatic potential of a homogeneously charged sphere with charge density $\tilde{\rho}$; i.e.,

$$\nabla^2\phi_1 = - \tilde{\rho}(\bar{r}, t)/\epsilon_0 \tag{45}$$

for sufficiently small a.

Equation (45) is called Poisson's equation; it arises directly from the definition of ϕ and the electrostatic field equations.

Also, as $a \to 0, \ddot{\phi}_1 \Rightarrow 0$, since if a is sufficiently small, we may write

$$\ddot{\phi}_1 = \frac{\ddot{\tilde{\rho}}(\bar{r}, t)}{4\pi\epsilon_0}\int_{R\le a}(1/R)\,dV' = \frac{\ddot{\tilde{\rho}}}{2\pi\epsilon_0}\int_0^{2\pi}\int_0^{\frac{\pi}{2}}\int_0^{a} r\sin\theta\,dr\,d\theta\,d\phi$$

$$= \frac{\ddot{\tilde{\rho}}}{\epsilon_0}\int_0^{a} r\,dr = \frac{a^2}{2\epsilon_0}\,\ddot{\tilde{\rho}} \to 0 \text{ as } a \to 0 \quad . \tag{46}$$

Therefore, it follows that as $a \to 0$,

$$\nabla^2\phi - \mu_0\epsilon_0\ddot{\phi} = \nabla^2(\phi_1 + \phi_2) - \mu_0\epsilon_0(\ddot{\phi}_1 + \ddot{\phi}_2) \to - \tilde{\rho}(\bar{r}, t)/\epsilon_0 \quad . \tag{47}$$

Thus equation (35) is a solution for the scalar potential in the inhomogeneous wave equation (32). In an exactly analogous manner, it can be seen that each Cartesian coordinate of equation (36) is a solution of the corresponding inhomogeneous wave equation, noting that in the process we would substitute for $\tilde{\rho}$ the appropriate component of $\sqrt{\mu_0 \epsilon_0}\, \tilde{j}$. Thus, equation (36) satisfies the inhomogeneous wave equation (32) for the vector potential.

Note that since $\tilde{\rho}$ and $\tilde{j}$ satisfy the continuity equation (34), equations (35) and (36) may be seen to satisfy the Lorentz condition of equation (31).

One may regard $\bar{A}$ and ϕ in equations (34) and (35) as arising from contributions from each volume element in space. Note that $\sqrt{\mu_0 \epsilon_0}\, R$ is the time required for light to travel from $\bar{r}'$ to $\bar{r}$. Equations (34) and (35) are therefore called retarded potentials.

We now use the following identities:

$$\operatorname{div}'[\bar{P}] = [\operatorname{div}' \bar{P}] + \frac{\sqrt{\mu_0 \epsilon_0}}{R} \bar{R} \cdot [\dot{\bar{P}}]$$

and (48)

$$\operatorname{curl}'[\bar{M}] = [\operatorname{curl}' \bar{M}] + \frac{\sqrt{\mu_0 \epsilon_0}}{R} \bar{R} \times [\dot{\bar{M}}] \quad ,$$

where

$$\bar{R} = \bar{r} - \bar{r}' \, ,$$

to write equations (35) and (36) as

$$\phi = -\frac{1}{4\pi\epsilon_0} \int \left\{ \frac{1}{R} \operatorname{div}'[\bar{P}] - \frac{\sqrt{\mu_0 \epsilon_0}}{R^2} \bar{R} \cdot [\dot{\bar{P}}] \right\} dV'$$

(49)

$$\bar{A} = \frac{\mu_0}{4\pi} \int \left\{ \frac{1}{R} \operatorname{curl}'[\bar{M}] - \frac{\sqrt{\mu_0 \epsilon_0}}{R^2} \bar{R} \times [\dot{\bar{M}}] + \frac{[\dot{\bar{P}}]}{R} \right\} dV' \quad .$$

Equation (46) will now be rewritten by modifying the vector identities

$$\operatorname{div}(\bar{P}/R) = (1/R) \operatorname{div} \bar{P} + \bar{P} \cdot \operatorname{grad}(1/R)$$

and (50)

$$\operatorname{curl}(\bar{M}/R) = (1/R) \operatorname{curl} \bar{M} - \bar{M} \times \operatorname{grad}(1/R) \, .$$

According to the divergence theorem,

$$\oint_S \bar{C} \cdot \bar{n}\, dS = \int_V \nabla \cdot \bar{C}\, dV \quad , \tag{51}$$

where $\bar{C}$ is any vector field $\bar{C}(\bar{r})$ defined within a volume V surrounded by the closed surface S.

Equation (51) may be used to write equations (50) as

$$\int (1/R)(\bar{n} \cdot \bar{P})\, dS = \int \{(1/R)\, \mathrm{div}\bar{P} + \bar{P} \cdot \mathrm{grad}(1/R)\}\, dV$$

and (52)

$$\int (1/R)(\bar{n} \times \bar{M})\, dS = \int \{(1/R)\, \mathrm{curl}\, \bar{M} - \bar{M} \times \mathrm{grad}(1/R)\}\, dV,$$

where we have integrated over an arbitrary finite domain, letting $\bar{n}$ be the unit outward normal to the surface.

Assume now that the region of space where $\bar{P}$ and $\bar{M}$ differ from zero (the substance) remains within a finite closed surface. If the integrals in equations (49) are extended over the volume inside this surface, the surface integrals in equations (52) vanish, and equations (49) can be written as

$$\phi = \frac{1}{4\pi\epsilon_0} \int \left\{ [\bar{P}] \cdot \mathrm{grad}'(1/R) + \frac{\sqrt{\mu_0\epsilon_0}}{R^2}\, \bar{R} \cdot [\dot{\bar{P}}] \right\} dV'$$

$$\bar{A} = \frac{\mu_0}{4\pi} \int \left\{ [\bar{M}] \times \mathrm{grad}'(1/R) - \frac{\sqrt{\mu_0\epsilon_0}}{R^2}\, \bar{R} \times [\dot{\bar{M}}] + [\dot{\bar{P}}]/R \right\} dV' \quad . \tag{53}$$

Let us now consider the substance itself. We shall regard matter as being composed of interacting particles embedded in the vacuum. As long as the region over which our averages are taken is large compared with the particle dimensions, the electromagnetic properties of each particle may be simply described by electric and magnetic dipoles.

We shall now consider a small sphere centered on a particular molecule, with a radius that is large compared to the linear dimensions of the molecule. Neglecting molecular structure outside the sphere we assume that the polarization $\bar{P}$ is constant. We shall assume that the molecules inside the sphere cause no resulting field at the central molecule. We therefore have a molecule situated in a spherical region, inside of which there is vacuum and outside of which there is a homogeneously polarized medium.

Now, ϕ must be determined for this case, namely ϕ for the free charges on the spherical discontinuity surface where $\bar{P}$ changes from zero (interior) to a constant exterior

value. Consider the potential $\tilde{\phi}$ of the complementary configuration, that of a homogeneously polarized sphere surrounded by vacuum. The superposition of these two configurations is a homogeneously polarized surface with no boundary. Therefore, the potential caused by the boundary is zero and

$$\phi + \tilde{\phi} = 0 \quad . \tag{54}$$

The term $\tilde{\phi}$ is just the scalar potential stated in equation (53), but with $\overline{P}$ being a constant; thus,

$$\phi = - \tilde{\phi} = - \frac{1}{4\pi\epsilon_0} \overline{P} \cdot \int \text{grad}'(1/R)\, dV' \quad . \tag{55}$$

Now since $R = \{(x - x')^2 + (y - y')^2 + (z - z')^2\}^{1/2}$, grad′ can be replaced in equation (55) by − grad and equation (55) can be written as

$$\phi = - \tilde{\phi} = \frac{1}{4\pi\epsilon_0} \overline{P} \cdot \text{grad} \int (1/R)\, dV' = - \overline{P} \cdot \text{grad}\phi_0 \quad , \tag{56}$$

where

$$\phi_0 = - \frac{1}{4\pi\epsilon_0} \int (1/R)\, dV' \quad . \tag{57}$$

The term ϕ_0 is interpreted as the potential of a uniformly charged sphere of charge density $\rho = -1$. Then by Poisson's equation,

$$\nabla^2\phi_0 = 1/\epsilon_0 \quad . \tag{58}$$

Now, by using equation (56),

$$-\partial\phi/\partial x = \frac{\alpha}{\alpha x} (P_x \partial\phi_0/\partial x + P_y \partial\phi_0/\partial y + P_z \partial\phi_0/\partial z)$$

$$= P_x \partial^2\phi_0/\partial x^2 + P_y \partial^2\phi_0/\partial x\partial y + P_z \partial^2\phi_0/\partial x\partial z \tag{59}$$

with similar expressions for $\partial\phi/\partial y$ and $-\partial\phi/\partial z$. Now, by symmetry it is known that at the center of the sphere

$$\partial^2\phi_0/\partial x\partial y = \partial^2\phi_0/\partial x\partial z = \partial^2\phi_0/\partial y\partial z = 0 \tag{60}$$

and

$$\partial^2\phi_0/\partial x^2 = \partial^2\phi_0/\partial y^2 = \partial^2\phi_0/\partial z^2 = \frac{1}{3\epsilon_0} \quad , \tag{61}$$

where equation (58) has been used in equation (61).

By using equation (59) and similar expressions and noting equations (60) and (61),

$$-\nabla\phi = \hat{i}\, P_x \partial^2\phi_0/\partial x^2 + \hat{j}\, P_y \partial^2\phi_0/\partial y^2 + \hat{k}\, P_z \partial^2\phi_0/\partial z^2 = \frac{\overline{P}}{3\epsilon_0} \quad . \tag{62}$$

The total field inside the sphere, $\overline{E}'$, which is the effective field acting on the central molecule, is obtained by adding the mean field $\overline{E}$ to equation (62), which yields

$$\overline{E}' = \overline{E} + \frac{\overline{P}}{3\epsilon_0} \quad . \tag{63}$$

It will be assumed that for each molecule the electric dipole moment $\overline{p}$ established under the influence of the field is proportional to the effective field $\overline{E}'$; i.e.,

$$\overline{p} = \alpha\overline{E}' \quad , \tag{64}$$

where α represents the mean polarizability. Thus, with N molecules per unit volume the total electric moment $\overline{P}$ per unit volume is

$$\overline{P} = N\overline{p} = N\alpha\overline{E}' \quad . \tag{65}$$

Assuming that $\overline{P}$ is proportional to $\overline{E}$, that is,

$$\overline{P} = \eta\overline{E} \quad , \tag{66}$$

where η = dielectric susceptibility, we have, by eliminating $\overline{E}'$ between equations (63) and (65), that

$$\frac{\eta\overline{E}}{N\alpha} = \overline{E} + \frac{\eta\overline{E}}{3\epsilon_0} \tag{67}$$

or

$$\eta = \frac{N\alpha}{1 - \frac{N\alpha}{3\epsilon_0}} \tag{68}$$

Now using equation (20)

$$\overline{D} = \epsilon_0\overline{E} + \overline{P} = \epsilon\overline{E} = \epsilon_0\overline{E} + \eta\overline{E} \quad , \tag{69}$$

where an isotropic medium has been assumed with

$$\overline{D} = \epsilon\overline{E} \quad , \tag{70}$$

where ϵ = permittivity. Thus, from equation (69)

$$\epsilon = \epsilon_0 + \eta \quad . \tag{71}$$

Substituting equation (68) into equation (71) yields

$$\epsilon = \frac{\epsilon_0 + \frac{2N\alpha}{3}}{1 - \frac{N\alpha}{3\epsilon_0}} \quad , \tag{72}$$

and solving equation (72) for α yields

$$\alpha = \frac{3\epsilon_0}{N}\left(\frac{\epsilon - \epsilon_0}{\epsilon + 2\epsilon_0}\right) = \frac{3\epsilon_0}{N}\left(\frac{n^2 - 1}{n^2 + 2}\right) \quad , \tag{73}$$

where the Maxwell relation $\epsilon/\epsilon_0 = n^2$ for nonmagnetic substances has been used. Equation (73) is called the Lorentz-Lorenz formula.

Equation (73) will be used to obtain the Maxwell Garnett formulation. Note first that by using equations (63), (65), and (73),

$$\overline{E}' = \overline{E} + \frac{n^2 - 1}{n^2 + 2}\overline{E}' \tag{74}$$

Let us now consider light of a wavelength λ falling on a metal ball with radius a and optical constants $\hat{n}$, the real coefficient of refraction, and κ, the absorption index. The total field inside the sphere is then given by equation (74), subject to

$$n = \hat{n}(1 - i\kappa) \quad . \tag{75}$$

If we now consider light falling on a medium consisting of many small metal spheres distributed in a vacuum, many to a wavelength, and integrate over a unit volume, this has the effect of summing the field contributions of the spheres, and equation (74) becomes

$$\overline{E}' = \overline{E} + (4\pi N' a^3/3)\frac{n^2 - 1}{n^2 + 2}\overline{E}' \quad , \tag{76}$$

where

N' = number of metal spheres per unit volume of medium

$4\pi N' a^3/3$ = percent metal per unit volume of medium.

Now $\overline{E}'$ represents the effective field in the new medium. It has been assumed that the medium under consideration extends throughout a space of dimensions which in no direction are smaller than the order of a wavelength.

Thus we have a medium with a revised polarization $\overline{P}'$, which by definition means that

$$\overline{E}' = \overline{E} + \frac{\overline{P}'}{3\epsilon_0} \tag{77}$$

and by comparing equations (76) and (77) we have

$$\overline{P}' = 4\pi N' a^3 \epsilon_0 \left(\frac{n^2 - 1}{n^2 + 2}\right)\overline{E}' \quad . \tag{78}$$

By eliminating $\overline{E}'$ from equations (77) and (78) and assuming that

$$P' = \eta' \overline{E},$$

where η' is the dielectric susceptibility for new medium, we have

$$\frac{\eta' \overline{E}}{4\pi N' a^3 \epsilon_0}\left(\frac{n^2 + 2}{n^2 - 1}\right) = \overline{E} + \frac{\eta' \overline{E}}{3\epsilon_0}$$

or

$$\eta' = \frac{1}{(4\pi N' a^3 \epsilon_0)^{-1}\left(\frac{n^2 + 2}{n^2 - 1}\right) - \frac{1}{3\epsilon_0}} \quad . \tag{79}$$

The dielectric constant ϵ' for the medium is defined as

$$\epsilon' = \epsilon_0 + \eta' \quad . \tag{80}$$

Substitution of equation (79) into equation (80) yields

$$\epsilon' = \epsilon_0 + \frac{4\pi N' a^3 \epsilon_0 \left(\frac{n^2 - 1}{n^2 + 2}\right)}{1 - \frac{4\pi N' a^3}{3}\left(\frac{n^2 - 1}{n^2 + 2}\right)} \quad . \tag{81}$$

Now, if $\mu = 4\pi N' a^3/3$,

$$\epsilon' = \epsilon_0 + \frac{3\mu\epsilon_0 \frac{n^2 - 1}{n^2 + 2}}{1 - \mu \frac{n^2 - 1}{n^2 + 2}} \quad . \tag{82}$$

If the metal spheres are situated in glass of refractive index υ instead of a vacuum, $\epsilon_0 \rightarrow \epsilon''$ in equation (82), where ϵ'' is the dielectric constant of the glass, yielding

$$\frac{\epsilon'}{\epsilon''} = 1 + \frac{3\mu\left(\frac{\epsilon}{\epsilon''} - 1\right)/\left(\frac{\epsilon}{\epsilon''} + 2\right)}{1 - \mu \frac{\left(\frac{\epsilon}{\epsilon''} - 1\right)}{\left(\frac{\epsilon}{\epsilon''} + 2\right)}} \quad , \tag{83}$$

where

$$n^2 = \epsilon/\epsilon_0 \rightarrow \epsilon/\epsilon'' .$$

Equation (83) may be written as

$$\frac{\epsilon'}{\epsilon_0} = \frac{\epsilon''}{\epsilon_0} + \frac{3\mu \frac{\epsilon''}{\epsilon_0}\left(\frac{\frac{\epsilon}{\epsilon_0} - \frac{\epsilon''}{\epsilon_0}}{\frac{\epsilon}{\epsilon_0} + 2\frac{\epsilon''}{\epsilon_0}}\right)}{1 - \mu\left(\frac{\frac{\epsilon}{\epsilon_0} - \frac{\epsilon''}{\epsilon_0}}{\frac{\epsilon}{\epsilon_0} + 2\frac{\epsilon''}{\epsilon_0}}\right)} . \tag{84}$$

Now by noting that

$$\epsilon''/\epsilon_0 = \upsilon^2 ,$$

and defining

$$(\bar{n}')^2 = [n'(1 - i\kappa')]^2 = \epsilon'/\epsilon_0 ,$$

we have

$$(\bar{n}')^2 = \upsilon^2 + \frac{3\mu\upsilon^2 \frac{n^2 - \upsilon^2}{n^2 + 2\upsilon^2}}{1 - \mu\frac{n^2 - \upsilon^2}{n^2 + 2\upsilon^2}} \tag{85}$$

where $\bar{n}'$ is the effective refractive index of the new medium. Note that equation (85) may be rewritten as

$$\frac{\bar{n}'^2 - \upsilon^2}{\bar{n}'^2 + 2\upsilon^2} = \mu\frac{n^2 - \upsilon^2}{n^2 + 2\upsilon^2} , \tag{86}$$

since from equation (86)

$$\bar{n}'^2 = \frac{v^2 + 2v^2\mu\dfrac{n^2 - v^2}{n^2 + 2v^2}}{1 - \mu\dfrac{n^2 - v^2}{n^2 + 2v^2}}$$

$$= v^2 + \frac{3\mu v^2\dfrac{n^2 - v^2}{n^2 + 2v^2}}{1 - \mu\dfrac{n^2 - v^2}{n^2 + 2v^2}} \quad .$$

Equation (86) is the Maxwell Garnett relation which describes the effective refractive index, $\bar{n}'$, of a dielectric embedded with many metallic spheres per wavelength of light in terms of the optical constants of the dielectric and the individual spheres. It should be noted that $\bar{n}'$ depends on μ, the relative volume of metal, rather than on the individual sphere radii. Thus, the spheres may be of quite various radii, provided that they are present in sufficient numbers.

B. Results Using the Maxwell Garnett Theory

Now, following the method of Malé [44], we proceed as follows. Rearranging equation (86) yields

$$\bar{n}'^2\left[1 - \mu\frac{(n^2 - v^2)}{(n^2 + 2v^2)}\right] - v^2 = 2\mu v^2\frac{(n^2 - v^2)}{(n^2 + 2v^2)} \tag{87}$$

or

$$\bar{n}'^2(1 - \mu r) - v^2 = 2v^2\mu r \quad , \tag{88}$$

where, in polar form

$$r = \frac{n^2 - v^2}{n^2 + 2v^2} = Ae^{i\alpha} \quad . \tag{89}$$

Solving for $\bar{n}'^2$ in equation (87), we have

$$\bar{n}'^2 = \upsilon^2 \frac{(2\mu r + 1)}{1 - \mu r} = -2\upsilon^2 \frac{\left(\mu + \frac{1}{2r}\right)}{\left(\mu - \frac{1}{r}\right)} \tag{90}$$

or

$$\bar{n}' = \upsilon \left[-2 \frac{\left(\mu + \frac{1}{2r}\right)}{\left(\mu - \frac{1}{r}\right)} \right]^{1/2} = \upsilon B e^{i\beta} = n' - i n' \kappa' \quad , \tag{91}$$

where the definition of $\bar{n}'$ has been noted and rewritten in polar form.

Now let us define the following points in the complex plane:

$$N = -1/2r \quad D = 1/r \quad Q = \mu \quad . \tag{92}$$

The graphical solution for $\bar{n}' = \upsilon B e^{i\beta}$ can now be written since

$$B = (2QN/QD)^{1/2} \quad \text{and} \quad \beta = \frac{\widehat{DQN} + \pi}{2} \quad . \tag{93}$$

Further, since $\bar{n}' = n' - i n' \kappa'$,

$$n' = -\upsilon B \cos\beta \quad \text{and} \quad n'\kappa' = \upsilon B \sin\beta \quad . \tag{94}$$

Let us now evaluate r for our case, letting $\upsilon = 1.5$, $\hat{n} = 2.42$, and $\hat{n}\kappa = 4.45$ [46], where we have used the definitions in equation (75). From equation (89), it is found that

$$r = \frac{n^2 - \upsilon^2}{n^2 + 2\upsilon^2} \quad .$$

Therefore, by definition of n we may write

$$r = \frac{(\hat{n} - i\kappa\hat{n})^2 - \upsilon^2}{(\hat{n} - i\kappa\hat{n})^2 + 2\upsilon^2} = \frac{(\hat{n}^2 - \kappa^2\hat{n}^2 - \upsilon^2) - 2i\kappa\hat{n}^2}{(\hat{n}^2 - \kappa^2\hat{n}^2 + 2\upsilon^2) - 2i\kappa\hat{n}^2} \quad . \tag{95}$$

Now substituting numerically into equation (95),

$$r = \frac{-16.2 - 21.6\,i}{-9.45 - 21.6\,i} = \frac{(-16.2 - 21.6i)(-9.45 + 21.6i)}{(-9.45 - 21.6i)(-9.45 + 21.6i)}$$

$$= 1.12 - 0.262\,i = Ae^{i\alpha} \tag{96}$$

$$A = \{(1.12)^2 + (0.262)^2\}^{1/2} \quad \text{and} \quad \alpha = \tan^{-1}(-0.262/1.15)$$

$$= 1.15 \quad . \tag{97}$$

Now, by using equation (92),

$$N = -1/2r = -0.434\, e^{-i\alpha} \quad ,$$

$$D = 1/r = 0.87\, e^{-i\alpha} \quad , \tag{98}$$

$Q = \mu = 0.15$, 0.25, and 0.45 for our three cases, as estimated from the electron micrographs.

By using the plot in Figure 32 and proceeding in accordance with the method of Malé, the following cases are obtained:

Case I. 30 Percent Lead Films

$Q = \mu = 0.15$.

Now, from Figure 32, it is found that

$$\overline{QN} = 5.78 \quad \overline{QD} = 7.26 \quad \widehat{DQN} = 174.2^\circ \quad .$$

Therefore, from equation (93),

$$B = (2\overline{QN}/\overline{QD})^{1/2} = 1.26 \qquad \beta = \frac{\widehat{DQN} + \pi}{2} = 177^\circ\, 6' \quad .$$

Now by using these results in equation (94),

$$n' = -vB\cos\beta = 1.89 \qquad n'\kappa' = vB\sin\beta = 0.096 \quad .$$

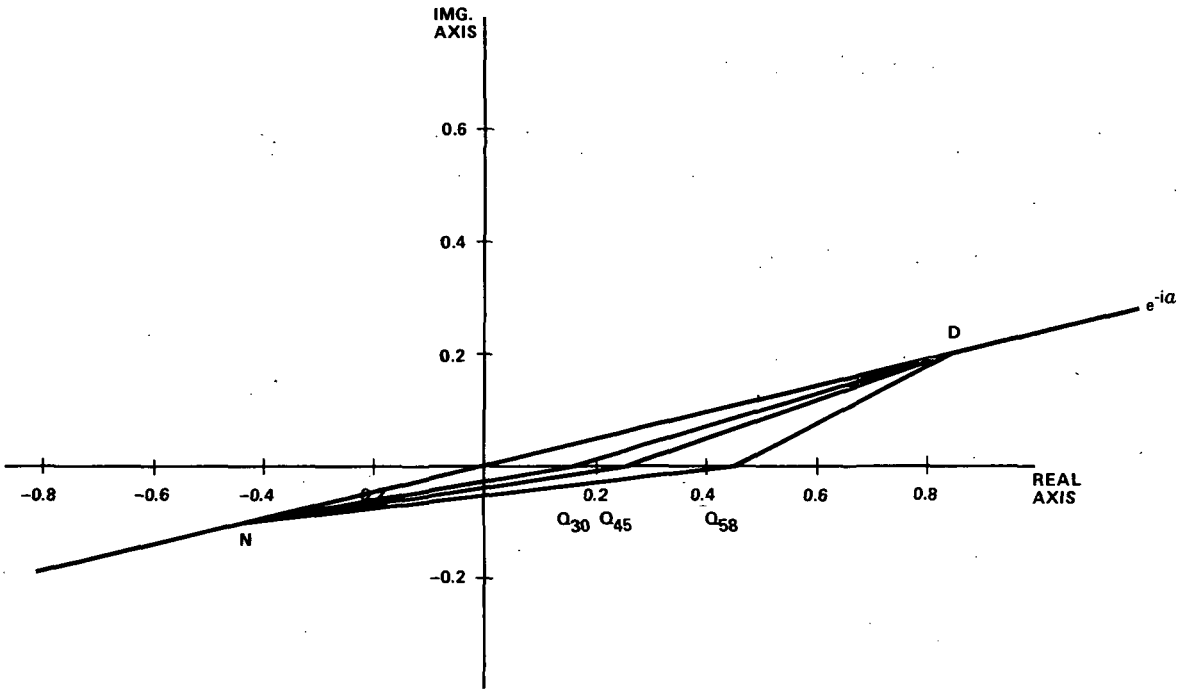

Figure 32. Malé's method for solution of the Maxwell Garnett equations.

Similar procedure for the other cases yields the following:

Case II. 45 Percent Lead Films

$Q = \mu = 0.25$,

$n' = 2.18$,

and

$n'\kappa' = 0.19$.

Case III. 58 Percent Lead Films

$Q = \mu = 0.45$,

$n' = 2.91$,

and

$n'\kappa' = 0.49$.

The above results are listed in Table 4, along with the extreme values obtained experimentally.

TABLE 4. THEORETICAL AND EXTREME EXPERIMENTAL REFRACTIVE INDICES

Lead Content of Film (Percent by Volume)	n′(Real Part of Index)		n′κ′(Imaginary Part of Index)	
	Theoretical	Experimental	Theoretical	Experimental
30 ± 3	1.89	1.95 to 2.18	0.10	0.03 to 0.41
45 ± 5	2.18	2.10 to 2.32	0.19	0.06 to 0.30
58 ± 6	2.91	1.73 to 2.83	0.49	0.57 to 2.94

Note: $n'_{complex} = n' - in'\kappa'$

VII. CONCLUSIONS

As a result of the physical and optical examinations of the thin lead dielectric cermet films studied in this report, one may conclude the following.

A. Internal Film Structure

Direct transmission electron miscroscopic examination of lead dielectric cermet films indicates that increases in the lead content of the films from 30 to 45 to 58 percent vary the film structure drastically. In the 30 percent lead films the structure consists of 10- to 30-nm-diameter lead spheres embedded in a fairly homogeneous dielectric medium. As the lead content is increased to 45 percent, the spheres grow to well-defined oblate spheroids which are 400 to 800 nm in diameter. Further addition of lead (to 58 percent) results in many additional spheroids in the 400- to 800-nm-size range which join together to form a connecting network as the film thickens.

B. Film Surface Structure

Replicas of film surfaces reveal mounds and pits that are roughly the size of the underlying metal particles. These features can be interpreted as manifestations of the film's metal structure, which juts out of the film plane in some areas and depresses the film

surface in other areas. Thus, there appears to be a gratifying correspondence between the replica and direct electron microscopy studies.

C. Film Refractive Indices

The refractive indices of lead-dielectric cermet films as measured by ellipsometry agree acceptably with the theoretical values predicted by the Maxwell Garnett theory for those films whose structure fits that of the Maxwell Garnett model; i.e., for those low- and intermediate-lead content films whose structure consists of tiny metal balls embedded in a dielectric. As expected, the experimental values for the highly metallic network structure films diverge from the Maxwell Garnett values. This is especially noticeable for the imaginary part of the refractive index. Thus the Maxwell Garnett theory may be applied to thin cermet films of suitable structure.

D. Effects of Film Thickness Variations

Electron micrographs reveal no outstanding thickness trend in the range observed except for the case of the 58-percent lead films, which seem to show an increase in the definition of their metallic structures as film thickness increased. All films examined were continuous at 20 nm.

The ellipsometer measurements reveal a definite thickness trend for the real part of the refractive index. This may be seen clearly in Figures 26 through 28. No existing theories have predicted such a trend.

APPENDIX A. USE OF THE ELLIPSOMETER

1. Theory of the Ellipsometer

Ellipsometry is the measurement of the change in the state of polarization of light on reflection from the surface of a dielectric or metal covered with a film. The ellipsometer in its modern form was developed by Rothen [47] in 1944. Motivated by the need of measuring thin film thicknesses quickly and accurately, he designed an apparatus, which he called an ellipsometer, based upon the fundamental principles established by Drude [37] concerning the change in the state of polarization of light upon reflection from a bare surface or a surface with a film on it. Rothen's apparatus followed the general form shown in Figure A-1. With the advent of modern electronic computers the application of the somewhat cumbersome exact Drude equations became routine, and ellipsometry became a powerful technique for measuring the thicknesses and refractive indices of films. An excellent review of the historical development of ellipsometry has been written by Rothen [35].

In understanding the use of the ellipsometer in analyzing polarized light, it is convenient to utilize the Poincaré sphere representation of polarized light. This representation will now be developed by use of Stokes parameters and will, in general, follow the presentation of McCrackin, et al. [48] in relating the Poincaré sphere representation of ellipsometry.

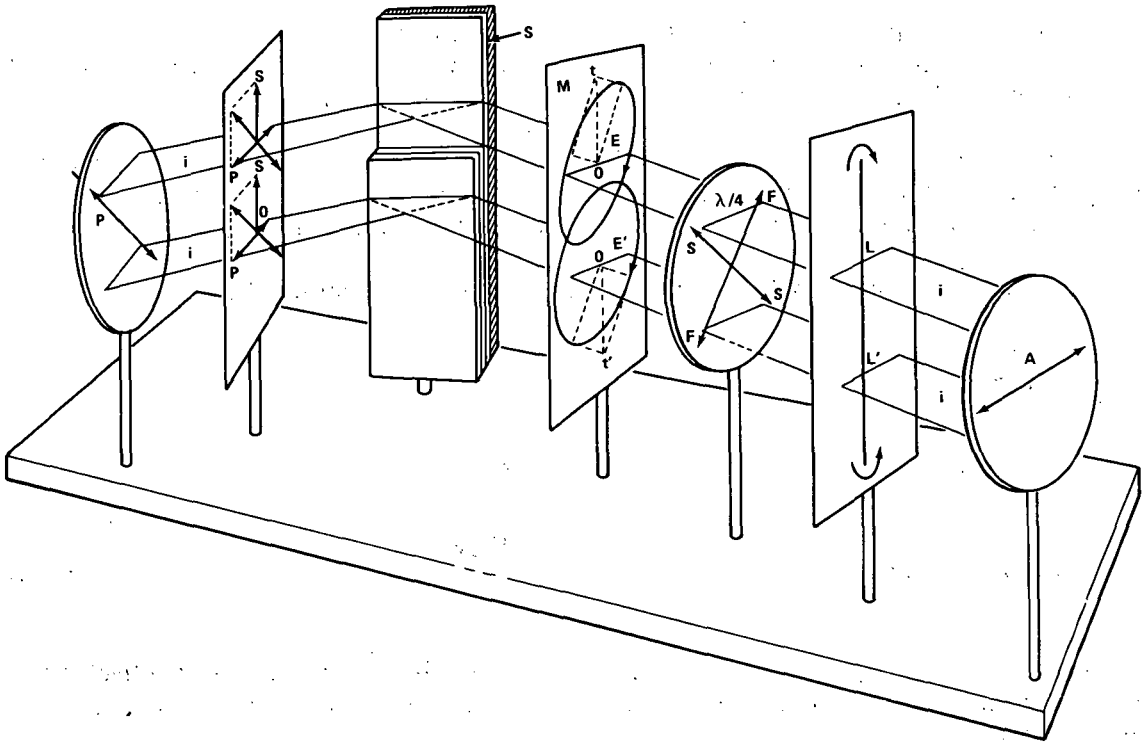

Figure A-1. Schematic representation of the halfshade ellipsometer [46].

Consider a plane monochromatic wave traveling along the axis of a coordinate system. For elliptically polarized light, the electric vector of the wave is

$$E_x = a_1 \cos(\tau + \delta_1) \quad ,$$

$$E_y = a_2 \cos(\tau + \delta_2) \quad ,$$

and (A-1)

$$E_z = 0 \quad ,$$

where

$\tau = \omega(t - z/v)$

ω = angular frequency

v = linear velocity of the light

a_i = component amplitude

The polarization can be described by the phase difference, $\delta = \delta_2 - \delta_1$, and the amplitudes, a_1 and a_2, of the components. In a stationary plane whose normal is parallel to the z axis, the locus of the electric vector's end is the ellipse shown in Figure A-2.

The ellipse may also be described in relation to coordinates x′ and y′ along the axis of the ellipse. Thus, the semiaxes, a and b, of the ellipse and the inclination ϕ of these coordinates also describe the polarization of the light.

Now, the auxiliary angles α and χ are introduced and defined by

$$\tan \alpha = a_2/a_1 \qquad \text{(A-2)}$$

and

$$\tan \chi = \pm b/a \quad . \qquad \text{(A-3)}$$

The angles ϕ and χ are called the azimuth and ellipticity of the light, respectively; and representation may be made either in terms of ϕ, χ and $a_1 + a_2$; a_1, a_2, and δ; or α, δ, and $a_1 + a_2$.

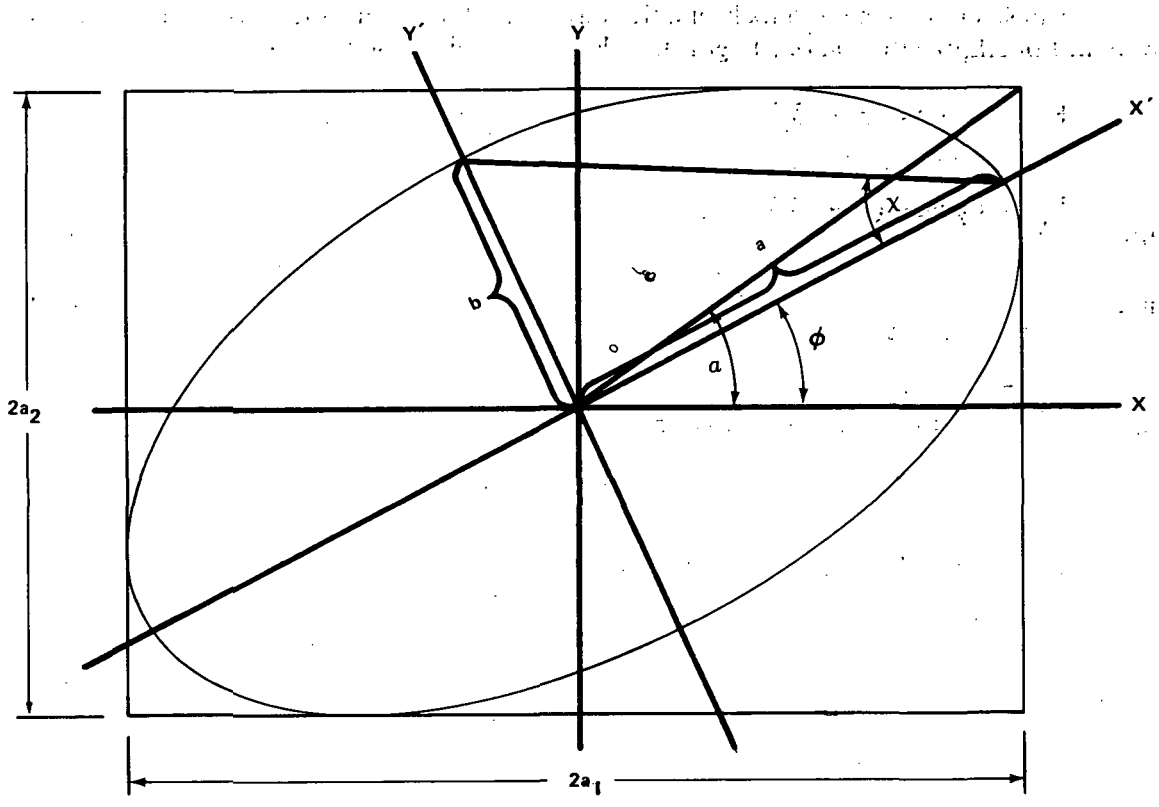

Figure A-2. Locus of the electric vector for elliptically polarized light in a plane normal to the direction of propagation.

Still another representation of the state of polarization, and one which leads quite naturally to the Poincaré sphere, is by parameters which all have the same physical dimensions. These are called Stokes parameters and can be defined as

$$S_0 = a_1^2 + a_2^2 \quad ,$$

$$S_1 = a_1^2 - a_2^2 \quad ,$$

$$S_2 = 2a_1a_2 \cos\delta \quad ,$$

and (A-4)

$$S_3 = 2a_1a_2 \sin\delta \quad .$$

Note that $S_0^2 = S_1^2 + S_2^2 + S_3^2$, so that the Stokes parameters are not all independent.

The Stokes parameters are also given by

$$S_1 = S_0 \cos 2\chi \cos 2\phi \quad ,$$

$$S_2 = S_0 \cos 2\chi \sin 2\phi \quad ,$$

and (A-5)

$$S_3 = S_0 \sin 2\chi \quad .$$

The proof of equations (A-5) follows [45].

Returning to equations (A-1), they are rewritten as follows:

$$E_x/a_1 = \cos\tau \cos\delta_1 - \sin\tau \sin\delta_1$$

and (A-6)

$$E_y/a_2 = \cos\tau \cos\delta_2 - \sin\tau \sin\delta_2 \quad .$$

Hence,

$$(E_x/a_1) \sin\delta_2 - (E_y/a_2) \sin\delta_1 = \cos\tau \sin(\delta_2 - \delta_1)$$

and (A-7)

$$(E_x/a_1) \cos\delta_2 - (E_y/a_2) \cos\delta_1 = \sin\tau \sin(\delta_2 - \delta_1) \quad .$$

Squaring and adding yields

$$(E_x/a_1)^2 + (E_y/a_2)^2 - 2\frac{E_x E_y}{a_1 a_2} \cos\delta = \sin^2\delta \quad , \qquad \text{(A-8)}$$

where

$$\delta = \delta_2 - \delta_1 \quad .$$

Equation (A-8) is of the form

$$Ax^2 + Bxy + Cy^2 + Dx + Ey + F = 0 \tag{A-9}$$

where A, B, C, D, E, and F are constants, which is the general equation of second degree. If $B^2 - 4AC < 0$, then equation (A-9) represents an ellipse [49].

Comparison of equation (A-9) with equation (A-8) yields

$$B^2 - 4AC = (4\cos^2\delta)/(a_1^2a_2^2) - 4/(a_1^2a_2^2) = 4(\cos^2\delta - 1)/(a_1^2a_2^2)$$

$$= -4\sin^2\delta/(a_1^2a_2^2) < 0 \quad . \tag{A-10}$$

Therefore, equation (A-8) represents an ellipse, and equations (A-1) represent elliptically polarized light. The ellipse is inscribed into a rectangle whose sides are parallel to the coordinate axes and whose lengths are $2a_1$ and $2a_2$. The ellipse touches the sides at $(\pm a_1, \pm a_2 \cos\delta)$ and $(\pm a_1 \cos\delta, \pm a_2)$ and has its axis along the coordinates x' and y' (Fig. 5). Then, using the standard rotation matrix we have

$$E_{x'} = E_x \cos\phi + E_y \sin\phi$$

and (A-11)

$$E_{y'} = -E_x \sin\phi + E_y \cos\phi \quad .$$

Note that 2a and 2b ($a \leq b$, Fig. A-2) are the lengths of the axes of the ellipse, therefore

$$E_{x'} = a\cos(\tau + \delta_0)$$

and (A-12)

$$E_{y'} = \pm b\sin(\tau + \delta_0) \quad ,$$

where the two signs describe the two possible senses in which the end point of the electrical vector may describe the ellipse.

Comparison of equations (A-11) and (A-12) and use of equations (A-6) gives

$$a(\cos\tau\cos\delta_0 - \sin\tau\sin\delta_0) = a_1(\cos\tau\cos\delta_1 - \sin\tau\sin\delta_1)\cos\phi + a_2(\cos\tau\cos\delta_2 - \sin\tau\sin\delta_2)\sin\phi$$

and

$$\pm b(\sin\tau\cos\delta_0 + \cos\tau\sin\delta_0) = -a_1(\cos\tau\cos\delta_1 - \sin\tau\sin\delta_1)\sin\phi + a_2(\cos\tau\cos\delta_2 - \sin\tau\sin\delta_2)\cos\phi \quad . \tag{A-13}$$

Now, equating the coefficients of $\cos\tau$ and $\sin\tau$ yields

$$a\cos\delta_0 = a_1\cos\delta_1\cos\phi + a_2\cos\delta_2\sin\phi \quad , \tag{A-14}$$

$$a\sin\delta_0 = a_1\sin\delta_1\cos\phi + a_2\sin\delta_2\sin\phi \quad , \tag{A-15}$$

$$\pm b\cos\delta_0 = a_1\sin\delta_1\sin\phi - a_2\sin\delta_2\cos\phi \quad , \tag{A-16}$$

and

$$\pm b\sin\delta_0 = -a_1\cos\delta_1\sin\phi + a_2\cos\delta_2\cos\phi \quad . \tag{A-17}$$

Squaring and adding equations (A-14) and (A-15) and noting that $\delta = \delta_2 - \delta_1$ yields

$$a^2 = a_1^2\cos^2\phi + a_2^2\sin^2\phi + 2a_1a_2\cos\phi\sin\phi\cos\delta \quad . \tag{A-18}$$

Similarly, from equations (A-16) and (A-17),

$$b^2 = a_1^2\sin^2\phi + a_2^2\cos^2\phi - 2a_1a_2\cos\phi\sin\phi\cos\delta \quad . \tag{A-19}$$

Hence,

$$a^2 + b^2 = a_1^2 + a_2^2 \quad . \tag{A-20}$$

Then multiplying equation (A-14) by equation (A-16) and equation (A-15) by equation (A-17) and adding, one obtains

$$\pm ab = a_1 a_2(\cos \delta_1 \sin \delta_2 - \cos \delta_2 \sin \delta_1) = a_1 a_2 \sin \delta \quad . \tag{A-21}$$

Further, dividing equation (A-16) by equation (A-14) and equation (A-17) by equation (A-15) yields

$$\pm b/a = \frac{a_1 \sin \delta_1 \sin \phi - a_2 \sin \delta_2 \cos \phi}{a_1 \cos \delta_1 \cos \phi + a_2 \cos \delta_2 \sin \phi}$$

$$= \frac{-a_1 \cos \delta_1 \sin \phi + a_2 \cos \delta_2 \cos \phi}{a_1 \sin \delta_1 \cos \phi + a_2 \sin \delta_2 \sin \phi} \quad . \tag{A-22}$$

Rewriting equation (A-22) yields

$$\cos \phi \sin \phi \, (a_1^2 - a_2^2) = a_1 a_2(\cos \delta_1 \cos \delta_2 + \sin \delta_1 \sin \delta_2)$$

$$\times \quad (\cos^2 \phi - \sin^2 \phi)$$

or

$$(a_1^2 - a_2^2) \sin 2\phi = 2a_1 a_2 \cos \delta \cos 2\phi \quad . \tag{A-23}$$

Now, using α as defined in equation (A-2), equation (A-23) can be written as

$$\tan 2\phi = \frac{2a_1 a_2 \cos \delta}{a_1^2 - a_2^2} = \frac{2 \tan \alpha}{1 - \tan^2 \alpha} \cos \delta$$

or

$$\tan (2\phi) = (\tan 2\alpha) \cos \delta \quad . \tag{A-24}$$

Now, from equations (A-20) and (A-21), we have

$$\pm \frac{2ab}{a^2 + b^2} = \frac{2a_1 a_2 \sin \delta}{a_1^2 + a_2^2} = \frac{2 \tan \alpha}{1 + \tan^2 \alpha} \sin \delta$$

$$= 2 \sin \alpha \cos \alpha \sin \delta = (\sin 2\alpha) \sin \delta \quad , \tag{A-25}$$

and using χ as defined in equation (A-3), equation (A-25) becomes

$$\sin 2\chi = (\sin 2\alpha) \sin \delta \quad . \tag{A-26}$$

Now, from equations (A-4), (A-25), and (A-26), we have

$$S_3 = 2a_1a_2 \sin \delta = (a_1^2 + a_2^2) \sin 2\chi = S_0 \sin 2\chi \quad . \tag{A-27}$$

Further, it is noted from equations (A-4) and (A-24) that

$$S_2 = 2a_1a_2 \cos \delta = (a_1^2 - a_2^2) \tan 2\phi = S_1 \tan 2\phi \quad . \tag{A-28}$$

Now, noting that $S_0^2 = S_1^2 + S_2^2 + S_3^2$ and using equations (A-27) and (A-28), we have

$$S_0^2 = S_1^2 + S_1^2 \tan^2 2\phi + S_0^2 \sin^2 2\chi$$

which means that

$$S_1^2 = \frac{S_0^2(1 - \sin^2 2\chi)}{1 + \tan^2 2\phi} = S_0^2 \cos^2 2\chi \cos^2 2\phi$$

or

$$S_1 = S_0 \cos 2\chi \cos 2\phi \quad . \tag{A-29}$$

Substituting equation (A-29) into equation (A-28) yields

$$S_2 = S_0 \cos 2\chi \sin 2\phi \quad . \tag{A-30}$$

However, equations (A-27), (A-29), and (A-30) are just equations (A-5), which we desired to derive. We can now proceed with the Poincaré sphere representation of polarized light.

It should be noted that equations (A-5) are the transformation equations required to go from linear to spherical coordinates. Thus, the state of polarization may be described by a point on a sphere of radius S_0 by the spherical coordinates S_0, 2ϕ, and 2χ. Alternately, the Stokes parameters may be used as Cartesian coordinates to represent the polarization. This is shown in Figure A-3.

With the assumption that the law of conservation of energy holds and that the light intensity is unity, the point can be projected onto a sphere of unit radius. The coordinates are then given by

$$S_0 = 1,$$

$$S_1 = \frac{1 - \tan^2 \alpha}{1 + \tan^2 \alpha} = \cos 2\chi \cos 2\phi \quad ,$$

and (A-31)

$$S_2 = \frac{2 \tan \alpha \cos \delta}{1 + \tan^2 \alpha} = \cos 2\chi \sin 2\phi \quad ,$$

where $S_0 = a_1^2 + a_2^2 = 1$ and equations (A-2), (A-4), and (A-5) have been used.

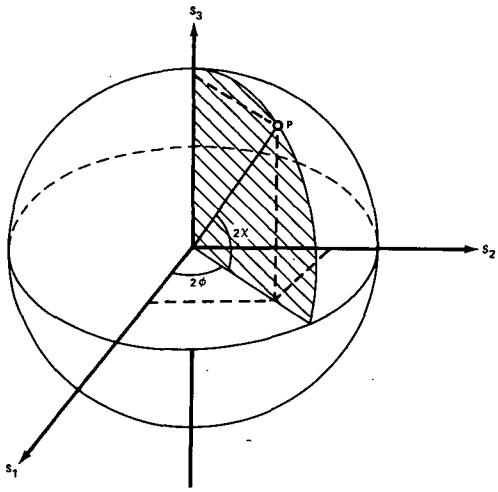

Figure A-3. Representation of polarized light on the Poincaré sphere.

Thus, light of a given polarization is represented by a point on the sphere with polar angles 2ϕ and 2χ, which represent, respectively, twice the azimuth and twice the ellipticity of the light. Consider an example. For plane polarized light, the ellipticity χ is zero and $S_3 = 0$. Thus, plane polarized light is represented by points on the equator of the Poincaré sphere. Again, consider circularly polarized light, with an ellipticity of 45 deg. Here, $S_1 = S_2 = 0$ and $2\chi = \pm\pi/2$, and circularly polarized light is represented by the poles of the sphere.

This representation may be used to define elliptically polarized light with respect to any physical axis, say x'' and y'' at an angle ϕ'' with the xy axes. The ellipticity χ is independent of the choice of axes, but the azimuth ϕ is changed by ϕ'' in going from the unprimed to the double prime system. Thus the S_1 and S_2 axes must be rotated about the S_3 axis by $2\phi''$.

The Poincaré sphere is convenient for representing the effects of double refracting plates and reflection on the state of polarization of a light beam. For example, let the polarized light in Figure A-2 pass through a double refracting plate of relative phase retardation θ. Choose the x and y axes in Figure A-2 along the fast and slow axes of the plate. Since the azimuth of the fast axis is zero, consideration of equations (A-31) shows it to be represented by the positive S_1 axis. The only effect of the plate is to change the relative phase of the components by θ; thus, a_1 and a_2 remain constant, and by equations (A-2) and (A-31), α and S_1 also remain constant. Thus, upon passing through the plate, the point representing the polarization will remain on the intersection of the sphere and the plane $S_1 = \text{constant}$. Consideration of equations (A-31) shows that this

intersection, as illustrated in Figure A-4, is a circle of radius $(2 \tan \alpha)/(1 + \tan^2 \alpha)$. The incident light is represented by the point P, and the transmitted light is represented by the point L. Therefore, the effect of the doubly refracting plate is to turn points on the sphere about the S_1 axis by an angle θ. If the plate had been oriented with its fast axis at a ϕ' azimuth with respect to the xy axes, the rotation by θ would have been about the line between the center of the sphere and the point $2\phi'$ on the equator.

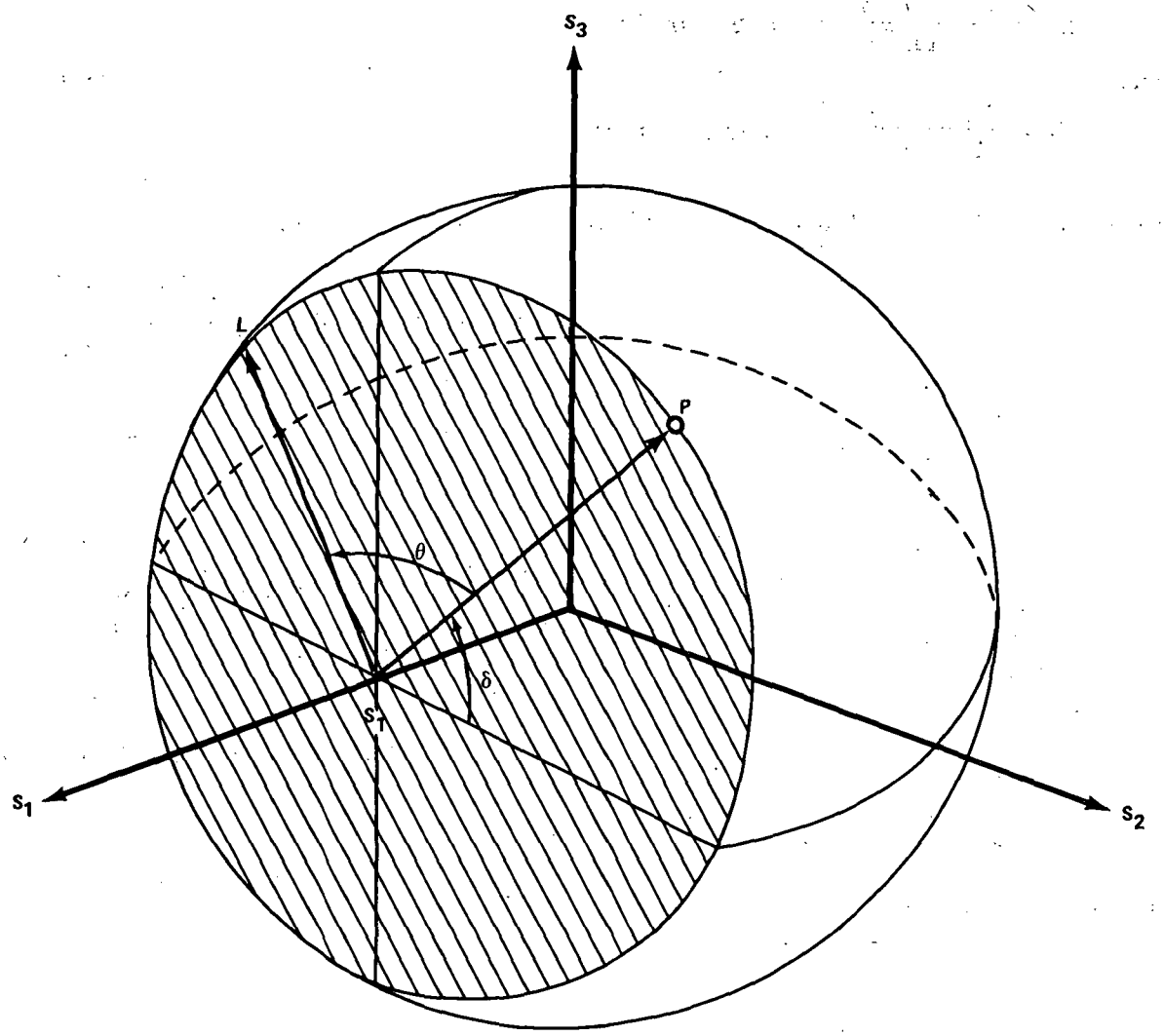

Figure A-4. Intersection of the Poincaré sphere and a plane normal to the S_1 axis.

Now, consider the Poincaré sphere representation of reflection at a metal surface. For this case, the incident light ray is resolved into components in the plane of incidence and normal to the plane of incidence (in the surface plane). The amplitude components $A_{0,p}$, $A_{0,s}$ of the incident waves and the corresponding components $R_{0,p}$, $R_{0,s}$ are related by the Fresnel relations derived in Appendix B and may be stated as

$$R_{0,p} = \frac{\tan(\theta_0 - \theta_1)}{\tan(\theta_0 + \theta_1)} A_{0,p}$$

and (A-32)

$$R_{0,s} = -\frac{\sin(\theta_0 - \theta_1)}{\sin(\theta_0 + \theta_1)} A_{0,s} \quad .$$

The quantities involved are further governed by Snell's law,

$$\sin\theta_1 = (n_0 \sin\theta_0)/n_1 \quad , \tag{A-33}$$

noting that since this case n_1 is complex; thus, θ_1 is complex also and no longer has the simple significance of an angle of refraction. Further, since θ_1 is complex, so are the ratios $R_{0,p}/A_{0,s}$ and $R_{0,s}/A_{0,s}$; i.e., characteristic phase changes occur on reflection. Thus, linearly polarized light will, in general, become elliptically polarized on reflection at the metal surface. Then, if δ_p and δ_s are the phase changes and ρ_p and ρ_s , which are the absolute values of the reflection amplitude coefficients, we have

$$R_{0,p}/A_{0,p} = \rho_p e^{i\delta_p} \text{ and } R_{0,s}/A_{0,s} = \rho_s e^{i\delta_s} \quad . \tag{A-34}$$

Further, if the incident light is linearly polarized in the azimuth ϕ_0 , we have

$$\tan\phi_0 = A_{0,s}/A_{0,p} \quad . \tag{A-35}$$

Thus

$$\rho = R_{0,p}/R_{0,s} = (\rho_p/\rho_s)\tan\phi_0 e^{i(\delta_p - \delta_s)} \quad , \tag{A-36}$$

or, more generally,

$$\rho = \tan\psi\, e^{i\Delta} \quad , \tag{A-37}$$

where ψ and Δ are functions of the optical constants of the surface, the angle of incidence, and the thickness and refractive index of any surface films present, and $\Delta = \delta_p - \delta_s$, representing the phase difference between the s and p components. Tan ψ is simply a measure of the relative absorption of the two components.

For consideration of the reflection process on the Poincaré sphere, represent the light with respect to Cartesian coordinates with the z axis in the direction of propagation and the x and y axes in and normal to the plane of incidence. Then $\tan \psi = a_s/a_p$. The Stokes parameters before reflection are given by equations (A-31) and after reflection by

$$S_1'' = \frac{1 - \tan^2 \alpha \cot^2 \psi}{1 + \tan^2 \alpha \cot^2 \psi} ,$$

$$S_2'' = \frac{2 \tan \alpha \cot \psi \cos (\delta + \Delta)}{1 + \tan^2 \alpha \cot^2 \psi} ,$$

and (A-38)

$$S_3'' = \frac{2 \tan \alpha \cot \psi \sin (\delta + \Delta)}{1 + \tan^2 \alpha \cot^2 \psi} ,$$

where it has been noted that the process of reflection introduces a phase difference Δ between the s and p components and changes the ratio of their amplitudes by $\tan \psi$. Further, it is noted that $\cot \psi e^{-i\Delta} = r_s/r_p$ and that $\tan \alpha = a_2/a_1$.

The reflection is represented on a Poincaré sphere in Figure A-5. The intersection of the S_1 axis with the sphere (the point I_p, with Cartesian coordinates 1, 0, 0) represents the orientation of the x axis, or the plane of incidence, as I_p corresponds to zero ellipticity χ and zero azimuth ϕ by equations (A-31). The point I_s has Cartesian coordinates (-1, 0, 0) corresponding to zero ellipticity and an azimuth of $\pi/2$; therefore, it represents the orientation of the y axis, or the plane of the surface. As in the case of the double refracting plate, the phase change rotates the point P, which represents the polarization of the incident light, around the S_1 axis through an angle Δ, the phase change produced by reflection, to the point L, which has the coordinates

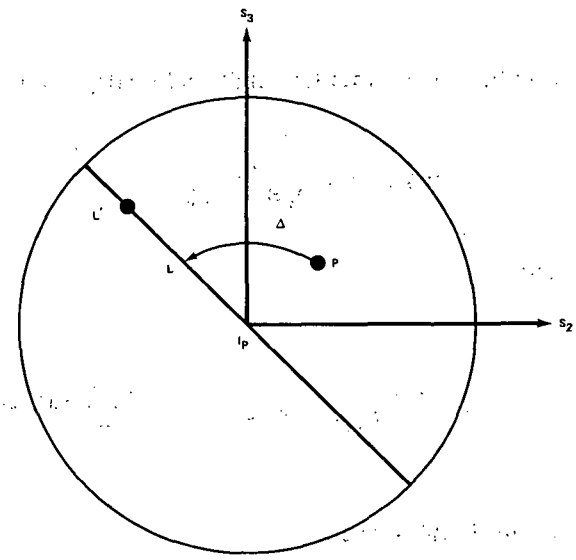

Figure A-5. Representation of metallic reflection on the Poincaré sphere, side A [48].

$$S_1' = \frac{1 - \tan^2 \alpha}{1 + \tan^2 \alpha} \quad ,$$

$$S_2' = \frac{2 \tan \alpha \cos (\delta + \Delta)}{1 + \tan^2 \alpha} \quad ,$$

and (A-39)

$$S_3' = \frac{2 \tan \alpha \sin (\delta + \Delta)}{1 + \tan^2 \alpha} \quad .$$

The point L is further translated to the point L', whose coordinates are given in equations (A-38), by the relative absorption of the components caused by reflection.

From equations (A-38) and (A-39), we have $S_3''/S_2'' = S_3'/S_2' = \tan(\delta + \Delta)$; i.e., points L and L' lie on the great circle given by the locus of points lying on the Poincare sphere satisfying $S_3/S_2 = \tan(\delta + \Delta)$. This locus is shown in Figure A-6 and is given by the intersection of the sphere with a plane normal to the S_1 axis and passing through the point L. Thus the point L is moved along the above great circle to the point L' to correctly represent the polarization of the reflected light. Let us now derive the location of L' on the great circle.

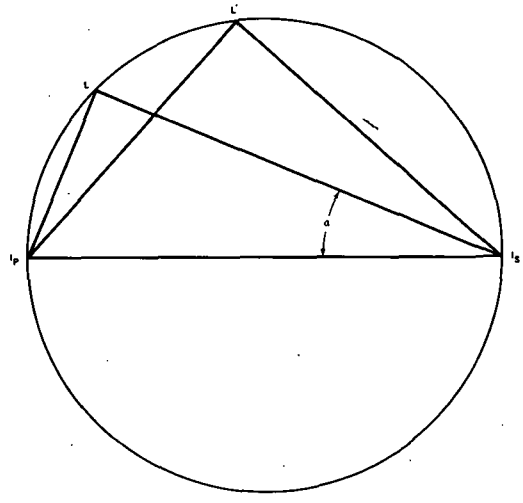

Figure A-6. Representation of metallic reflection on the Poincaré sphere, side B [48].

The coordinates of I_p and I_s are (1, 0, 0) and (-1, 0, 0), respectively, and those of L are given by equations (A-39). Therefore, the lengths of the chords I_pL and I_sL are

$$I_pL = \left\{\left(1 - \frac{1 - \tan^2 \alpha}{1 + \tan^2 \alpha}\right)^2 + \left[\frac{2 \tan \alpha \cos (\delta + \Delta)}{1 + \tan^2 \alpha}\right]^2 + \left[\frac{2 \tan \alpha \sin (\delta + \Delta)}{1 + \tan^2 \alpha}\right]^2\right\}^{1/2}$$

$$= \left[\frac{4 \tan^4 \alpha + 4 \tan^2 \alpha}{(1 + \tan^2 \alpha)^2}\right]^{1/2} = \frac{2 \tan \alpha}{(1 + \tan^2 \alpha)^{1/2}}$$

and

$$I_sL = \left[\frac{4 + 4 \tan^2 \alpha}{(1 + \tan^2 \alpha)^2}\right]^{1/2} = \frac{2}{(1 + \tan^2 \alpha)^{1/2}} \quad (A\text{-}40)$$

so that

$$\frac{I_p L}{I_s L} = \tan \alpha \quad . \tag{A-41}$$

$I_p L I_s$ is a right angle since it is inscribed in a semicircle; therefore, $I_p I_s L = \alpha$. Note that $\tan \alpha = a_2/a_1$ by equation (A-2).

Now, the position of L′ is determined by the angle $I_p I_s L'$. The tangent of this angle again gives the ratio of the amplitudes of the components of the reflected light, in analogy with equation (A-2). This ratio is given by $\tan \alpha / \tan \psi$. Therefore,

$$\frac{I_p L'}{I_s L'} = \tan (I_p I_s L') = \tan \alpha / \tan \psi \quad . \tag{A-42}$$

Using equations (A-38) as in equations (A-40) it is found that

$$I_p L' = \frac{2 \tan \alpha \cot \psi}{(1 + \tan^2 \alpha \cot^2 \psi)^{1/2}} \quad . \tag{A-43}$$

Moreover, using equations (A-41) and (A-42),

$$\tan \psi = \frac{(I_p L)/(I_s L)}{(I_p L')/(I_s L')} \quad ; \tag{A-44}$$

in general, the ratio of the chords between a point representing the state of polarization of a given light wave and two diametrically opposed points on the sphere is equal to the ratio of the amplitudes of the components when the electric vector of the light is resolved along axes represented by these two opposed points.

Let us now summarize the Poincaré sphere representation of the reflection of light from a surface with known complex coefficient $\tan \psi \, e^{i\Delta}$. The point P , representing the polarization state of the incident light, is moved by the reflection process through an angle Δ on the sphere in a plane normal to the S_1 axis to the point L . The chords $I_p L$ and $I_s L$ are measured and $\tan \alpha$ calculated by equation (A-41). The

chord I_pL' is calculated from equation (A-43), or the angle I_pI_sL' is calculated from equation (A-42), thus determining the state of polarization of the reflected light. It will later be shown how this representation can be used for the calculation of the effects occurring on reflection. First, however, still following the treatment of McCrackin, et al. [48], the instrumentation will be described briefly.

2. Instrumentation

The various components of the ellipsometer are shown in Figure A-7. Collimated monochromatic light, that of the mercury green line (546.073 nm), is used. The polarizer, a Glan-Thompson prism mounted in a graduated circle, serves to polarize the source light. The compensator, also mounted on a graduated circle, is a mica quarter-wave plate; it is used to convert the linearly polarized light into elliptically polarized light. The incident light has an azimuthal angle and ellipticity predictable from the polarizer and compensator settings. In general, this azimuth and ellipticity will be changed by reflection from the sample.

The aperture is an adjustable opening allowing a variation in the surface area examined and in the amount of light reaching the phototube. The analyzer, a second Glan-Thompson prism mounted on a graduated circle, can be rotated until a minimum intensity as indicated by the photometer is reached. If some ellipticity exists in the light reaching the analyzer, light extinction cannot be obtained by rotating the analyzer alone. In this case, the polarizer and analyzer must be adjusted alternately to remove this ellipticity and obtain extinction. Such an extinction, or null point, indicated that the light reflected from the sample is plane polarized.

It should be noted that while alignment of the ellipsometer is not too critical for thickness and refractive index measurements on thin films, it is critical for measurements on surfaces. A step-by-step alignment procedure has been presented by McCrackin, et al. [48].

3. Determination of Reflection Coefficient

The reflection of light from a surface is characterized by the complex reflection coefficient $\tan \psi \; e^{i\Delta}$, and hence by the two quantities ψ and Δ. Still following McCrackin, et al. [48], it will later be shown how the refractive index and thickness of films on a surface are calculated from Δ and ψ. Here, however, we shall deal with how Δ and ψ are determined from readings on the analyzer (A) and polarizer (P) scales.

For any given surface there is a multiplicity of polarizer, compensator, and analyzer scale readings that produce extinction by the analyzer of the reflected light from the surface. In explaining these numerous readings and how Δ and ψ may be computed from them, it should be remembered that all azimuthal angles are measured positive counterclockwise from the plane of incidence when looking into the light beam, and that the compensator is generally set so that its fast axis is at an azimuth of $\pm\pi/4$. The present discussion is for an instrument such as that shown in Figure A-7, with the light passing through the compensator before reflecting off the sample.

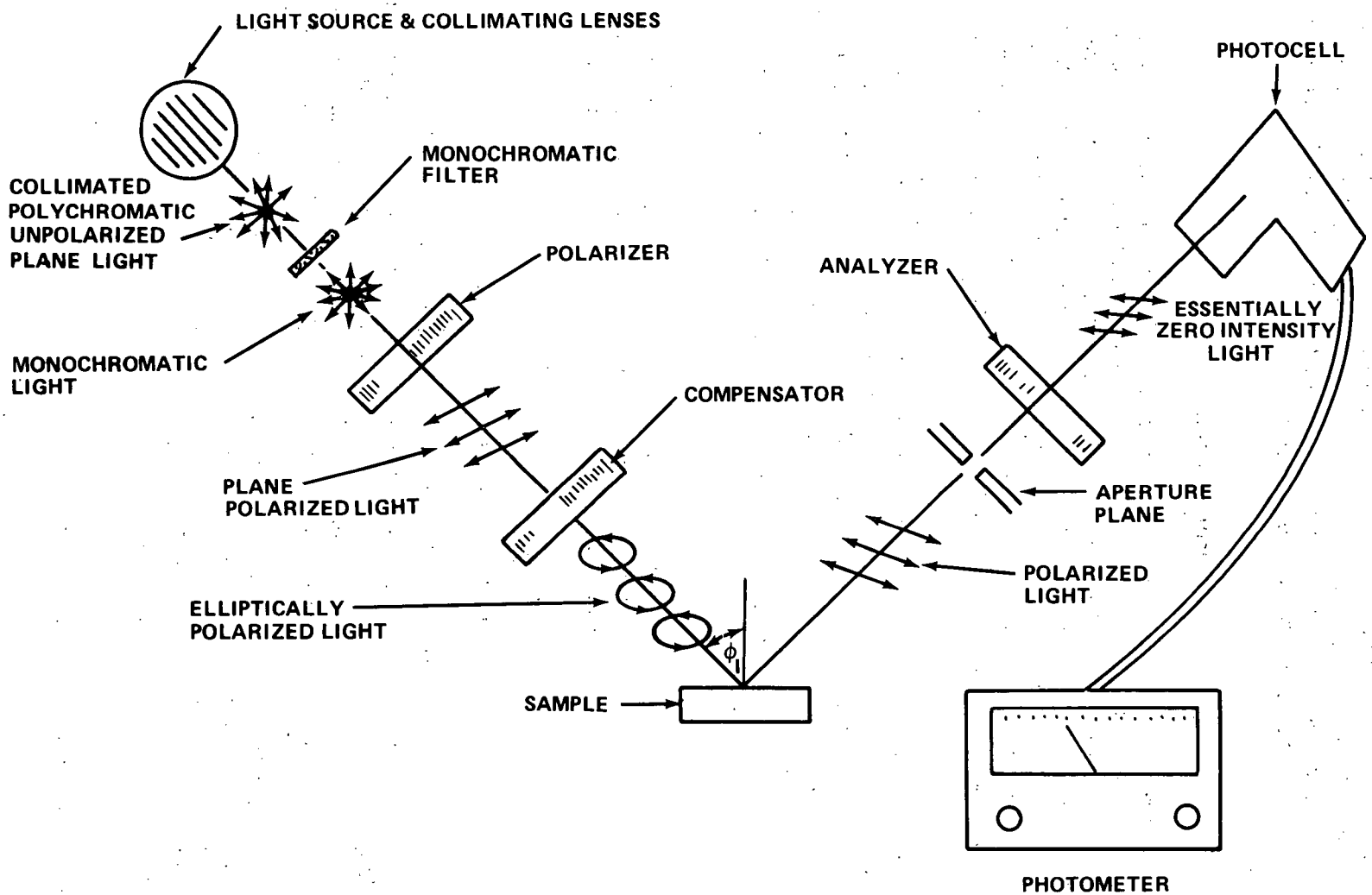

Figure A-7. The component parts of an ellipsometer [48].

The various readings fall into four sets or zones, two with the fast axis of the compensator set at $-\pi/4$, numbered 1 and 3, and two with it set at $+\pi/4$, numbered 2 and 4. In each zone there is one independent set of P and A readings, or a total of four. However, since both polarizer and analyzer may be rotated by π without affecting the results, there appear 16 P and A settings, indicating a null point. Further, since the compensator may be rotated by π without affecting the results, there are finally 32 possible sets of null point readings.

In calculating Δ and ψ, it is useful to calculate the three quantities p, a_p, and a_s from the P and A values, p being related to the P readings, a_p being related to the A readings in zones 1 and 4, and a_s being related to the A readings in zones 2 and 3. These quantities and their relations will now be examined, following the Poincaré sphere treatment of Winterbottom [50].

The following definitions and rules for use of the Poincaré sphere, which was shown in Figures A-3 through A-5, should be briefly noted:

a. The Poincaré sphere is a sphere of unit radius.

b. Use of the sphere may be compared to use of a globe in navigation. The sphere has north and south poles (which lie on the S_3 axis) and is divided by latitudes, longitudes, great circles, and other arcs as needed.

c. Latitudes on the Poincaré sphere show the ellipticity of the light or the ratio of the minor (b) axis to the major (a) axis of the ellipse. By definition, χ is the ellipticity. Then, 2χ is the latitude on the sphere and $\tan \chi = b/a$. For example, circularly polarized light has $b/a = 1$. Then $\tan \chi = 1$ and $\chi = 45$ deg. The latitude for circularly polarized light is then $2\chi = 90$ deg, which is at the poles. For linearly polarized light, $b/a = 0$. Then, $\tan \chi$ and χ are zero, and the points representing this polarization lie on the equator. Elliptically polarized light has χ between zero and one; therefore, all points except those on the equator and at the poles represent elliptically polarized light (Fig. A-8).

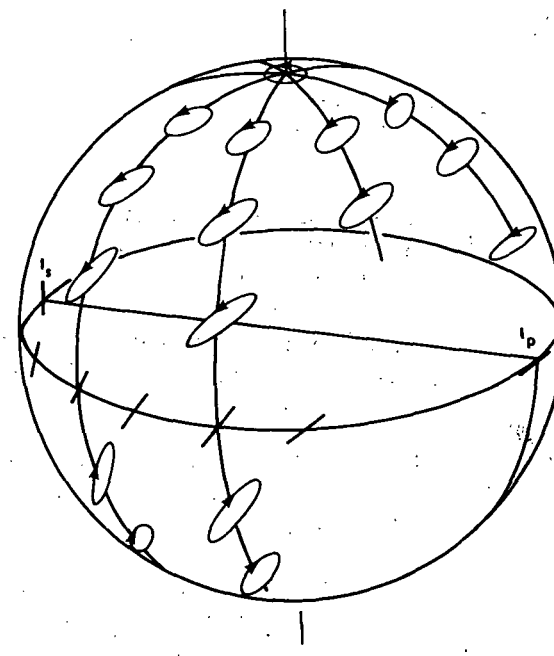

Figure A-8. Poincaré sphere, the general significance of the different areas.

d. Longitudes represent the angle of inclination of the major axis of the ellipse ϕ. At 0-deg longitude, which is the point I_p in Figure A-9 [51], the major axis is parallel to the equator. At 180 deg, or point I_s in Figure A-9, the major axis is perpendicular to the equator, $\phi = 90$ deg. Longitudes are measured clockwise from 0 to 360 deg; thus, the angle of the major axis turns from 0 to 180 deg.

e. The sense of rotation of the ellipse is counterclockwise in the southern hemisphere and clockwise in the northern hemisphere, using the traditional sense.

The compensation process will now be given in terms of the Poincaré sphere representation [51].

In Figure A-9, as in the case of metallic reflection, I_p marks the plane incidence and I_s marks the plane of the surface. In the ellipsometer, the corresponding planes are horizontal and vertical. Point C_f marks the fast axis of the compensator, which is set in this case at 270/2 or 135 deg to the plane of incidence, which is the same as at an azimuth of $-\pi/4$. The fast axis of the compensator is its optical axis. Point C_s marks the slow axis of the compensator, which is 180/2 or 90 deg from the fast axis. Point P is the polarizer angular reading, which in this case is roughly 40/2 or 20 deg clockwise from I_p.

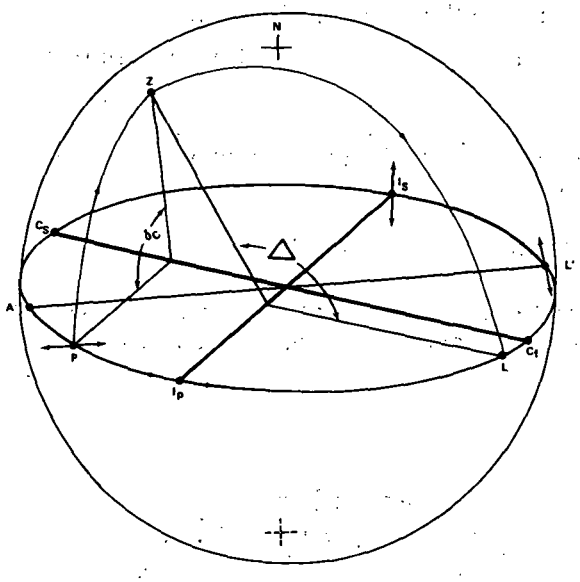

Figure A-9. Poincaré sphere, the ellipsometer compensation process [51].

The phase change caused by the compensator, δ_c, changes the linear polarization form at P into the elliptical form at Z. The phase change δ_c is $\pi/2$ for a perfect quarter-wave plate. As explained in the previous treatment of the double refracting plate, such a phase change rotates polarization forms clockwise on the sphere about the C_f - C_s axis as one looks from C_f - C_s through an angle equal in magnitude to the phase change.

Reflection of the elliptically polarized light Z from a metal surface produces a phase change Δ which rotates Z to L about the I_p - I_s axis. In addition to the phase change Δ, a relative absorption of the E_x and E_y components occurs which shifts the linear polarization from L to L'. This L' form is extinguished by setting the transmission plane of the analyzer A at 180/2 or 90 deg from L'. In this case, A is roughly 60/2 or 30 deg.

As noted before, polarizing prisms and quarter-wave compensators can be rotated by π without affecting the polarization forms. To avoid confusion, ellipsometer readings are grouped into four sets or zones.

Figure A-10 shows plane views of the Poincaré sphere which illustrate how the four zones arise. Zone 1 corresponds to the diagram in Figure A-9. The P and A readings

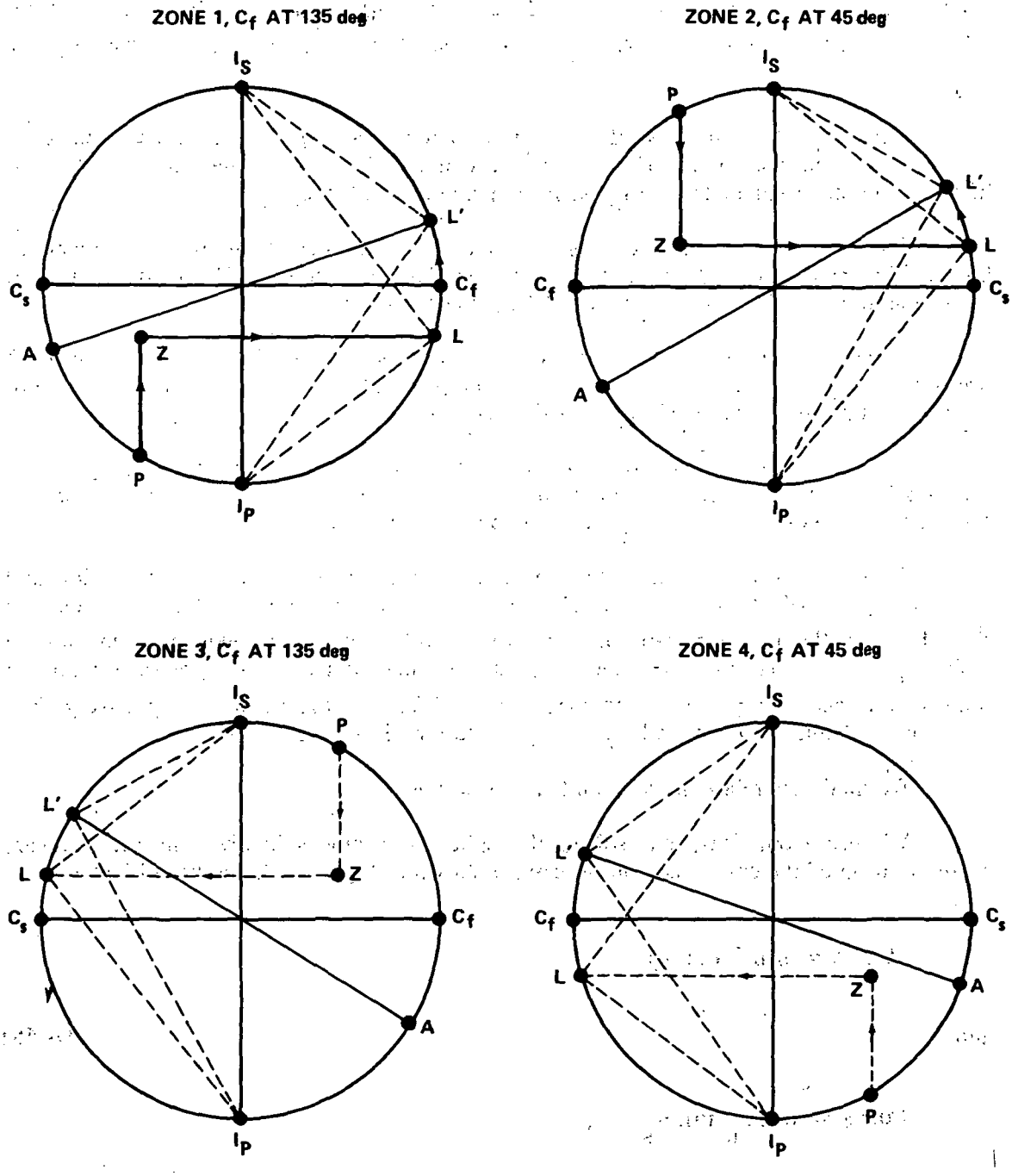

Figure A-10. Plane views of the Poincaré sphere [51].

in Zone 1 will be designated p and a_p, respectively. Since P and A can be rotated by π and still give the same polarization form as before, there are four possible readings in this zone. These readings are combinations of $P = p, p + \pi$ and $A = a_p, a_p + \pi$. In Zone 2, the case shown gives $P = \pi/2 - p, 3\pi/2 - p,$, and $A = a_s, a_s + \pi$. Zone 3 has $P = p + \pi/2, p + 3\pi/2$ and $A = \pi - a_s, 2\pi - a_s$. Zone 4 has $P = \pi - p, 2\pi - p$ and $A = \pi - a_p, 2\pi - a_p$.

Zone 1. The fast axis of the compensator is at $-\pi/4$. The polarizer plane of transmission makes an angle of $+p$ with the plane of incidence. The analyzer plane of transmission makes an angle of $+a_p$ with the plane of incidence.

Zone 2. The fast axis of the compensator is at $+\pi/4$. The polarizer plane of transmission makes an angle of $\pi/2 - p$ with the plane of incidence. The analyzer plane of transmission makes an angle of $+a_s$ with the plane of incidence.

Zone 3. The fast axis of the compensator is at $-\pi/4$. The polarizer plane of transmission makes an angle of $p + \pi/2$ with the plane of incidence. The analyzer plane of transmission makes an angle of $-a_s$ with the plane of incidence.

Zone 4. The fast axis of the compensator is at $+\pi/4$. The polarizer plane of transmission makes an angle of $-p$ with the plane of incidence. The analyzer plane of transmission makes an angle of $-a_p$ with the plane of incidence.

Thus, the term p is the angle between the polarizer plane of transmission and either the plane of incidence or the plane of the surface, while a_p and a_s represent the angle between the analyzer plane of transmission and the plane of incidence, being labeled either a_p or a_s, according to whether p is the angle between the polarizer plane of transmission and the plane of incidence or the plane of the surface, respectively. The relations of P and A to p and a_p or a_s are summarized in Table A-1.

We shall now relate p, a_p, and a_s to Δ and ψ.

Winterbottom [50] has solved the spherical triangles involved in the Poincaré representation of the compensation process, as shown in Figure A-7, and has obtained

$$-\tan \Delta = \sin \delta \cot 2p$$

and (A-45)

$$\tan^2 \psi = \tan a_p \tan a_s \quad ,$$

TABLE A-1. RELATION OF P AND A READINGS TO p, a_p, AND a_s [48]

Zone	Compensator	P	A
1	$-\pi/4$	p	a_p
		$p + \pi$	a_p
		p	$a_p + \pi$
		$p + \pi$	$a_p + \pi$
3	$-\pi/4$	$p + \pi/2$	$\pi - a_s$
		$p + 3\pi/2$	$\pi - a_s$
		$p + \pi/2$	$2\pi - a_s$
		$p + 3\pi/2$	$2\pi - a_s$
2	$+\pi/4$	$\pi/2 - p$	a_s
		$3\pi/2 - p$	a_s
		$\pi/2 - p$	$a_s + \pi$
		$3\pi/2 - p$	$a_s + \pi$
4	$+\pi/4$	$\pi - p$	$\pi - a_p$
		$2\pi - \pi$	$\pi - a_p$
		$\pi - p$	$2\pi - a_p$
		$2\pi - p$	$2\pi - a_p$

where δ is the relative retardation of the compensator. For a perfect quarter-wave plate ($\delta = \pi/2$), these reduce to

$$\Delta = \pi/2 + 2p$$

and (A-46)

$$\psi = a_p = a_s$$

Thus, by using Table A-1 and equations (A-45) or (A-46), it is possible to compute p and a_p or a_s from P and A, and hence compute Δ and ψ.

In practice, the values of p, a_p and a_s found from the P and A readings in the various zones are not identical. Experience shows that the averages from Zones 1 and 3 check very closely with the averages from Zones 2 and 4 for both p and a, so measurements are usually taken in Zones 1 and 3 only and averaged.

4. Computation of Film Indices and Thicknesses

A typical thin film under study consists of a film of index n_2 and thickness d_2 on substrate of index n_3 immersed in a medium of index n_1, as shown in Figure A-11. Let all media be isotropic and n_1 represent a real index of refraction, while

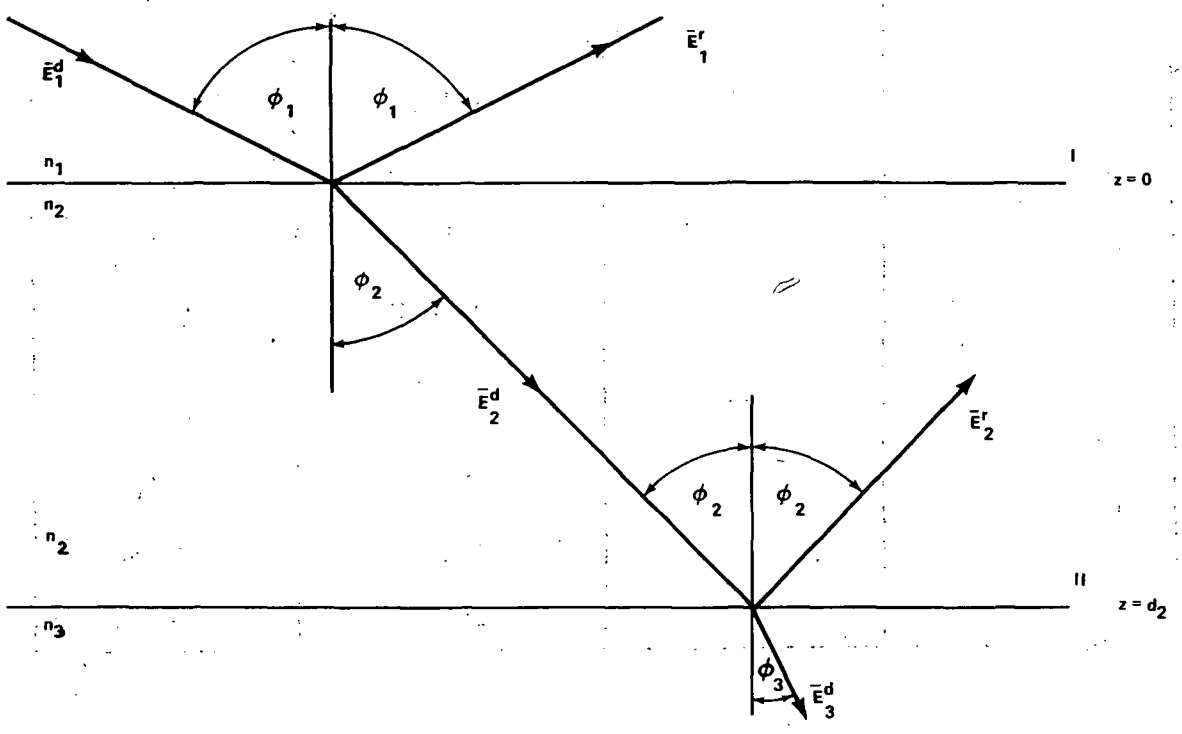

Figure A-11. Reflection and refraction of light by one thin film.

n_2 and n_3 may be complex. This system is treated in Appendix B, where it is shown that the parallel and normal reflection coefficients for light incident at the boundary between the immersion medium and film are

$$r_{12}^{p} = \frac{n_2 \cos \phi_1 - n_1 \cos \phi_2}{n_2 \cos \phi_1 + n_1 \cos \phi_2}$$

and (A-47)

$$r_{12}^{s} = \frac{n_1 \cos \phi_1 - n_2 \cos \phi_2}{n_1 \cos \phi_1 + n_2 \cos \phi_2}$$

Similar expressions hold for the reflection coefficients at the boundary between film and substrate, r_{23}^{p} and r_{23}^{s} . The $\cos \phi_i$ values needed for these reflection coefficients are given by Snell's law; i.e.,

$$\cos \phi_2 = [1 - (\sin \phi_1 \, n_1/n_2)^2]^{1/2} \qquad \text{(A-48)}$$

etc.

It is also shown in Appendix B that the total reflection coefficients that include the contributions of reflections from lower boundaries are given by:

$$R^{p} = \frac{r_{12}^{p} + r_{23}^{p} \exp D}{1 + r_{12}^{p} r_{23}^{p} \exp D}$$

and (A-49)

$$R^{s} = \frac{r_{12}^{s} + r_{23}^{s} \exp D}{1 + r_{12}^{s} r_{23}^{s} \exp D} \quad ,$$

where D is $-4\pi \, i \, n_2 \cos \phi_2 \, d_2/\lambda$.

The ratio of the total reflection coefficients defines ρ , where

$$\rho = R^{p}/R^{s} \qquad \text{(A-50)}$$

which may be further expressed as

$$\rho = \tan \psi \, e^{i\Delta} \quad . \tag{A-51}$$

As has been shown, we can calculate ρ from the ellipsometer readings.

Therefore, by knowing n_1 and n_3 and by making ellipsometer measurements, we can determine refractive indices for films of known thicknesses or thicknesses of films of known indices. Note that the equations cannot be solved for d and n_2 in closed form. The normal procedure is to assume a series of refractive indices and to calculate thicknesses from the experimental measurements. Since manual calculations of this type are impractical because of the complexity of the equations, the problem is normally solved by computer techniques. In this study, the ellipsometer computer program of McCrackin [36] was adopted to Fortran 4H by Mr. J.L. Zurasky, MSFC, for use in the MSFC XDS Sigma Five Computer. This program calculated the refractive indices used in this study from ellipsometric measurements made on a Gaertner Model L119 ellipsometer.

APPENDIX B. DERIVATION OF THE DRUDE EQUATIONS

Let us first derive Fresnel's formulas for the reflection and refraction of light on a boundary between two isotropic dielectrics. We proceed as follows.

Consider a plane light wave incident on a reflecting boundary. The medium from which the light ray is incident has permittivity ϵ_0 and refractive index n_0, and the other medium, in which the light ray is refracted, has permittivity ϵ_1 and refractive index n_1. The permeability of both mediums is that of a vacuum, μ_V. Vector orientation is as shown in Figure B-1.

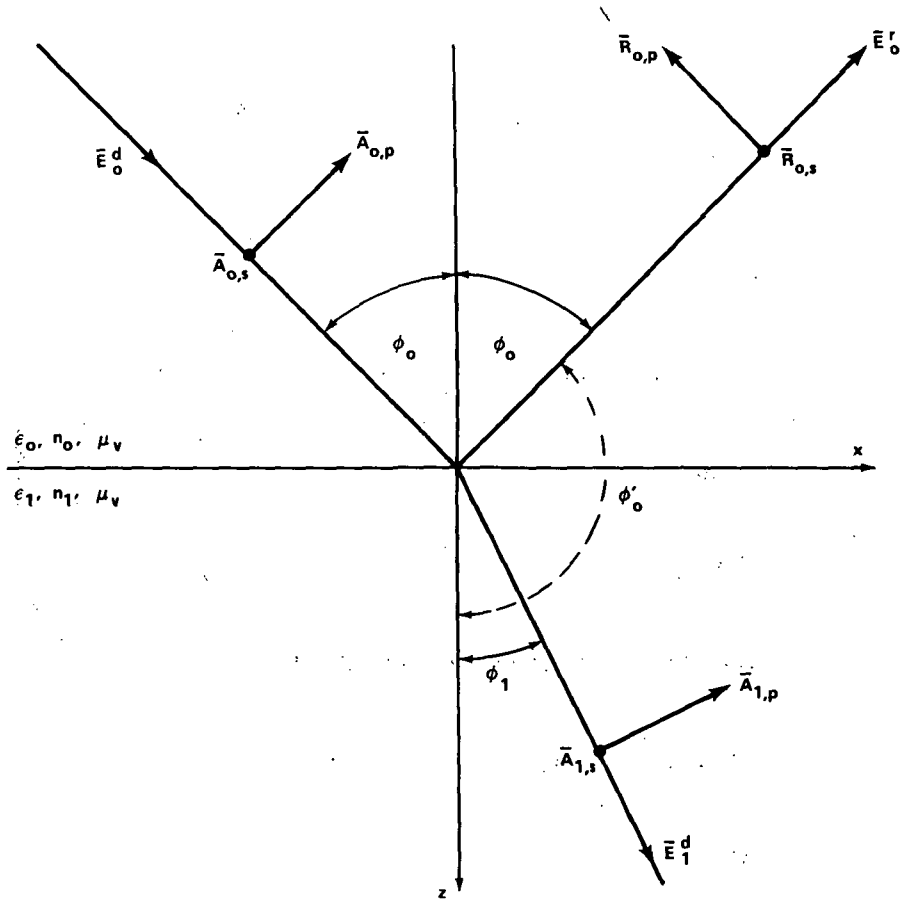

Figure B-1. Reflection and refraction of light at a plane boundary between two dielectrics.

It should be noted that the velocity of light in the first medium (with index 0) is given by

$$V_0 = 1/\sqrt{\epsilon_0 \mu_V} \tag{B-1}$$

and in the second medium (with index 1) by

$$V_1 = 1/\sqrt{\epsilon_1 \mu_v} \quad . \tag{B-2}$$

By using the complex form, where

$$\bar{E} = \text{electric field strength} = \bar{E}_0 e^{i\tau} \quad , \tag{B-3}$$

in which

$E_{0,x} = Ae^{i\delta_1}$,

$E_{0,y} = Be^{i\delta_2}$,

$E_{0,z} = Ce^{i\delta_3}$,

$\tau = \omega(t - z/v)$, where $\bar{z}$ is the direction of propagation ,

$\delta_1, \delta_2, \delta_3$ = phases ,

t = time ,

v = velocity of light in medium investigated ,

ω = angular frequency ,

$\omega = 2\pi f$,

f = frequency ,

the vector plane wave of the incident light can be written as

$$\bar{E}_0^d = \bar{A}_0 e^{i\tau_0^d} \quad ; \tag{B-4}$$

the vector reflected wave as

$$\bar{E}_0^r = \bar{R}_0 e^{i\tau_0^r} \quad ; \tag{B-5}$$

and the vector refracted wave as

$$\bar{E}_1^d = \bar{A}_1 e^{i\tau_1^d} \quad . \tag{B-6}$$

Note that for equations (B-4) through (B-6)

$$\tau_0^d = \omega\left(t - \frac{x\sin\phi_0 + z\cos\phi_0}{v_0}\right) \quad , \tag{B-7}$$

$$\tau_0^r = \omega\left(t - \frac{x\sin\phi_0' + z\cos\phi_0'}{v_0}\right) \quad , \tag{B-8}$$

and

$$\tau_1^d = \omega\left(t - \frac{x\sin\phi_1 + z\cos\phi_1}{v_1}\right) \quad , \tag{B-9}$$

where ϕ_0, ϕ_0', and ϕ_1 are defined as shown in Figure B-1.

The amplitude vectors in equations (B-4) through (B-6) are divided into components normal to and in the plane of incidence; i.e., A_0 is divided into $A_{0,p}$ and $A_{0,s}$, $\bar{R}_0$ is divided into $R_{0,p}$ and $R_{0,s}$, and $\bar{A}_1$ is divided into $A_{1,p}$ and $A_{1,s}$.

Now, the above vector light waves will be written out into components onto the coordinate axis, noting that the components of the s amplitudes lie in the y direction and that the p components have projections onto the x and z axes. This may be seen from Figure B-1.

Thus, the following equations are obtained for incident light

$$E^{d}_{0,x} = A_{0,p}\cos\phi_0 e^{i\tau^{d}_{0}} ,$$

$$E^{d}_{0,y} = A_{0,s} e^{i\tau^{d}_{0}} ,$$

and

$$E^{d}_{0,z} = -A_{0,p}\sin\phi_0 e^{i\tau^{d}_{0}} .$$

For reflected light we have

$$E^{r}_{0,x} = R_{0,p}\cos\phi'_0 e^{i\tau^{r}_{0}} ,$$

$$E^{r}_{0,y} = R_{0,s} e^{i\tau^{r}_{0}} ,$$

and (B-10)

$$E^{r}_{0,z} = -R_{0,p}\sin\phi'_0 e^{i\tau^{r}_{0}} ,$$

and for refracted light,

$$E^{d}_{1,x} = A_{1,p}\cos\phi_1 e^{i\tau^{d}_{1}} ,$$

$$E^{d}_{1,y} = A_{1,s} e^{i\tau^{d}_{1}} ,$$

and

$$E^{d}_{1,z} = -A_{1,p}\sin\phi_1 e^{i\tau^{d}_{1}} .$$

Now, by Maxwell's equations for isotropic homogeneous dielectrics containing no electric charges, which are

$$\mu_v \frac{\partial H_x}{\partial t} = \frac{\partial E_y}{\partial z} - \frac{\partial E_z}{\partial y} ,$$

$$\mu_v \frac{\partial H_y}{\partial t} = \frac{\partial E_z}{\partial x} - \frac{\partial E_x}{\partial z} ,$$

and (B-11)

$$\mu_v \frac{\partial H_z}{\partial t} = \frac{\partial E_x}{\partial y} - \frac{\partial E_y}{\partial x}$$

and by integration, using equations (B-10) in equations (B-11), the following equations are found for incident light

$$H^d_{0,x} = -n_0 \sqrt{\epsilon_v/\mu_v} A_{0,s} \cos\phi_0 e^{i\tau^d_0} ,$$

$$H^d_{0,y} = n_0 \sqrt{\epsilon_v/\mu_v} A_{0,p} e^{i\tau^d_0} ,$$

and

$$H^d_{0,z} = n_0 \sqrt{\epsilon_v/\mu_v} A_{0,s} \sin\phi_0 e^{i\tau^d_0} .$$

For reflected light we have

$$H^r_{0,x} = -n_0 \sqrt{\epsilon_v/\mu_v} R_{0,s} \cos\phi'_0 e^{i\tau^r_0} ,$$

$$H^r_{0,y} = n_0 \sqrt{\epsilon_v/\mu_v} R_{0,p} e^{i\tau^r_0} ,$$

and (B-12)

$$H^r_{0,z} = n_0 \sqrt{\epsilon_v/\mu_v} R_{0,s} \sin\phi'_0 e^{i\tau^r_0} ,$$

and for refracted light,

$$H^d_{1,x} = -n_1\sqrt{\epsilon_v/\mu_v}\,A_{1,s}\cos\phi_1 e^{i\tau^d_1} \quad ,$$

$$H^d_{1,y} = n_1\sqrt{\epsilon_v/\mu_v}\,A_{1,p}e^{i\tau^d_1} \quad ,$$

and

$$H^d_{1,z} = n_1\sqrt{\epsilon_v/\mu_v}\,A_{1,s}\sin\phi_1 e^{i\tau^d_1} \quad .$$

Now, for two dielectrics, the tangential components of $\overline{E}$ and $\overline{H}$ and the normal components of $\overline{B}$ and $\overline{D}$ are continuous across the interface [52]. Therefore, we may write

$$E^d_{0,x} + E^r_{0,x} = E^d_{1,x} \quad , \qquad H^d_{0,x} + H^r_{0,x} = H^d_{1,x} \quad ,$$

$$E^d_{0,y} + E^r_{0,y} = E^d_{1,y} \quad , \qquad H^d_{0,y} + H^r_{0,y} = H^d_{1,y} \quad , \tag{B-13}$$

$$\epsilon_0\left(E^d_{0,z} + E^r_{0,z}\right) = \epsilon_1 E^d_{1,z}, \quad \mu_v\left(H^d_{0,z} + H^r_{0,z}\right) = \mu_v H^d_{1,z} \quad .$$

Now, substituting equations (B-11) and (B-12) into equations (B-13), we obtain

$$A_{0,p}\cos\phi_0 e^{i\tau^d_0} + R_{0,p}\cos\phi'_0 e^{i\tau^r_0} = A_{1,p}\cos\phi_1 e^{i\tau^d_1} \quad , \tag{B-14}$$

$$A_{0,s}e^{i\tau^d_0} + R_{0,s}e^{i\tau^r_0} = A_{1,s}e^{i\tau^d_1} \quad , \tag{B-15}$$

$$\epsilon_0\left(A_{0,p}\sin\phi_0 e^{i\tau^d_0} + R_{0,p}\sin\phi'_0 e^{i\tau^r_0}\right) = \epsilon_1 A_{1,p}\sin\phi_1 e^{i\tau^d_1} \quad , \tag{B-16}$$

$$n_0\left(A_{0,s}\cos\phi_0 e^{i\tau^d_0} + R_{0,s}\cos\phi'_0 e^{i\tau^r_0}\right) = n_1 A_{1,s}\cos\phi_1 e^{i\tau^d_1} \quad , \tag{B-17}$$

$$n_0\left(A_{0,p}e^{i\tau_0^d} + R_{0,p}e^{i\tau_0^r}\right) = n_1 A_{1,p}e^{i\tau_1^d} \quad , \tag{B-18}$$

$$n_0\left(A_{0,s}\sin\phi_0 e^{i\tau_0^d} + R_{0,s}\sin\phi_0' e^{i\tau_0^r}\right) = n_1 A_{1,s}\sin\phi_1 e^{i\tau_1^d} \quad . \tag{B-19}$$

Now, by the law of reflection, it is known that $\cos\phi_0' = -\cos\phi_0$ and $\sin\phi_0 = \sin\phi_0'$, and by Snell's law of refraction it is known that $\sin\phi_0/\sin\phi_1 = n_1/n_0$. Therefore, equation (B-19) may be written as

$$A_{0,s}e^{i\tau_0^d} + R_{0,s}e^{i\tau_0^r} = A_{1,s}e^{i\tau_1^d}$$

which is the same as equation (B-15). Noting that $\epsilon_0 = n_0^2$ and $\epsilon_1 = n_1^2$, equation (B-16) may be rewritten as

$$n_0\left(A_{0,p}e^{i\tau_0^d} + R_{0,p}e^{i\tau_0^r}\right) = n_1 A_{1,p}e^{i\tau_1^d}$$

which is the same as equation (B-18).

Thus four conditions remain that must be satisfied at $z = 0$ for all t. These requirements are satisfied by the following conditions at $z = 0$.

a. Phase condition

$$\tau_0^d = \tau_0^r = \tau_1^d \tag{B-20}$$

b. Amplitude conditions

$$\begin{aligned}
&(A_{0,p} - R_{0,p})\cos\phi_0 = A_{1,p}\cos\phi_1 \quad , \\
&(A_{0,p} + R_{0,p})n_0 = A_{1,p}n_1 \quad , \\
&A_{0,s} + R_{0,s} = A_{1,s} \quad , \\
&(A_{0,s} - R_{0,s})n_0\cos\phi_0 = A_{1,s}n_1\cos\phi_1 \quad .
\end{aligned} \tag{B-21}$$

and for the reflected wave

$$\bar{E}_0^r = \bar{R}_0 \exp\left[i\omega \left(t - \frac{x \sin\phi_0 - z \cos\phi_0}{v_0} \right) \right] = \bar{R}_0 e^{i\tau_0^r} \quad . \tag{B-27}$$

In the film there are again two waves, the wave refracted by the first boundary, which includes all waves passing in the same direction after reflection at $z = 0$ and $z = d$, and the waves reflected at $z = d$. The wave refracted at $z = 0$ is written as

$$\bar{E}_1^d = \bar{A}_1 \exp\left[i\omega \left(t - \frac{x \sin\phi_1 + z \cos\phi_1}{v_1} \right) \right] = \bar{A}_1 e^{i\tau_1^d} \quad , \tag{B-28}$$

and the wave reflected by $z = d$ is written as

$$\bar{E}_1^r = \bar{R}_1 \exp\left[i\omega \left(t - \frac{x \sin\phi_1 - z \cos\phi_1}{v_1} \right) \right] = \bar{R}_1 e^{i\tau_1^r} \quad . \tag{B-29}$$

In the third medium, we have all waves refracted by $z = d$. This set of waves is regarded as one wave which is written as

$$\bar{E}_2^d = \bar{A}_2 \exp\left[i\omega \left(t - \frac{x \sin\phi_2 + z \cos\phi_2}{v_2} \right) \right] = \bar{A}_2 e^{i\tau_2^d} \quad . \tag{B-30}$$

In general, $\bar{A}_0$, $\bar{R}_0$, $\bar{A}_1$, $\bar{R}_1$, $\bar{A}_2$, and $\bar{R}_2$ are complex numbers.

Now, at boundaries I and II, we may apply Fresnel's formulas, equations (B-22) through (B-25), which yield the following relations.

$$\begin{aligned} r'_p &= R^I_{0,p} / A^I_{0,p} = \frac{\tan(\phi_0 - \phi_1)}{\tan(\phi_0 + \phi_1)} \quad , \\ r'_s &= R^I_{0,s} / A^I_{0,s} = -\frac{\sin(\phi_0 - \phi_1)}{\sin(\phi_0 + \phi_1)} \end{aligned} \tag{B-31}$$

$$t'_p = A^I_{1,p}/A^I_{0,p} = \frac{2\sin\phi_1\cos\phi_0}{\sin(\phi_0+\phi_1)\cos(\phi_0-\phi_1)} \quad ,$$

$$t'_s = A^I_{1,s}/A^I_{0,s} = \frac{2\sin\phi_1\cos\phi_0}{\sin(\phi_0+\phi_1)} \quad , \tag{B-32}$$

$$r''_p = R^{II}_{1,p}/A^{II}_{1,p} = \frac{\tan(\phi_1-\phi_2)}{\tan(\phi_1+\phi_2)}$$

$$r''_s = R^{II}_{1,s}/A^{II}_{1,s} = -\frac{\sin(\phi_1-\phi_2)}{\sin(\phi_1+\phi_2)} \tag{B-33}$$

$$t''_p = A^{II}_{2,p}/A^{II}_{1,p} = \frac{2\sin\phi_2\cos\phi_1}{\sin(\phi_1+\phi_2)\cos(\phi_1-\phi_2)} \quad ,$$

$$t''_s = A^{II}_{2,s}/A^{II}_{1,s} = \frac{2\sin\phi_2\cos\phi_1}{\sin(\phi_1+\phi_2)} \quad . \tag{B-34}$$

Note that equations (B-10) are still valid for the components of $\bar{E}_0{}^d$, $\bar{E}_0{}^r$, and $\bar{E}_1{}^d$. Analogously, we may write for the components of $\bar{E}_1{}^r$ and $\bar{E}_2{}^r$ the following:

$$E^r_{1,x} = -R_{1,p}\cos\phi_1 e^{i\tau^r_1} \quad ,$$

$$E^r_{1,y} = R_{1,s} e^{i\tau^r_1} \quad ,$$

$$E^r_{1,z} = -R_{1,p}\sin\phi e^{i\tau^r_1} \quad , \tag{B-35}$$

$$E^d_{2,x} = A_{2,p}\cos\phi_2 e^{i\tau^d_2} \quad ,$$

$$E^d_{2,y} = A_{2,s} e^{i\tau^d_2} \quad ,$$

$$E^{d}_{2,z} = -A_{2,p} \sin\phi_2 e^{i\tau^{d}_{2}} \quad . \qquad \text{(B-35) (Con't)}$$

Equations (B-12) for the components of $\bar{H}_0^{d}$, $\bar{H}_0^{r}$, and $\bar{H}_1^{d}$ are also still valid. Analogously, we may write for the components of $\bar{H}_1^{r}$ and $\bar{H}_2^{d}$ the following:

$$\begin{aligned}
H^{r}_{1,x} &= n_1 \sqrt{\epsilon_v/\mu_v} R_{1,s} \cos\phi_1 e^{i\tau^{r}_{1}} , \\
H^{r}_{1,y} &= n_1 \sqrt{\epsilon_v/\mu_v} R_{1,p} e^{i\tau^{r}_{1}} , \\
H^{r}_{1,z} &= n_1 \sqrt{\epsilon_v/\mu_v} R_{1,s} \sin\phi_1 e^{i\tau^{r}_{1}} , \\
H^{d}_{2,x} &= -n_2 \sqrt{\epsilon_v/\mu_v} A_{2,s} \cos\phi_2 e^{i\tau^{d}_{2}} , \\
H^{d}_{2,y} &= n_2 \sqrt{\epsilon_v/\mu_v} A_{2,p} e^{i\tau^{d}_{2}} , \\
H^{d}_{2,z} &= n_2 \sqrt{\epsilon_v/\mu_v} A_{2,s} \sin\phi_2 e^{i\tau^{d}_{2}} .
\end{aligned} \qquad \text{(B-36)}$$

As boundary conditions we have the continuity of the tangential components of the electric and magnetic field strength over boundaries I and II. This means that

$$
\begin{aligned}
E^{d}_{0,x} + E^{r}_{0,x} &= E^{d}_{1,x} + E^{r}_{1,x} \quad , \\
E^{d}_{0,y} + E^{r}_{0,y} &= E^{d}_{1,y} + E^{r}_{1,y} \quad , \\
H^{d}_{0,x} + H^{r}_{0,x} &= H^{d}_{1,x} + H^{r}_{1,x} \quad , \\
H^{d}_{0,y} + H^{r}_{0,y} &= H^{d}_{1,y} + H^{r}_{1,y} \quad ,
\end{aligned}
\tag{B-37}
$$

and

$$
\begin{aligned}
E^{d}_{1,x} + E^{r}_{1,x} &= E^{d}_{2,x} \quad , \\
E^{d}_{1,y} + E^{r}_{1,y} &= E^{d}_{2,y} \quad , \\
H^{d}_{1,x} + H^{r}_{1,x} &= H^{d}_{2,x} \quad , \\
H^{d}_{1,y} + H^{r}_{1,y} &= H^{d}_{2,y} \quad .
\end{aligned}
\tag{B-38}
$$

Note that because of the discussion following equation (B-19), it is necessary to consider the requirements for continuity of the normal components of the electric and magnetic induction across the boundaries, since these conditions are contained implicitly in equations (B-37) and (B-38).

The above boundary conditions are satisfied by the following assumptions:

a. The phase conditions $\tau_0{}^{d} = \tau_0{}^{r} = \tau_1{}^{d}$ and $\tau_1{}^{d} = \tau_1{}^{r} = \tau_2{}^{d}$ are satisfied at $z = 0$ and $z = d$, respectively.

b. The following amplitude conditions are satisfied:

At Boundary I (z = 0)

$$\begin{aligned}
&(A^{I}_{0,p} - R^{I}_{0,p})\cos\phi_0 = (A^{I}_{1,p} - R^{I}_{1,p})\cos\phi_1 \\
&(A^{I}_{0,p} + R^{I}_{0,p})\, n_0 = (A^{I}_{1,p} + R^{I}_{1,p})\, n_1 \\
&A^{I}_{0,s} + R^{I}_{0,s} = A^{I}_{1,s} + R^{I}_{1,s} \\
&(A^{I}_{0,s} - R^{I}_{0,s})\, n_0 \cos\phi_0 = (A^{I}_{1,s} - R_{1,s})\, n_1 \cos\phi_1 \quad .
\end{aligned} \tag{B-39}$$

At Boundary II (z = d)

$$\begin{aligned}
&(A^{II}_{1,p} - R^{II}_{1,p})\cos\phi_1 = A^{II}_{2,p}\cos\phi_2 \\
&(A^{II}_{1,p} + R^{II}_{1,p})\, n_1 = A^{II}_{2,p}\, n_2 \\
&A^{II}_{1,s} + R^{II}_{1,s} = A^{II}_{2,s} \\
&(A^{II}_{1,s} - R^{II}_{1,s})\, n_1 \cos\phi_1 = A^{II}_{2,s}\, n_2 \cos\phi_2 \quad .
\end{aligned} \tag{B-40}$$

The amplitude conditions are obtained by substituting equations (B-10), (B-35), (B-12), and (B-36) into equations (B-37) and (B-38) and letting the phase conditions be fulfilled.

Now, we must consider the phase relations between the amplitudes; i.e., we must introduce the principle of the interference of light into the calculation. From equations (B-26) through (B-30), it may be seen that we are concerned with a factor of ω times the optical path difference, which is the product of the distance and the refractive index n(n = c/v, where c = speed of light in a vacuum);i.e., for a beam of monochromatic light that has been split and recombined, the phase difference between the two recombining beams is $2\pi/\lambda$ times (optical path difference), or

$$\text{Phase difference} = 2\pi/\lambda \left(\sum_i n_i d_i - \sum_j n_j d_j\right) \quad . \tag{B-41}$$

Now, Jenkins and White [54] show that the optical path in Figure B-2 is such that we have a phase difference of

$$x = \text{phase difference} = (2\pi/\lambda)\, 2n_1 d \cos\phi_1 \quad . \tag{B-42}$$

Remembering that $\omega z/v = (2\pi/\lambda)cz/v = (2\pi/\lambda)nz$, we have

$$A^{I}_{1,p} = A^{II}_{1,p} \exp\left(\frac{i\omega\, d\cos\phi_1}{v_1}\right) = A^{II}_{1,p} e^{\frac{1}{2}ix} \quad ,$$

$$R^{I}_{1,p} = R^{II}_{1,p} \exp\left(\frac{i\omega\, d\cos\phi_1}{v_1}\right) = R^{II}_{1,p} e^{-\frac{1}{2}ix} \quad , \tag{B-43}$$

$$A^{I}_{1,s} = A^{II}_{1,s} e^{\frac{1}{2}ix}; \quad R^{I}_{1,s} = R^{II}_{1,s} e^{-\frac{1}{2}ix} \quad .$$

Now we may combine equations (B-39) and (B-40) as:

$$\left(A^{I}_{0,p} - R^{I}_{0,p}\right)\cos\phi_0 = \left(A^{II}_{1,p} e^{\frac{1}{2}ix} - R^{II}_{1,p} e^{-\frac{1}{2}ix}\right)\cos\phi_1 \quad ,$$

$$\left(A^{I}_{0,p} + R^{I}_{0,p}\right)n_0 = \left(A^{II}_{1,p} e^{\frac{1}{2}ix} + R^{II}_{1,p} e^{-\frac{1}{2}ix}\right)n_1 \quad ,$$

$$A^{I}_{0,s} + R^{I}_{0,s} = A^{II}_{1,s} e^{\frac{1}{2}ix} + R^{II}_{1,s} e^{-\frac{1}{2}ix} \quad , \tag{B-44}$$

$$\left(A^{I}_{0,s} - R^{I}_{0,s}\right)n_0 \cos\phi_0 = \left(A^{II}_{1,s} e^{\frac{1}{2}ix} - R^{II}_{1,s} e^{-\frac{1}{2}ix}\right)n_1 \cos\phi_1 \, .$$

Now noting that from equations (B-33) that $R^{II}_{1,p} = r^{n}_{p} A^{II}_{1,p}$ and $R^{II}_{1,s} = r^{n}_{s} A^{II}_{1,s}$ and substituting $e^{-\frac{1}{2}ix} = z$ and $e^{\frac{1}{2}ix} = 1/z$, we obtain

$$
\begin{aligned}
\left(A^{I}_{0,p} - R^{I}_{0,p}\right)\cos\phi_0 &= \frac{1 - r''_p z^2}{z} A^{II}_{1,p}\cos\phi_1 \quad , \\
\left(A^{I}_{0,p} + R^{I}_{0,p}\right) n_0 &= \frac{1 + r''_p z^2}{z} A^{II}_{1,p} n_1 \quad , \\
A^{I}_{0,s} + R^{I}_{0,s} &= \frac{1 + r''_s z^2}{z} A^{II}_{1,s} \quad , \\
\left(A^{I}_{0,s} - R^{I}_{0,s}\right) n_0 \cos\phi_0 &= \frac{1 - r''_s z^2}{z} A^{II}_{1,s} n_1 \cos\phi_1 \quad .
\end{aligned}
\tag{B-45}
$$

Considering first the last two equations of (B-45), we may write

$$
\frac{A^{I}_{0,s} + R^{I}_{0,s}}{A^{I}_{0,s} - R^{I}_{0,s}} = \frac{\left(1 + r''_s z^2\right) n_0 \cos\phi_0}{\left(1 - r''_s z^2\right) n_1 \cos\phi_1} \quad . \tag{B-46}
$$

Now, note that by equation (B-31), we have

$$
r'_s = - \frac{\sin(\phi_0 - \phi_1)}{\sin(\phi_0 + \phi_1)} = \frac{n_0\cos\phi_0 - n_1\cos\phi_1}{n_0\cos\phi_0 + n_1\cos\phi_1} \quad .
$$

Therefore,

$$
\frac{1 + r'_s}{1 - r'_s} = \frac{n_0\cos\phi_0}{n_1\cos\phi_1} \quad , \tag{B-47}
$$

and equation (B-46) becomes

$$
\frac{A^{I}_{0,s} + R^{I}_{0,s}}{A^{I}_{0,s} - R^{I}_{0,s}} = \frac{\left(1 + r''_s z^2\right)\left(1 + r'_s\right)}{\left(1 - r''_s z^2\right)\left(1 - r'_s\right)} \quad . \tag{B-48}
$$

Rewriting, we have

$$A^I_{0,s}[(1 - r''_s z^2)(1 - r'_s) - (1 + r''_s z^2)(1 + r'_s)]$$

$$= R^I_{0,s}[-(1 + r''_s z^2)(1 + r'_s) - (1 - r''_s z^2)(1 - r'_s)] \qquad \text{(B-49)}$$

or

$$\frac{R^I_{0,s}}{A^I_{0,s}} = r_s e^{i\delta_s}$$

$$= \frac{[(1 + r''_s z^2)(1 + r'_s) - (1 - r''_s z^2)(1 - r'_s)]}{[(1 + r''_s z^2)(1 + r'_s) + (1 - r''_s z^2)(1 - r'_s)]} \qquad \text{(B-50)}$$

$$= \frac{r''_s z^2 + r'_s}{1 + r''_s r'_s z^2} = \frac{r'_s + r''_s e^{-ix}}{1 + r'_s r''_s e^{-ix}} .$$

Now considering the first two equations of equations (B-45) we have

$$\frac{A^I_{0,p} + R^I_{0,p}}{A^I_{0,p} - R^I_{0,p}} = \frac{(1 + r''_p z^2)\, n_1 \cos\phi_0}{(1 - r''_p z^2)\, n_0 \cos\phi_1} . \qquad \text{(B-51)}$$

Note that by equation (B-31) we have

$$r'_p = \frac{\tan(\phi_0 - \phi_1)}{\tan(\phi_0 + \phi_1)} = \frac{n_1 \cos\phi_0 - n_0 \cos\phi_1}{n_1 \cos\phi_0 + n_0 \cos\phi_1} . \qquad \text{(B-52)}$$

Therefore,

$$\frac{1 + r'_p}{1 - r'_p} = \frac{n_1 \cos\phi_0}{n_0 \cos\phi_1} , \qquad \text{(B-53)}$$

and equation (B-51) becomes

$$\frac{A^I_{0,p} + R^I_{0,p}}{A^I_{0,p} - R^I_{0,p}} = \frac{(1 + r''_p z^2)(1 + r'_p)}{(1 - r''_p z^2)(1 - r'_p)} \quad . \tag{B-54}$$

Rewriting we have

$$\begin{aligned} A^I_{0,p}[(1 - r''_p z^2)(1 - r'_p) - (1 + r''_p z^2)(1 + r'_p)] \\ = R^I_{0,p}[- (1 + r''_p z^2)(1 + r'_p) - (1 - r''_p z^2)(1 - r'_p)] \end{aligned} \tag{B-55}$$

or

$$\begin{aligned} \frac{R^I_{0,p}}{A^I_{o,p}} = r_p e^{i\delta_p} &= \frac{(1 + r''_p z^2)(1 + r'_p) - (1 - r''_p z^2)(1 - r'_p)}{(1 + r''_p z^2)(1 + r'_p) + (1 - r''_p z^2)(1 - r'_p)} \\ &= \frac{2r''_p z^2 + 2r'_p}{2 + 2r''_p r'_p z^2} = \frac{r'_p + r''_p e^{-ix}}{1 + r'_p r''_p e^{-ix}} \quad . \end{aligned} \tag{B-56}$$

We have thus obtained the exact Drude equations for the reflection coefficients for a film-covered surface in the form

$$\begin{aligned} R^p = r_p e^{i\delta_p} &= \frac{r'_p + r''_p e^{-ix}}{1 + r'_p r''_p e^{-ix}} \quad , \\ R^s = r_s e^{i\delta_s} &= \frac{r'_s + r''_s e^{-ix}}{1 + r'_s r''_s e^{-ix}} \quad , \end{aligned} \tag{B-57}$$

where x is $(2\pi/\lambda)(2n_1\ d\ \cos\ \phi_1)$ and r_s', r_s'', r_p', and and r_p'' are the well-known Fresnel amplitude coefficients.

It should be noted that the derivation just presented treated the case of a dielectric (nonabsorbing) media. We shall follow the common approach of extending our results to include the case of conducting (absorbing) media by replacing the real index of refraction by a complex quantity (n + ik, where k = 0 for a dielectric media). The extension proves to be approximately correct and is in accordance with a careful development of the Fresnel coefficients by Stratton [55]. This extension is also discussed by Nestall [56].

We note further that the classical Fresnel equations, while generally inadequate in metal optics, are applicable here since the frequency involved is below the plasma frequency, ω_p. At ω_p and above, the effects of polarization waves must be considered. For most metals, ω_p lies in the ultraviolet. This facet of the Fresnel equations is discussed by Melnyk and Harrison [57], who point out that when polarization fields become important the classical Fresnel equations no longer apply. However, for frequencies up to and including visible light frequencies, there are no measurable bulk charge densities in metals; hence no polarization fields.

REFERENCES

1. Sella, C., Conjeaud, P., and Trillat, J.J.: C.R. Acad. Sci. Paris, 249, 1987, 1959.
2. Bethge, H.: Phys. Stat. Sol. 2, 3, 1962a.
3. Walton, D.: J. Chem. Phys. 37, 2182, 1962a.
4. Bassett, G.A.: Phil. Mag. 3, 1042, 1958.
5. Adamsky, R.F., and LeBlanc, R.E.: J. Vac. Sci. Tech. 2, 79, 1965.
6. Pashley, D.W., Stowell, M.J., Jacobs, M.H., and Law, T.J.: Phil. Mag. 10, 127, 1964.
7. Miller, N.C., and Shirn, G.A.: Appl. Phys. Lett. 10, 86, February 1, 1967.
8. Glang, R., Holmwood, R.A., and Herd, S.R.: J. of Vac. Sci. and Tech. 4, 163, 1967.
9. Beckerman, M., and Thun, R.E.: Tran., 8th Nat. Vac. Symp. Am. Vac. Soc. 2, 905, 1961.
10. Frenkel, J.: Phys. Rev. 36, 1604, 1930.
11. Emtage, P.R., and Tantraporn, W.: Phys. Rev. Lett. 8, 267, 1962.
12. Stratton, R.: Phys. Chem. Solids. 23, 1177, 1962.
13. Hartman, T. E., Blair, J. C., and Bauer, R.: J. of Appl. Phys. 37, 2468, 1966.
14. Hill, R.M.: Thin Solid Films. 1, 39, 1967.
15. Gundlach, K.H., and Simmons, J.G.: Thin Solid Films. 4, 61, 1969.
16. Neugebauer, G.A., and Webb, M.B.: J. of Appl. Phys. 33, 74, January 1962.
17. Hartman, T.E.: J. Appl. Phys. 34, 943, 1963.
18. Parker, R.L., and Krinsky, A.: J. of Appl. Phys. 34, 2700, 1963.
19. Weitzenkamp, L.A., and Bashara, N.M.: Trans. Metallurgical Soc. of AIME. 236, 351, 1966.
20. Herman, D.S., and Rhodin, T.N.: J. Appl. Phys. 37, 1594, 1966.
21. Milgram, A.A., and Lu, Chih-shun: J. of Appl. Phys. 37, 4774, 1966.
22. Swanson, J.G., Campbell, D.S., and Anderson, J.C.: Thin Solid Films. 1, 325, 1967/68.

REFERENCES (Continued)

23. Hill, R.M.: Proc. Roy. Soc. A. 309, 377, 1969.

24. Morris, J.E.: J. Appl. Phys. 39, 6107, 1968.

25. Christen, T.E., and Hewitt, J.B., Jr.: Proc. 1970 Electronics Components Conference. 63, 1970.

26. Abelés, F.: J. Optical Soc. of Am. 47, 473, 1957.

27. Maxwell Garnett, J.C.: Phil. Trans. 203, 385, 1904.

28. Heavens, O.S.: Optical Properties of Thin Solid Films. Butterworks Scientific Publications, Ltd., London, 1955.

29. Mie, G.: Ann. Physik. 25, 377, 1908.

30. Schopper, H.: Z. Physik. 130, 565, 1951.

31. Rasigni, G., and Rouard, P.: J. Opt. Soc. Am. 53, 604, 1963.

32. Doremus, R.H.: J. of Appl. Phys. 37, 2775, 1966.

33. Doremus, R.H.: Thin Solid Films. 1, 379, 1967/68.

34. Tekucheva, I.A.: Soviet Phys. J. 84-87, January-February 1965.

35. Passaglia, E., Stromberg, R.R., and Kruger, J., ed.: Ellipsometry in the Measurement of Surfaces and Thin Films. National Bureau of Standards, 1964.

36. McCrackin, F.L.: A Fortran Program for Analysis of Ellipsometer Measurements. NBS Technical Note 479, April 1969.

37. Holland, L.: Thin Film Microelectronics. John Wiley & Sons, Inc., New York, 1965.

38. Tolansky, S.: Multiple-Beam Interferometry of Surface and Films. Clarendon Press, Oxford, 1949.

39. Jenkins, R., and DeVries, J.L.: Practical X-Ray Spectrometry. Phillips Technical Library, The Netherlands, 1967.

40. McKinley, T.D., Heinrich, K.F.J., and Wittry, D.B., ed.: The Electron Microprobe. John Wiley & Sons, Inc., New York, 1966.

41. Heidenreich, R.D.: Fundamentals of Transmission Electron Microscopy. John Wiley & Sons, Inc., New York, 1964.

REFERENCES (Concluded)

42. Drude, P.: Ann. Physik. 272, 532, 865, 1889.

43. American Society for Testing and Materials: X-Ray Emission Line Wavelengths and Two-Theta Tables. ASTM Data Series DS 37, Philadelphia, Pa., 1965.

44. Malé, D.: C.R. Acad. Sci. Paris, 230, 286, 1950.

45. Born, M., and Wolf, E.: Principles of Optics. The Macmillan Co., New York, 1959.

46. National Research Council of the United States of America: International Critical Tables of Numerical Data, Physics, Chemistry and Technology. V, McGraw-Hill Book Co. Inc., New York, p. 250, 1929.

47. Rothen, A.: Review of Scientific Instruments. 16, 26, February 1945.

48. McCrackin, F.L., Passaglia, E., Stromberg, R. R., and Steinberg, H.L.: J. of Research of NBS. 67A, July-August 1963.

49. Rainville, E.D.: Unified Calculus and Analytic Geometry. The Macmillan Co., New York, 1961.

50. Winterbottom, A.B.: Optical Studies of Metal Surfaces. The Royal Norwegian Scientific Society Report No. 1, F. Burns, Norway, 1955.

51. Bornong, B.J.: Use of the Ellipsometer in the Measurement of Thin Films. AD 658063, Technical Report, U.S. Army Weapons Command, July 1967.

52. Reitz, J. R., and Milford, F.J.: Foundations of Electromagnetic Theory. Addison-Wesley Publishing Co., Reading, Mass., 1960.

53. Vašíček, A.: Optics of Thin Films. North-Holland Publishing Co., Amsterdam, 1960.

54. Jenkins, F.A., and White, H.E.: Fundamentals of Optics. McGraw-Hill Book Co., Inc., New York, 1957.

55. Stratton, J. A.: Electromagnetic Theory. McGraw-Hill Book Co., Inc., New York, pp. 490-494, 1941.

56. Nestall, J.E., Jr., and Christy, R.W.: Am. J. of Phys. 39, 313, 1971.

57. Melnyk, A.R., and Harrison, M.J.: Phys. Rev. B2, 835, 1970.

NATIONAL AERONAUTICS AND SPACE ADMINISTRATION
WASHINGTON, D.C. 20546

OFFICIAL BUSINESS
PENALTY FOR PRIVATE USE $300

FIRST CLASS MAIL

POSTAGE AND FEES PAID
NATIONAL AERONAUTICS AND
SPACE ADMINISTRATION
451

U.S.MAIL

POSTMASTER: If Undeliverable (Section 158 Postal Manual) Do Not Return

"The aeronautical and space activities of the United States shall be conducted so as to contribute . . . to the expansion of human knowledge of phenomena in the atmosphere and space. The Administration shall provide for the widest practicable and appropriate dissemination of information concerning its activities and the results thereof."

—NATIONAL AERONAUTICS AND SPACE ACT OF 1958

NASA SCIENTIFIC AND TECHNICAL PUBLICATIONS

TECHNICAL REPORTS: Scientific and technical information considered important, complete, and a lasting contribution to existing knowledge.

TECHNICAL NOTES: Information less broad in scope but nevertheless of importance as a contribution to existing knowledge.

TECHNICAL MEMORANDUMS: Information receiving limited distribution because of preliminary data, security classification, or other reasons. Also includes conference proceedings with either limited or unlimited distribution.

CONTRACTOR REPORTS: Scientific and technical information generated under a NASA contract or grant and considered an important contribution to existing knowledge.

TECHNICAL TRANSLATIONS: Information published in a foreign language considered to merit NASA distribution in English.

SPECIAL PUBLICATIONS: Information derived from or of value to NASA activities. Publications include final reports of major projects, monographs, data compilations, handbooks, sourcebooks, and special bibliographies.

TECHNOLOGY UTILIZATION PUBLICATIONS: Information on technology used by NASA that may be of particular interest in commercial and other non-aerospace applications. Publications include Tech Briefs, Technology Utilization Reports and Technology Surveys.

Details on the availability of these publications may be obtained from:

SCIENTIFIC AND TECHNICAL INFORMATION OFFICE

NATIONAL AERONAUTICS AND SPACE ADMINISTRATION

Washington, D.C. 20546